Poznań University of Technology

Faculty of Civil and Transport Engineering

Doctoral Thesis

Carbon Nanotubes Applications for Friction Reduction in Transport Engineering

Author:
mgr inż. Mohanad J. Hameed Al-Karawi

Supervisor

dr hab. inż. Jarosław Kałużny prof. PP

Co-supervisor

dr inż. Marek Nowicki

Poznań 2024

Table of Contents

List of Figures

List of Tables

List of Abbreviations

AFM	Atomic Force Microscope
AFR	Air-Fuel Ratio
Al_2O_3	Aluminium Oxide
CCVD	Catalytic Chemical Vapor Deposition Method
CH_4	Methane
CI engine	Compression-Ignition Engine
CuO	Copper (II) oxide or Cupric Oxide
CNFs	Carbon Nanofibers
CNTs	Carbon Nanotubes
CNTFET	Carbon Nanotube Field-Effect Transistor
C60	Carbon 60 (a molecule made up of 60 carbon atoms)
CVD	Chemical Vapor Deposition
CxHy	Hydrocarbons
EDS	Energy Dispersive Spectrometer
EN	Engineered Nanomaterial
ESEM	Environmental Scanning Electron Microscope
EU	European Union
Fe_2O_3	Iron (III) Oxide
FWCNTs	Few Walled Carbon Nanotubes
HCOOH	Formic Acid
HCl	Hydrogen Chloride
HSMs	High Shear Mixers
HSR	High Shear Reactors
IF	Inorganic Fullerene
KOH	Potassium Hydroxide
LAMMPS	Large-scale Atomic/Molecular Massively Parallel Simulator
MD	Molecular Dynamics
MM	Molecular Mechanics
MWCNTs	Multi-Walled Carbon Nanotubes
NH_3	Ammonia
QM	Quantum Mechanical
SEM	Scanning Electron Microscope
SWCNT	Single-Walled Carbon Nanotubes
USA	United States of America
UV	Ultraviolet Radiation
PBT	Polybutylene Terephthalate
PECVD	Plasma-Enhanced Chemical Vapor Deposition
PRCL	Piston Ring and Cylinder Liner
POM	Polyoxymethylene
RBM	Radial Breathing Mode
RPM	Revolutions Per Minute
Ru	Ruthenium
SF6	Sulfur Hexafluoride
SiO_2	Silicon Dioxide
STM	Scanning Tunneling Microscope
TEM	Transmission Electron Microscope
ZDDPs	Zinc Dialkyl Dithiophosphates

List of Symbols

$\overrightarrow{a_i}$	The Acceleration of Each Atom
F_k	Force of Kinetic Friction
μ	The Coefficient of Friction
μ_k	The Coefficient of Kinetic Friction
λ	Air-Fuel Ratio
F_N	The Normal Force
F_T	The Tangential Force
$F(dt)$	The New Energy of Each Atom After a Small Increment of Time
m_T	Sitting Mass
m_H	Hanging Mass
m_i	The Mass of Atom
V	Volume
$\overrightarrow{v_i}(dt)$	The Velocity of Each Atom After a Small Increment of Time
T	Temperature
N	Number of Atoms
$F_{1\to2}$	Force Applied by Atom 1 on Atom 2
U_{12}	The Energy Interaction Between Atom 1 and Atom 2
U_{col}	Coulombic Interaction Energy
U_{vdw}	Van der Waals Interaction
U_{tot}	Total Energy
$U(dt)$	The New Energy of Each Atom After a Small Increment of Time
$\overrightarrow{r_i}(dt)$	The New Position of Each Atom After a Small Increment of Time
q_1	The Signed Magnitudes of The Charge for Atom One
q_2	The Signed Magnitudes of The Charge for Atom Two

Abstract

This thesis aims to understand the tribological functions of carbon nanotubes (CNTs) and their practical applications for internal combustion engines lubrication.

Until now the vast majority of scientific studies aiming at tribological applications of CNTs were conducted under idealized tribometer conditions [1, 3]. This thesis is focused on the industrial applications of CNTs, with special regard to the transport engineering and combustion engines. It is obvious that the main source of friction losses in an internal combustion engine is related to the sliding friction, whereby the main friction components are pistons, piston rings and journal bearings. Thereby the main part of this work was an engine test, where the CNTs were introduced into engine lubricating oil. The overall engine friction was measured and compared for reference oil and research oil, whereby only trace amounts of CNTs were introduced, to obtain the CNTs mass concentration in research oil as low as 0.03%. The engine motoring torque was reduced significantly, moreover a surprisingly high reduction in engine vibrations was observed. The vibration acceleration measured on the engine block, close to the main bearing was reduced by up to 30% for the research oil containing trace amounts of CNTs. The vibrations were measured for hot engine, the beneficial role of CNTs was confirmed at various engine working conditions like coolant temperature, engine speed and load. The final experimental result of this work confirmed the thesis that the CNTs introduced into lubricating oil can reduce sliding friction significantly, reducing vibrations at the same time.

Friction on sliding surfaces is closely linked to the dissipation and release of thermal energy, which is crucial for understanding friction. A large portion of the surface phenomena relies on temperature. For better understanding of the CNTs induced friction phenomena observed in the engine a series of complementary tests were conducted. A precise understanding of the interaction between surfaces in contact at the atomic or nanoscale level is necessary to determine crucial friction characteristics, including friction coefficient, adhesion, energy dissipation, and wear. To gain this insight Amsler tribometer tests and molecular dynamics calculations were conducted, as an extension to the engine tests. It turned out that the phenomena related to the CNTs in the lubricating oil could not be explained to their full extent at this point. The LAMMPS molecular dynamics simulation model allows for some insights into friction at atomic scale, however real engine journal bearings working conditions are too complex to be reproduced at a molecular scale.

Streszczenie

Zastosowania Nanorurek Węglowych w Inżynierii Transportu w Celu Zmniejszenia Tarcia

Niniejsza praca ma na celu zrozumienie mechanizmów tarcia nanorurek węglowych (ang.: Carbon Nanotubes, CNTs) i ich praktycznego wykorzystania w tłokowych silnikach spalinowych.

Dotychczas znakomita większość badań CNTs jest ograniczona do wyidealizowanych warunków które panują w tribometrach [1,3]. W tej pracy ważniejsze są jednak przemysłowe zastosowania CNTs, ze szczególnym uwzględnieniem zagadnień transportowych i tłokowych silników spalinowych. W tłokowym silniku spalinowym dominującą formą tarcia jest tarcie ślizgowe które występuje w głównych węzłach tarcia takich jak tłoki, pierścienie tłokowe i łożyska ślizgowe. Z tego powodu główną część niniejszej pracy stanowi eksperyment silnikowy który polegał na wprowadzeniu CNTs do oleju smarującego. Do oleju referencyjnego wprowadzono śladowe ilości CNTs uzyskując stężenie masowe równe 0,03%, następnie porównano straty tarcia dla oleju referencyjnego i wzbogaconego nanorurkami. Zaobserwowano znaczne zmniejszenie strat tarcia w warunkach napędu zewnętrznego silnika, ponadto nanorurki spowodowały zaskakująco silne zmniejszenie drgań. Czujnik drgań zamontowano na kadłubie silnika, w pobliżu łożysk głównych wału korbowego. W różnych warunkach pracy silnika określonych temperaturą cieczy chłodzącej, prędkością obrotową i obciążeniem zarejestrowano zmniejszenie maksymalnego przyspieszenia drgań sięgające 30%. Główny eksperyment wykonany w ramach tej pracy potwierdza tym samym hipotezę, że CNTs wprowadzone do oleju smarującego mogą znacząco zmniejszyć tarcie ślizgowe, jednocześnie przyczyniając się do znacznego zmniejszenia drgań.

Do zrozumienia procesów tarcia ślizgowego kluczowe jest uwzględnienie rozpraszania energii w formie energii cieplnej. Wiele zjawisk zachodzących na powierzchni trących jest ściśle związane z ciepłem wyzwolonym przez tarcia. Dla głębszego zrozumienia wyników testów silnikowych wykonano dodatkowe badania. Określenie podstawowych parametrów związanych z tarciem, takich jak współczynnik tarcia, adhezja, dyssypacja energii i zużycie powierzchni wymaga zrozumienia zjawisk na poziomie atomowym. Aby to umożliwić przeprowadzono dodatkowe testy w tribometrze Amslera oraz symulacje tarcia z użyciem modelu dynamiki molekularnej. Obecnie nie jest jeszcze możliwe pełne zrozumienie zjawisk w skali atomowej. Model LAMMPS pozwala jedynie na ograniczone odwzorowanie złożonych zjawisk zachodzących w łożysku ślizgowym tłokowego silnika spalinowego.

1 Introduction

1.1 Introduction

In moving mechanical systems, which consume enormous quantities of energy, increase the temperature significantly, and reduce output precisely, friction and wear are inevitable. In most mechanical situations, a variety of lubricants were used to minimize friction and wear and the efficiency of lubricants greatly affects the performance of moving mechanical systems. The addition of various additives into conventional lubricants, such as Copper (II) oxide (CuO), Iron (III) oxide (Fe_2O_3), Cu, graphene oxide, has attracted considerable attention in recent years [1].

The additives can significantly improve the friction and wear performance of lubricants. Nanoparticles have their unique advantages as a relatively new class of lubricant additives. Nanoparticles enter the region of contact thanks to their small size, which is the most significant aspect of their action [1]. Studies have demonstrated that incorporating nanostructured carbon, particularly CNTs (carbon nanotubes), into lubricating oil can decrease friction loss. CNTs are an allotropic form of carbon and are characterized by mechanical and chemical properties. That makes them extremely important when producing engines [2], due to their tiny size, which is the most important feature of nanoparticles, Fig. 1.1.

The nanoparticles are made to be excellent lubricant additives by certain other potential properties such as low reactivity to other lubricant additives, a high possibility of film formation on various surface types, high non-volatility to withstand high temperatures, and increased durability [1].

CNTs have drawn a lot of interest since they were discovered in 1991. They have a fascinating structure and a large number of possible applications, including field emitters and electronic nanoscale equipment, which have already been investigated [4]. The mechanical characteristics of nanotubes also show promise. The resistance of carbon nanotubes to bending has already been observed and studied [5]. Nanotubes can also have interesting tribological properties with their nanometric size, they can easily be active in the contact area, and their structure without dangling bonds confers them a chemical inertness [4, 5].

1.2 Background

Research has demonstrated that incorporating CNTs enhances the lubrication properties of lubricants. Several independent studies have shown that the incorporation of nanostructured carbon, particularly CNTs, into lubricating oil can reduce friction loss [1, 4]. It is important to acknowledge that these studies were mainly carried out in controlled tribometer settings [3].

CNTs have been found to possess advantageous tribological characteristics in various studies conducted primarily under ideal tribometer conditions. J. Kałużny et al [6], and Joly-Pottuz et al [4] have reported the advantageous tribological properties of CNTs and a reduction in friction coefficient during the sliding of C60 films against a 52100 steel ball in multiple engine tests. MWCNTs were employed as a coating on the piston skirt, resulting in a maximum reduction of 16% in the tested engine's overall measured friction [6].

The combustion engine employs multiple friction components composed of diverse metal and plastic materials, functioning concurrently at varying speeds, contact pressures, and temperatures that are subject to dynamic changes. The practical testing of lubricants presents challenges in studying tribological phenomena due to the engine's overall friction being a combination of various friction phenomena, including dry and Elasto-hydrodynamic friction regimes [3].

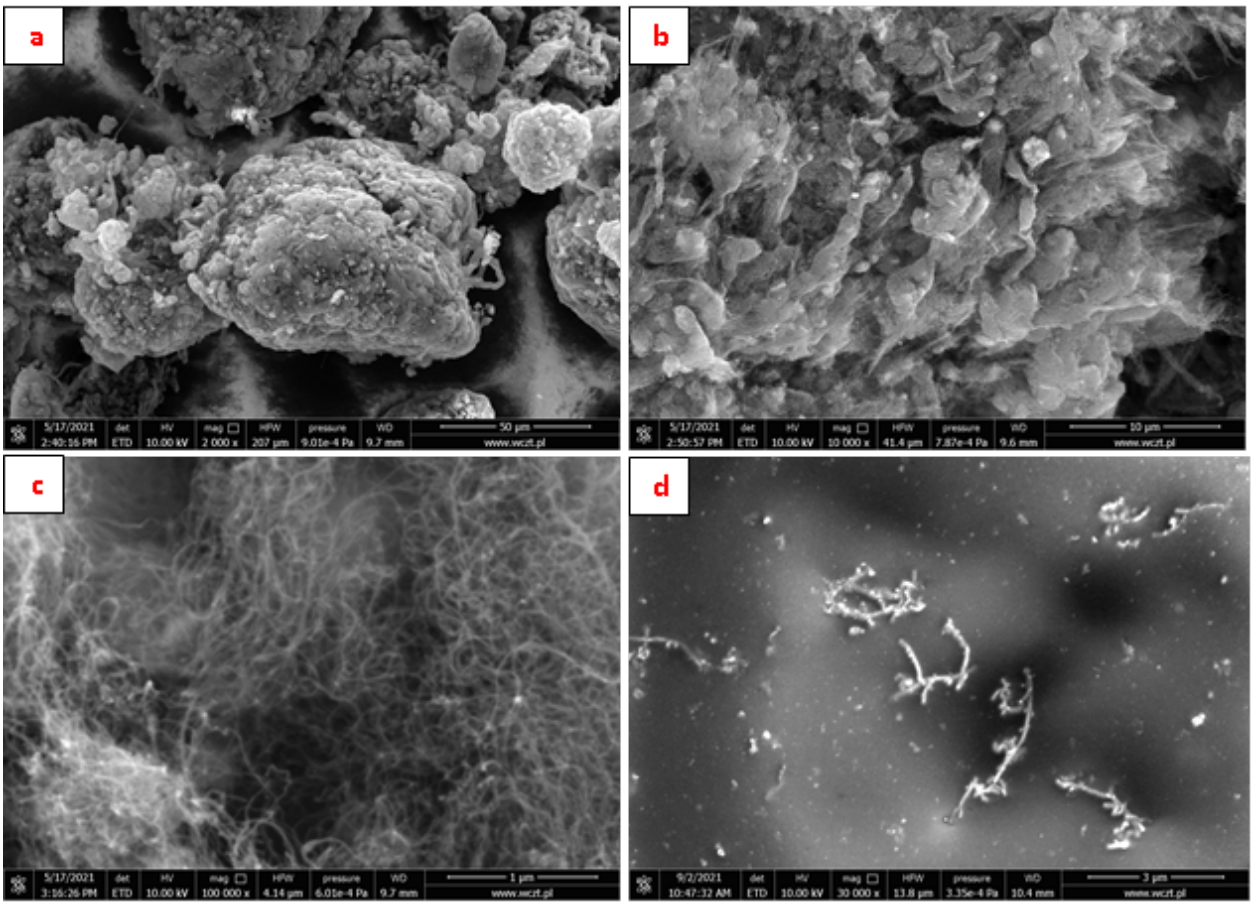

Fig. 1.1. Carbon nanotubes NC 7000 produced by Nanocyl® in scanning electron microscopy; a-c pristine CNTs powder at various magnification, d: CNTs remnants found in the grease covering bearing race after lubrication test; author's own research

The findings suggest an intricate nature of tribological phenomena occurring in actual machinery that employs oil modified with CNTs. Further investigation is required to fully comprehend the various tribological functions of CNTs and their involvement in friction mechanisms [3].

CNTs were found to significantly reduce friction in lubricating oil during full engine tests, as reported in [7]. Despite the abundance of tribometer research reports, there have been only a limited number of tests involving CNTs in actual machines thus far. The favorable tribological properties of CNTs have been studied at a microscopic scale and using tribometers, but their effectiveness in engines has not been confirmed [8]. To date, there have been no reported studies on the tribological characteristics of CNTs as a solid lubricant or as an additive to lubricating oil or grease [6].

1.3 Problem Statement

To enhance the environmental sustainability and performance of internal combustion engines, by minimizing friction losses and consequently decreasing fuel consumption. Internal combustion engines currently dominate the powertrain applications in cars and are expected to continue to do so in the coming

decades, despite the popular belief that reciprocating engines will take over. This is attributed to the well-to-wheel energy balance and comprehensive estimation of emissions across all stages of production and distribution [8].

Friction loss is a factor in the engine's energy balance, as indicated by its mechanical efficiency. Moreover to increase fuel economy and, in particular, the overall mechanical efficiency, the determination of the friction losses for combustion engines is a main subject in current engine development. Based on current challenges for manufacturers including stricter CO_2 emission limits from the legislative side, changing customer preferences (away from product towards function, e.g., car-sharing and car rental), and a general focus on the environmental impact, it is nowadays crucial to develop highly efficient vehicles [9].

The engine components generate frictional force akin to that of high load due to their continuous motion. So in order to improve the engine performance and have some representation of frictional losses, a study will be developed to describe the friction force from the piston assembly friction, the piston skirt friction, as well as the bearing friction. The frictional loss of the engine will be compared to give a better understanding of the lubrication condition and the efficiency of lubrication [10].

Detailed knowledge of mechanisms of tribological action must be gained for the successful industrial application of CNTs for friction, vibration and wear reductions in machines. Where CNTs have been of interest for various applications over the past decade. However, due to the chemical inertness of CNTs, their dispersion in solvents remains a challenge. Therefore, in the context of lubricant additives, the issue that should be addressed first is its stability in the base oil [11, 12].

Detailed molecular dynamics simulations are unavoidable to understand the processes occurring at an atomic scale during the friction process. A CNT is an ideal object for understanding the atomic scale aspects of interface interaction and friction. Among the many properties of CNTs that have sparked the interest of researchers is their high Young's modulus in the direction of the nanotube axis. However, studies have shown that nanotubes have a very low Young's modulus perpendicular to the nanotube axis, and simulations and experiments show that nanotubes can withstand a significant compressive force [13, 14].

Tribometer and real machine tests will be performed in this work to test the results of molecular dynamics calculations. If properly designed the nanolubricants containing CNTs should reduce friction, vibration and wear significantly.

1.4 Research Objectives

The goal of this work is to test and understand the tribological mechanisms related to the CNTs added to the lubricants with special regard to the sliding friction. The thesis is focused on the main friction components of an internal combustion engine. Recognizing the significant potential of CNTs in reducing friction and vibration, through an understanding of their tribological properties, can facilitate their effective use as lubricants, leading to the development of a novel category of lubricants.

1.5 Brief on Methodology

This study's major goal was to use CNTs in engine lubricants to lessen friction losses and wear. This study showed how adding CNTs, which have been proven to improve lubrication properties in lubricating oils in the past, can be done. According to the research findings reported in Hwang et al. [15], the lubrication performance notably improved as the size of the particles suspended in the mineral oil shrank.

Therefore, the impetus for doing this research was the conviction that it was necessary to confirm the findings of tribological tests of engine oil with the inclusion of CNTs. Therefore this work was characterized by focusing on the testing and understanding of the tribological mechanisms related to the

CNTs added to the lubricants and the dominant role of the CNTs. This work will allow for efficient applications for friction and vibration reductions thanks to understanding the tribological roles of CNTs.

Like other nanomaterials, CNTs exhibit a great propensity to aggregate. As a result, the findings of the tribological tests reveal that a crucial element in influencing friction conditions is the CNTs' dispersion in the oil. This prompted an explanation and discussion of the phenomenon related to CNTs' dispersion in engines. Thus, investigating the effects of friction at trace CNT concentrations was the objective. A rather considerable reduction in engine friction and vibration was still found at this concentration level, when the re-agglomeration effects were well reduced.

1.6 Scope and Limitation of the Study

The core of this research was improving the design of internal combustion engines by using CNTs. Which is the application of nanomaterial described as attempts to use CNTs in order to improve the functional properties of various engine components and improve the mechanical efficiency of internal combustion engines, in particular, to reduce losses caused by friction [2]. Figure 1.2. shows the structure of the thesis.

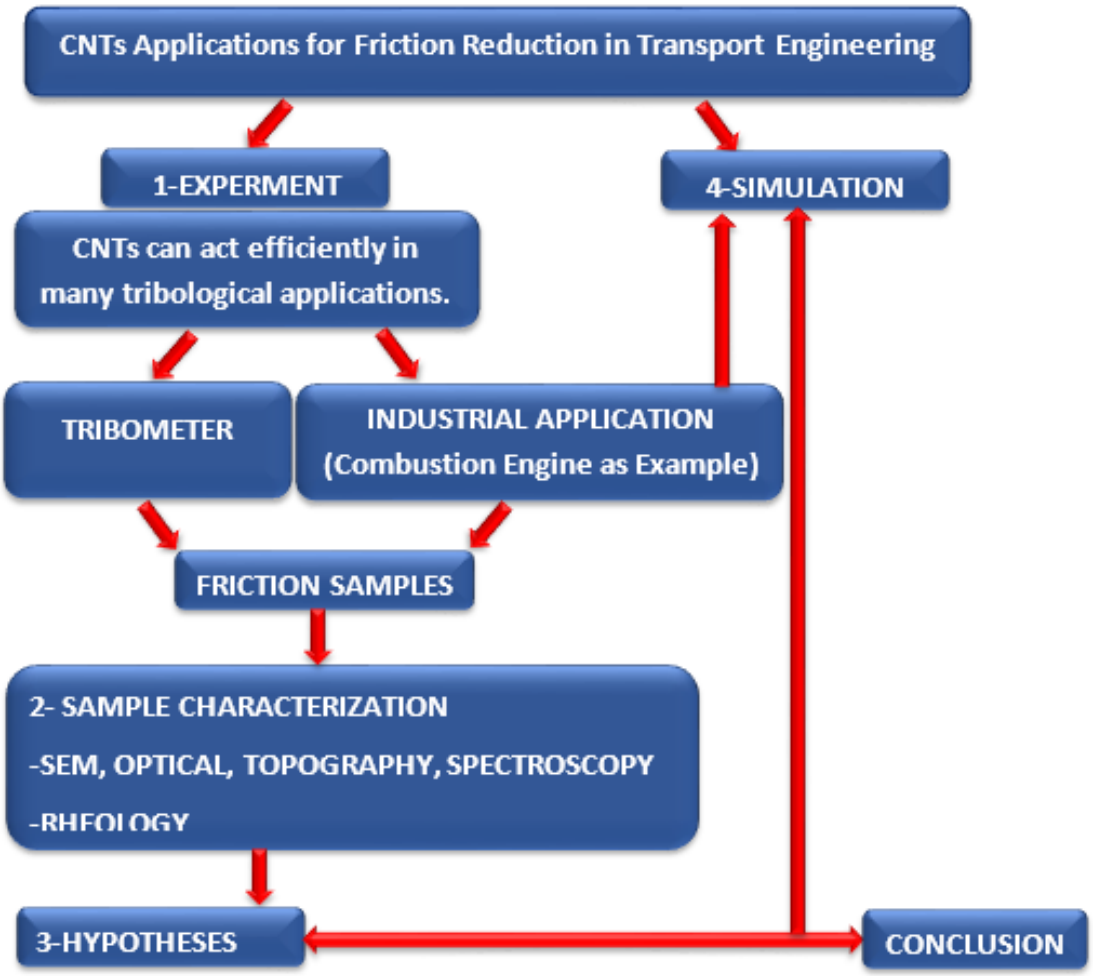

Fig. 1.2. Project flow chart

The tests will be conducted, and the surfaces wear morphology, and microstructure of CNTs will be observed using a scanning electron microscope (SEM). The survival of the CNTs and their resilience to the chemical environment and mechanical loads were confirmed by the photos of the samples acquired during engine testing that were recorded using SEM [1, 4]. Furthermore, energy dispersive spectrometer (EDS) analysis can be used to see whether CNTs have the capacity to adhere foreign particles to their surface. In the technical assessment of CNT images, these particles that become attached during engine operation may be referred to as pollution, but from a tribological perspective, they may really be advantageous. This capability can be used to purposefully add nanoparticles to the CNTs that have demonstrated beneficial tribological capabilities [6].

An experimental work consisted of determining the friction coefficient of CNTs by the method of molecular dynamics simulation using LAMMPS and C++ software for dynamic processes. In order to understand the atomic process, which results in macroscopic parameters like friction coefficient, wear, adhesion, and energy dissipation, it is necessary to study phenomena and properties at the atomic or molecular levels. This is done using a computer simulation method that analyzes the physical movements of atoms and molecules. Where carbon nanotubes are an ideal object for understanding the atomic scale aspects of interface interaction and friction [13].

2

Nanomaterials in Mechanical Engineering

2.1 Introduction to Nanomaterials

The cornerstones of nanoscience and nanotechnology are nanomaterials. The science and technology of nanostructures is a wide and interdisciplinary field of research and development interest that has developed explosively worldwide in recent years. It has the ability to revolutionize the way materials and goods are made and the range and scope of open features. It already has a major commercial influence, which will undoubtedly grow in the future [16].

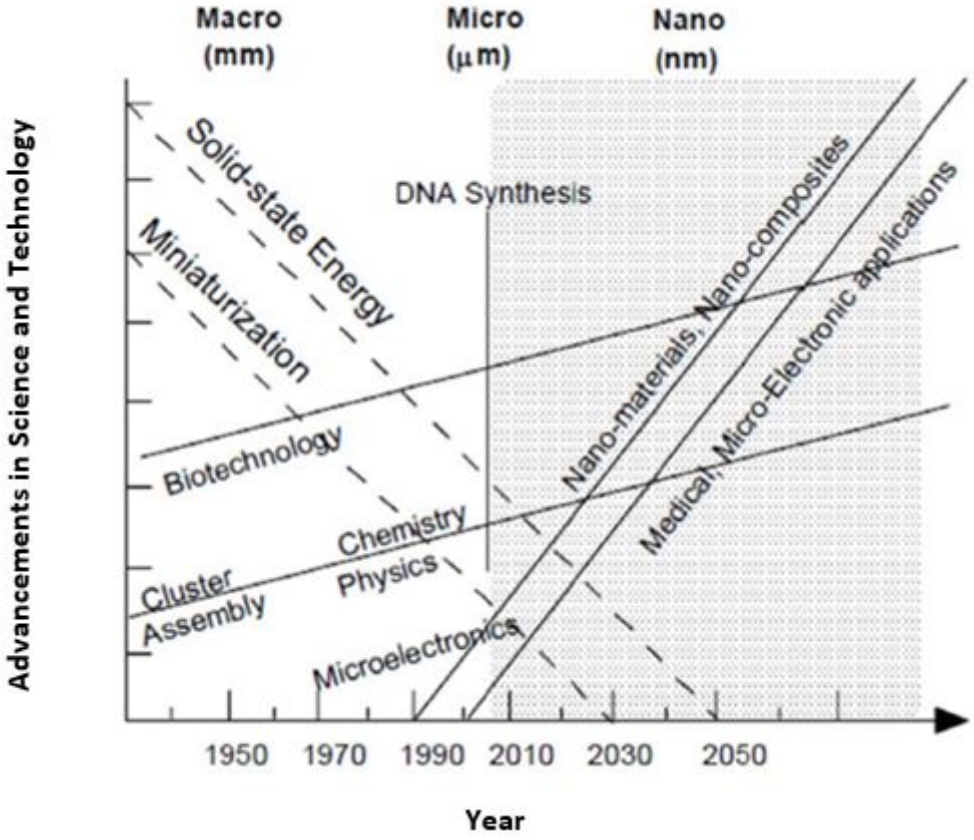

Fig. 2.1. Evolution of technology, science, and the future [16]

The presence of nanosized particles is not a new phenomenon in the workplace. The concept of "ultrafine particles" was described as early as 1997 by the Deutsche Forschungsgemeinschaft (German Research Foundation) by the Commission for the Investigation of the Health Hazards of Chemical Compounds in the working field [17].

The Commission for Investigating the Health Hazards of Chemical Compounds in the working field has defined the concept of “ultrafine particles” in its list of maximum workplace concentration (Maximale Arbeitsplatz-Konzentration MAK) and Biological agent tolerance value (Biologischer Arbeitsstoff Toleranzwert BAT). The values of the concept of "ultrafine particles" for the workplace mainly reflect the concept of nanoparticles used in science and technology today [17].

Nanoparticles are not an invention of science in regards to the concept of particle size or as a scientific accomplishment. They were nevertheless still smoke elements. Their use as natural iron oxide and carbon black particles has already been used in ancient cave paintings such as Altamira, etc. Due to their increasing agglomerate tendency, nanosized particles vary from coarser particles. These agglomerates are considered single particles in a microscopic context and can disintegrate into their primary particles in biological material [17, 18].

The Nanomaterial definition does not yet exist. It is understood that the traditional physical and chemical rules cannot extend to the nanoscale in full, and can vary from those of the bulk equivalents. These nanoscale characteristics of nanomaterials are derived from certain parameters, such as their shape, size, surface chemistry, specific surface area, and additional parameters. Where the definition has legal implications, lawmakers prefer a simple and concise distinction, i.e. what is legal or authorized and what is not allowed [19].

Nanomaterials can be described as materials with outer dimensions of at least 1-100 nm, and which have different physical and chemical characteristics from those they express when in their bulk forms. The technical definition of a nanomaterial is important to implement risk valuation and risk organization measures for nanomaterials. Formulating a science-based description is challenging because of the understanding of these novel materials, the measurement and imaging techniques needed to assess them are still fast developing.

An excessively broad description of the materials for which they are not applicable may enforce nano-specific requirements. On the other hand, a too-restrictive concept could make nanomaterials accessible on the market without being subject to appropriate risk evaluation and management measures.

The EU is the only competence in which nanomaterials have a wide legal meaning. Moreover, EU legislation unique to the sector, such as cosmetics and biocidal goods has distinct, yet to be harmonized meanings. The EU definition calls into question by various stakeholders as too broad or too restrictive. Technical challenges exist to its implementation and revisions with the assistance of the Joint Research Center that are being considered currently by the EU Commission [20].

Some nanomaterials are natural, but engineered nanomaterial (EN) has a specific interest, which was developed for and used in several commercial products and processes. They are used in medicine for diagnosis, imaging, and drug delivery, for example in solar screens, cosmetics or sporting goods, treads, electronics, and many other everyday articles [16].

Engineered nanomaterials are resources designed at the molecular (nanometer) level to take advantage of their small size and novel properties which are generally not seen in their conventional, bulk counterparts. The two main reasons why materials at the nanoscale can have different properties are increased relative surface area and new quantum effects. The surface area to volume ratio for a nanomaterial is much greater than the traditional forms, which can result in and greatly affect the chemical reaction and their strength. Quantum effects can also become even more relevant in nanoscales when assessing the properties and characteristics of materials leading to new magnetic, electrical, and optical behaviors.

Nanomaterials are in commercial use already, some for several years or decades. Today's wide range of commercial items including textiles, cosmetics, sunscreens, electronics, paints, and lacquer, which have no stains or wrinkles, is available.

Nanocomposites and Nanocoatings are used in a variety of consumer goods like sports equipment, windows, bikes, cars, and other nano-composites. There are new layers that block UV rays on the

bottles to protect the drinks from sunlight damage and long-lasting tennis balls using butyl rubber/nano clay compounds.

Nanoscale titanium dioxide is utilized in cosmetics, sunscreens, and self-cleaning windows, while nano silica is used as fillers in various products, such as dental fillings and cosmetics [16].

Nanomaterials have been present since the formation of nanostructures in early meteorites following the big bang. Subsequently, nature produced additional nanostructures, including seashells and skeletons. Early humans produced nanoparticles present in smoke while using fire [16].

The history of nanomaterials, from a scientific perspective, commenced at a later time. Michael Faraday synthesized colloidal gold particles in 1857, which is among the earliest scientific reports on the subject. Nanostructured catalysts have been studied for more than 70 years. In the early 1940s, silica nanoparticles in the form of precipitates and fumes were produced and marketed in the United States and Germany as a replacement for ultrafine carbon black in the reinforcement of rubber.

Amorphous silica nanoparticles are widely used in various consumer products, including coffee creamer, tires, optical fibers, and catalyst supports. Metallic nanopowders were developed in the 1960s and 1970s for magnetic recording tapes. In 1976, Granqvist and Buhrman [16] introduced Nanocrystals using the inert gas evaporation technique.

Maya blue paint has been discovered to be a hybrid material with a nanostructure. The composition of the material, which exhibits color and resistance to acids and biocorrosion, remains unclear. However, analyses of genuine samples from Jaina Island indicate that the material comprises needle-shaped palygorskite crystals that create a superlattice with a 1.4 nm period. The intercalates of an amorphous silicate substrate contain metal (Mg) nanoparticles. The synthetic samples demonstrate that the presence of both nanoparticles and superlattice is necessary to achieve the aesthetically pleasing blue color tone.

Nanophase engineering is increasingly applied to a variety of inorganic and organic materials, enabling the manipulation of their mechanical, catalytic, electric, magnetic, optical, and electronic properties [16].

Nanophase or cluster-assembled materials are typically produced by creating small clusters that are subsequently fused into a bulk-like material or embedded into a compact liquid or solid matrix. Nanophase silicon possesses distinct physical and electronic properties that can be utilized in the development of novel devices through integration with macroscopic semiconductor processes. Doping ordinary glass with quantized semiconductor colloids can result in a high-performance optical medium that has potential applications in optical computing [16].

Nanomaterials are very small and have a maximum size of 100 nm or less. Nanomaterials can have nanoscales in one (i.e. surface films) dimension, two (i.e. beams or fibers) dimensions, or three (i.e. particles) dimensions. They can exist with circular, tubular, and irregular shapes in single fuse, aggregate, or agglomerated forms or even alone. Common kinds of nanomaterial comprise dendrimers, fullerenes, and quantum dots nanotubes.

Nanomaterials exhibit distinct physical and chemical properties compared to conventional chemicals, such as carbon nanotubes, silver nanoparticles, carbon nanoparticles, fullerenes, and silica photocatalysts. They find applications in the field of nanotechnology. Siegel's classification of nanostructured materials includes zero-dimensional, one-dimensional, two-dimensional, and three-dimensional structures [16].

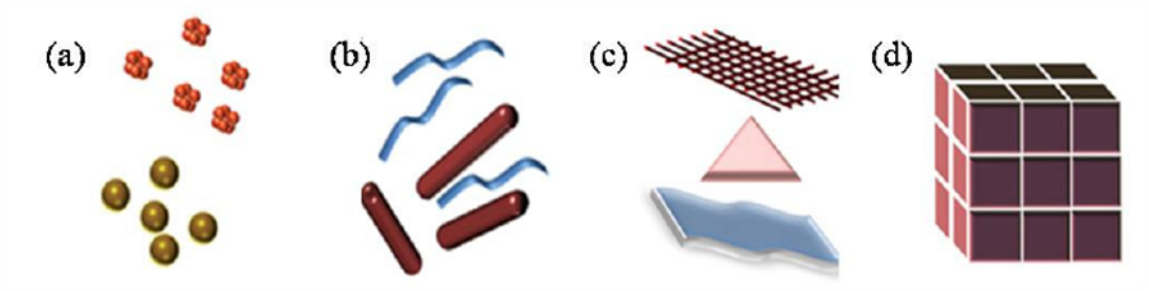

Fig. 2.2 Nanomaterials classified into four categories: (a) 0D spheres and clusters, (b) 1D nanofibers, nanowires, and nanorods, (c) 2D nanofilms, nanoplates, and networks, and (d) 3D nanomaterials [16]

2.2 What is Nanotechnology

The term "nano" originates from the Greek word for small. Nanotechnology, which involves scientific manipulation at the atomic level using specialized tools, has gained prominence as a field of study over the last thirty years.

The term "nanotechnology" was first introduced by Norio Taniguchi in Japan in 1974. According to Norio Taniguchi, nanotechnology involves the manipulation of materials at the atomic or molecular level through processes such as separation, standardization, and distortion. Nanotechnology is a broad field that explores many pieces of evidence about the properties and structures of materials [21].

Nanotechnologies have created considerable science and engineering interest in the past years, and they are necessarily interdisciplinary. Nanomaterials are present in all parts of the world and have been environmentally friendly since the formation of our earth some 4.5 billion years ago [22].

Nanotechnology is the knowledge and control of the material at the scale of 1 to 100 nanometers (one billionth of a meter is a nanometer), where special phenomena allow for new applications.

Nanotechnology includes the imaging, calculation, modeling, and manipulation of matter on this scale. Nanoscale research, engineering, and technology are included. The material's biological, physical, and chemical properties could vary fundamentally and have valuable properties of single atoms and molecules or bulk matter. Research and development in nanotechnology are directed at understanding and producing improved materials and systems that fulfill these novel needs [23].

Human creativity and visions also lead to new science and technology. From these visions, nanotechnology, a boundary of the 21st century, came in. While human-made nanoparticles have existed throughout the whole of human history, they have increased dramatically since the industrial revolution [24].

Studying nanoparticles is not new. Richard Zsigmondy, recipient of the Nobel Prize in Chemistry in 1925, first put forward the idea of a "nanometer". He was the first to quantify the particle size, such as golden colloids, with a microscope that coined the term nanometer specifically for characteristics of particle size.

The new nanotechnology had been the brainchild of Richard Feynman in 1959, the Nobel Prize winner for Physics in 1965. He gave a talk entitled “There’s Plenty of Room at the Bottom” during the American Physical Society Meeting in Caltech in 1959, in which he introduced a principle of atomic manipulation. This new concept showed new ways of thinking and the theories of Feynman have proved to be correct. This is why he is regarded as the founder of modern nanotechnology [24].

Almost fifteen years on from Feynman's lecture, Norio Taniguchi, a Japanese scientist was the first person to identify semiconductor processes in order to use nanotechnology.

The Nanotechnology's Golden Age started in the 1980s when Smalley, Kroto, and Curl discovered fullerenes then Eric Drexler from Massachusetts Institute of Technology (MIT) used the concept from

Feynman's "There is Plenty of Room at the Bottom" and Taniguchi's concept nanotechnology from his book in 1986, "Engines of Creation: The Coming Era of Nanotechnology" [24].

Drexler suggested a nanoscale concept "assembler" that could create a copy of the arbitrary complexity of itself and of other objects. The nanotechnology vision of Drexler is known as "molecular nanotechnology". The study of nanotechnology was further advanced when another Japanese scientist, Iijima, developed carbon nanotubes. The interest in the new fields of nanoscience and nanotechnology grew at the beginning of the 21st century. The stature of Feynman and his concept of atomic material manipulation have played a major role in shaping national science priorities in the United States. During the speech at Caltech on January 21, 2000, President Bill Clinton advocated for funding research into this new technology. In 2003, President George W. Bush signed the 21st Century Nanotechnology Act of Research and Development [24].

Nanotechnology research became a national priority through legislation and the created National Nanotechnology Initiative (NNI). Today the National Science and Technology Council (NSTC) of the President's Cabinet level operates the NNI and its Committee on Technology [24].

2.3 Carbon Nanotubes (CNTs)

CNTs can be defined as nanostructures derived from rolling graphene sheets and having different physical and chemical properties [25]. CNTs are cylinder-shaped large molecules composed of a hybridized carbon atom hexagonal system that is created by rolling up a single graphene sheet known as single-walled carbon nanotubes, SWCNTs or by rolling up several graphene sheets known as multiwalled carbon nanotubes, MWCNTs and were first described in 1991 [26] Fig. 2.3.

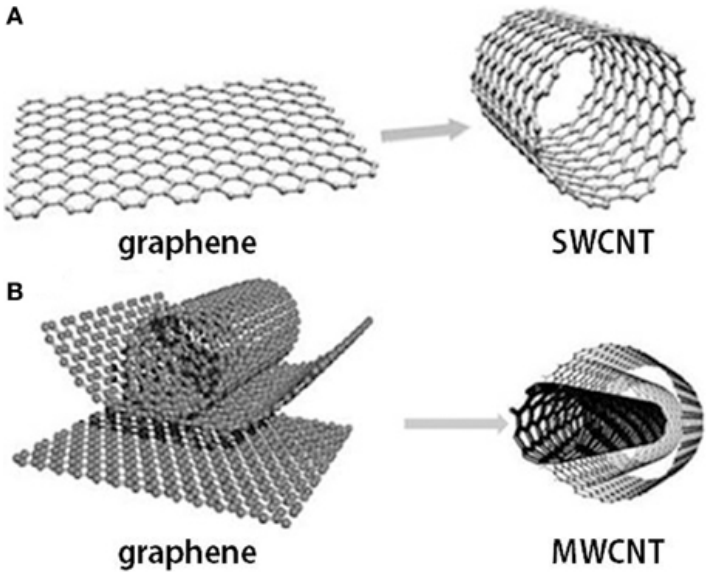

Fig. 2.3. Graphene and carbon nanotubes as (A) single-wall carbon nanotube (SWCNT) and (B) multi-wall carbon nanotube (MWCNT) structures [27]

Carbon is a chemical element, which has an atomic number 6 with six electrons occupying an atomic orbital as 1 s^2, 2 s^2, and $2p^2$. Carbon can be hybridized in sp, sp^2, or sp^3 forms. Discoveries of extremely constant nanometer scale sp^2 carbon-bonded materials like graphene [27], fullerenes [28], and CNTs [29] have encouraged further investigation and research in this field.

Graphene is the source of much of the physical properties of carbon nanotubes. Carbon atoms are arranged densely in graphene in a regular sp^2-bonded atomic-scale honeycomb (hexagonal) pattern, which is a basic structure for other sp^2 carbon-bonded materials (allotropes) like CNTs and fullerenes.

Numerous properties and applications of CNTs are available which completely benefit from their specific properties such as, thermal conductivity, mechanical strength, electrical and aspect ratio [30].

The practical significance of the conductivity of CNTs was substantial. CNTs with specific N and M structural parameters exhibit high conductivity, suggesting their metallic nature. The conductivity of CNTs is dependent on their chirality and diameter. CNTs exhibit either metallic or semiconducting properties based on their electrical behavior.

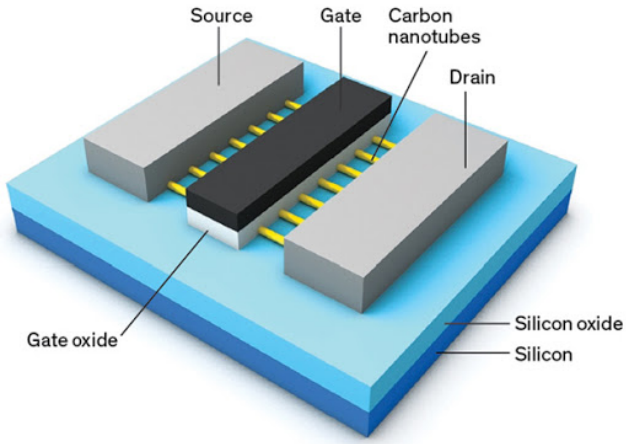

Fig. 2.4 CNTs electrical conductivity [31]

The conductivity of MWCNTs is intricate. Some armchair-structured CNTs exhibit superior conductivity compared to other metallic CNTs. In addition, intrawall reactions in MWCNTs have been observed to cause a non-uniform redistribution of current across individual tubes. Uniform current is observed across various segments of metallic SWCNTs. The transport current of semi-conducting SWCNT ropes exhibits abrupt changes at different locations on the CNTs [30].

The electrical properties of SWCNT ropes were characterized by electrode placement at various locations along the nanotubes. Specifically, the conductivity and resistivity were measured. The resistivity of SWCNT ropes was approximately 10^{-4} ohm.cm at a temperature of 27°C. SWCNT ropes exhibit the highest conductivity among all known carbon fibers. The achieved current density was 107 A/cm^2, but SWCNT ropes have the potential to sustain stable current densities as high as 1013 A/cm^2.

Individual SWCNTs may exhibit defects, as reported. These defects fortuitously enable SWCNTs to function as transistors. The connection of CNTs can result in the creation of transistor-like structures. A nanotube possessing a junction between a straight metallic segment and a chiral semiconducting segment exhibits rectifying diode behavior, thereby functioning as a half-transistor within a solitary molecule. Recent reports indicate that SWCNTs can function as high-speed electrical signal interconnects on semi-conducting devices, with speeds of up to 10 GHz [30].

The carbon atoms in a graphene sheet of graphite are arranged in a planar honeycomb lattice, with each atom bonded to three adjacent atoms via strong chemical bonds. Graphite exhibits a high basal-plane elastic modulus due to its strong interatomic bonds. CNTs are anticipated to be the ultimate high-strength fibers. SWCNTs exhibit high stiffness and exceptional resistance to physical damage. Applying pressure to the nanotube's tip induces bending while preserving its structural integrity. So that upon removal of the force, the tip reverts to its initial state. CNTs are highly valuable as probe tips for high-resolution scanning probe microscopy due to this property of theirs [30].

Quantifying these effects has proven challenging, and a precise numerical value remains elusive. The application of an atomic force microscope (AFM) can displace the unanchored ends of a freestanding nanotube from their equilibrium position, allowing for the measurement of the necessary force. Young's modulus of SWCNT is currently estimated at approximately 1 Tera Pascal, although there is some controversy surrounding this value. Some studies have reported a higher value of up to 1.8 TPa.

Several higher values have also been reported. The observed disparities may stem from variations in the experimental measurement methodologies. Previous studies have demonstrated that Young's modulus is contingent upon the dimensions and chirality of the SWCNT, with values ranging between 1.22 TPa and 1.26 TPa. A value of 1.09 TPa has been computed for a nanotube of a generic nature. Although various MWCNTs have been studied, it has been observed that the modulus measurements obtained through AFM techniques are not significantly influenced by the diameter. The authors contend that the MWCNTs' modulus is linked to the level of disorder in their walls. The outermost layers of MWCNTs are the first to break, as reported in reference [30].

Recent research conducted at the University of Pennsylvania suggests that CNTs exhibit superior thermal conductivity compared to all other known materials. Ultra-small SWCNTs have demonstrated superconductivity at temperatures below 20ºK. Exotic strands, known for their exceptional strength and capacity to exhibit the electrical properties of semiconductors or perfect metals, may potentially serve as miniature heat conduits in various materials and devices, according to research.

The exceptional strength and stiffness of in-plane graphitic C-C bonds are due to their strong resistance against axial strains. The SWCNT exhibits a nearly negligible thermal expansion within the plane, but a significant expansion between planes. This suggests a robust in-plane connection and substantial flexibility in response to nonaxial strains. CNTs have been suggested for various applications, including nanoscale molecular electronics, sensing and actuating devices, and reinforcing additive fibers in functional composite materials [30].

Recent experiments have been conducted on the preparation and mechanical characterization of CNT-polymer composites. The measurements indicate slight improvements in the strength properties of polymer matrixes with embedded CNTs in comparison to those without. Initial experiments and simulations indicate that CNTs exhibit exceptionally high thermal conductivity. Nanotube reinforcements in polymeric materials are anticipated to considerably enhance the thermal and thermo-mechanical characteristics of composites [30].

Field emission occurs when electrons tunnel from a metal tip into a vacuum under the influence of a strong electric field. The favorable field emission properties of CNTs can be attributed to their small diameter and high aspect ratio. The sharpness of supported CNTs results in the development of a strong electric field at their free end, even at moderate voltages.

De Heer et al. at EPFL reported this observation in 1995. The author promptly recognized the potential superiority of field emitters over traditional electron sources and their potential widespread use in various applications, particularly in flat-panel displays. After only five years, it is remarkable that Samsung actually realized a very bright color display, which will be shortly commercialized using this technology.

CNTs are conductive additives with a high aspect ratio that can be used in various types of plastics. The high aspect ratio of CNTs allows for achieving the same electrical conductivity with a lower loading (concentration) of CNTs compared to other conductive additives. The reduced loading of the polymer resins retains their toughness, particularly at low temperatures, while also preserving the essential performance characteristics of the matrix resin. CNTs are effective in enhancing the electrical conductivity of plastics. The high aspect ratio of these materials, approximately 1000:1, results in lower electrical conductivity loadings compared to traditional additives like carbon black, chopped carbon fiber, or stainless steel fiber [30].

2.4 Structure of Carbon Nanotubes

The structure of CNTs consists of an enrolled cylindrical graphitic sheet (called graphene) rolled up into a seamless cylinder with a diameter in the order of a nanometer. It is understood that CNTs are the material lying in between fullerenes and graphite as a quite new member of carbon allotropes [32].

CNTs are hollow tubular channels, formed either by one wall (SWCNT) or several walls (MWCNTs), of rolled graphene sheets [33, 34].

They have thus far been receiving an ever-increasing scientific and industrial interest due to their exceptional physical and chemical properties that render them suitable for numerous potential applications ranging from living matter structure manipulation to nanometer-sized computer circuits and composites.

CNTs exhibit great mechanical properties along with extremely high aspect ratios (length-to-diameter ratio) ranging from 30 to more than many thousand, in fact, because of their size (ranging from 1 nm to tens of nm) and aspect ratios, CNTs can be distributed in a much finer scale than common fibers.

However, the properties and dimensions of CNTs strongly depend on the deposition parameters and the nature of the synthesis method, i.e., arc discharge, laser ablation, or chemical vapor deposition (CVD). From the perspective of a commercial application, the CVD technique is the only one that can offer a path toward low-cost and large-scale production [34].

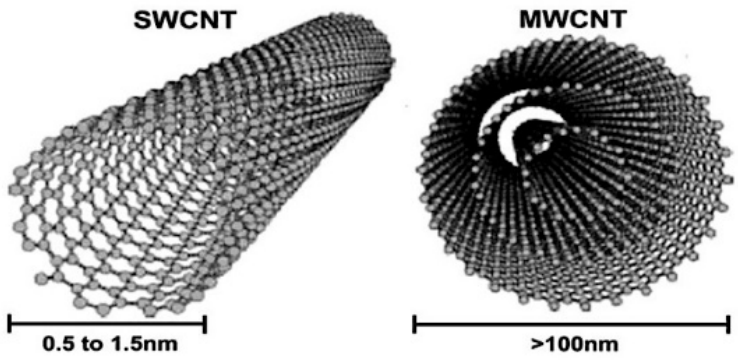

Fig. 2.5 Single-walled (SWCNT) and multi-walled (MWCNTs) carbon nanotubes [35]

2.5 Methods of Carbon Nanotube Growth

Synthesizing CNTs requires a carbon source, an energy source, and in most cases, a catalyst. Three main methods share this principle, cited below in decreasing order of importance in terms of overall contemporary production capacity. Others do exist but they are miscellaneous and do not contribute significantly in this regard (the template-based method will, however, also be cited later):

1) The catalytic chemical vapor deposition method (CCVD) and the variety of related methods, for example, plasma-enhanced, radiofrequency enhanced, fluidized bed, spray pyrolysis, and so on;
2) The electric arc plasma method;
3) The pulsed laser vaporization method, which is now abandoned when preparing CNTs for commercial purposes [36].

Initially, high-temperature methods like arc discharge or laser ablation were employed for the synthesis of CNTs. However, low-temperature chemical vapor deposition (CVD) techniques (<800 ºC)

have now superseded these methods due to their ability to precisely regulate the orientation, alignment, length, diameter, purity, and density of CNTs. The majority of these techniques necessitate the use of auxiliary gases and a vacuum. Gas-phase techniques are appropriate for industrial-scale synthesis methods and applications that require significant amounts of nanotubes, such as composite materials. This is due to their volumetric nature, which makes them economically feasible. Gas-phase synthesis methods have drawbacks such as low catalyst yields, short catalyst lifetimes, and low catalyst number density [25].

CNTs preparation results in the production of impurities, the nature and quantity of which are contingent upon the employed methodology. The described techniques produce powders with a low concentration of CNTs and other carbon-based particles, such as nanocrystalline graphite, amorphous carbon, fullerenes, and metal catalysts (typically Fe, Co, Mo, or Ni) used in the synthesis process. The presence of impurities hinders the desired properties of CNTs and poses challenges to their characterization and practical use. One of the primary challenges in this field is the creation of effective and uncomplicated purification techniques. The prevalent purification techniques involve acid treatment of synthesized CNTs [25].

CNTs can be synthesized using arc discharge methods at temperatures exceeding 1700 ºC, which leads to CNTs with fewer structural defects in comparison to other methods. The electric arc method is a widely used and simple approach for CNT synthesis, initially utilized for C60 fullerene production. MWCNTs were first discovered by Iijima in 1991 via arc-discharge evaporation [26].

SWCNTs were intentionally produced in 1993. This method utilized an electric arc between graphite electrodes to generate high temperatures that cause carbon sublimation. MWCNTs or SWCNTs can result from the cooling and condensation of carbon vapors. MWCNTs are typically produced without catalyst particles between graphite electrodes, while SWCNTs can be synthesized by introducing Fe, Ni, or Co catalysts. Metal powder can be packed into an anode hole to introduce catalysts. The metal and graphite undergoes consumption, resulting in the formation of catalyst particles that promote the production of small-diameter SWCNTs.

The purity and yield of MWCNTs were found to be highly dependent on the gas pressure within the reaction vessel. Various atmospheres significantly impact the ultimate morphology of CNTs. DC arc discharge was employed with graphite electrodes in helium and methane. Thick nanotubes adorned with numerous carbon nanoparticles were produced through evaporation in the presence of high-pressure methane gas and a high arc current. Thin and long MWCNTs were synthesized using a 6 mm diameter anode, a methane gas pressure of 50 Torr, and an arc current of 20 A. The study revealed that CNT morphology varied more significantly during evaporation in methane gas compared to helium gas.

SWCNTs can be synthesized with the aid of transition metal catalysts. Their growth in arc discharge involves a composite anode and is typically carried out in a hydrogen or argon atmosphere. The anode is typically composed of graphite and metal, including but not limited to Ni, Fe, Co, Pd, Ag, and Pt. Alternatively, it may consist of mixtures of Co, Fe, and Ni with other elements, such as Co-Ni, Fe-Ni, Fe-No, Co-Cu, Ni-Cu, and Ni-Ti. The catalyst is crucial for the process yield. Maintaining a constant gap distance between the electrodes is necessary for achieving high process efficiency. This ensures stable current density and anode consumption rate. Undesirable byproducts, including MWCNTs and fullerenes, are also typically generated during this procedure [25].

The laser ablation method uses a pulsed and continuous laser to vaporize a graphite target in an oven, which is filled with an inert helium or argon gas to keep pressure. The laser ablation is similar to the arc discharge, both taking advantage of the very high temperature generated, with the similar optimum background gas and catalyst mix observed. The very similar reaction conditions are needed to indicate that the reactions probably occur with the same mechanism for both the laser ablation and electric arc methods. SWCNT was prepared by continuous wave carbon dioxide laser ablation without applying

additional heat to the target. They found that the average diameter of SWCNT produced by carbon dioxide laser increased with increasing laser power [25, 37].

Pandey et al. [25] and Stramel et al. [38] separately used commercial MWCNTs and MWCNTs-polystyrene targets (PSNTs) to deposit composite thin films onto silicon substrates through a Programmable logic device (PLD) with a pulsed, diode-pumped, Tm laser. The hypothesis is that the use of holmium and thulium doping in LuLF laser, a laser host material LuLF (LuLiF4), will result in the production of laser light at approximately 2 mm. The utilization of pure MWCNT targets results in a thin film comprising superior quality MWCNTs in comparison to PSNT targets. Thin films of MWCNTs were deposited through PLD techniques using the Nd: YAG laser to ablate commercially available polystyrene-nanotube pellets onto alumina substrates. This was reported in [25].

Arc discharge and laser ablation are plasma-based synthesis methods. Thermal synthesis employs only thermal energy, and the reaction hot zone temperature does not exceed 1200 ºC, even in plasma-enhanced CVD. CNTs can be synthesized via catalytic chemical vapor deposition using carbon feedstock and active catalysts like Fe, Ni, and Co. Mo and Ru can promote the activity of feedstock for CNT formation. Thermal synthesis includes various chemical vapor deposition methods. Chemical Vapor Deposition, flame synthesis and Carbon monoxide synthesis are some of the processes utilized [25, 39].

Catalytic chemical vapor deposition (CVD) involves heating gaseous carbon-containing molecules using plasma or a resistively heated coil, after introducing a carbon source into the gas phase. Heat is employed to induce molecular cracking, resulting in the formation of reactive atomic carbon. Transition metals, particularly Fe, Co, or Ni, are the commonly employed catalysts. The catalysts are occasionally doped with additional metals, such as Au. Hydrocarbons, particularly methane, ethane, ethylene, acetylene, xylene, their mixtures, isobutane, and ethanol, are the preferred carbon sources in CVD. The efficient growth of CNTs from gaseous carbon sources is highly dependent on the concentration and reactivity of gas phase intermediates, which are produced during hydrocarbon decomposition along with reactive species and free radicals.

The studies demonstrated that growth efficiency is significantly influenced by the concentration and reactivity of gas-phase intermediates generated through intricate gas-phase reactions. Gas phase production of efficient intermediates capable of chemisorption or physisorption on the catalyst surface is expected to initiate CNT growth. The growth kinetics are influenced by the interplay and competition between gas-phase and surface reactions [25].

Plasma-enhanced chemical vapor deposition (PECVD) systems have been utilized for the synthesis of SWCNTs and MWCNTs. PECVD is a broad term that includes various synthesis methods. PECVD can be either direct or remote. These systems are suitable for producing MWCNTs field emitter towers and certain SWCNTs. A remote PECVD technique can be utilized for the synthesis of both MWCNTs and SWCNTs. The SWCNTs were synthesized via the direct PECVD method using a CH_4-H_2 gas mixture at 500 mT, with the substrate heated to 550-850 ºC and an externally applied magnetic field, while applying 900 W of plasma power. The PECVD technique employs a high-frequency voltage to induce a glow discharge within a chamber or reaction furnace, utilizing both electrodes. A substrate is positioned on the electrode that is grounded. The uniform film is formed by supplying the reaction gas from the opposite plate. Catalytic metals, including Fe, Ni, and Co, are deposited on a substrate of Si, SiO_2, or glass through thermal CVD or sputtering techniques. PECVD and HWCVD represent a hybrid of plasma-based growth and CVD synthesis. PECVD synthesis utilizes feedstock gases like CH_4 and CO as a source of carbon, eliminating the requirement for a solid graphite source, unlike arc discharge, laser ablation, and solar furnace. Argon-assisted plasma is utilized to decompose feedstock gases into reactive carbon species such as C2, CH, and CxHy, enabling growth at low pressure and temperature [25, 39].

2.6 Carbon Nanotubes Applications

Nanotechnology is one of the latest and most developed technologies, presenting many advantages and benefits for new materials with significantly improved properties. Nanotechnology can be used in different applications in various fields, including nano-medicine, energy, the environment, and in sensors. Although the fields of nanotechnology are vast and new materials come into use regularly the potential of CNTs is the most promising.

Since their discovery by Iijima in 1991, CNTs have been the most rapidly developing nanomaterials in the field of nanotechnology due to their various realized and potential applications. Many investigators and researchers have dedicated much effort to the creation of new properties and to expanding the number of new applications in varied fields, from materials science, electronics, medicine and energy storage, with many studies concentrating on nanotechnology and the usage of CNTs as fillers. More attractive applications of CNTs can be attained by using them for applications that need conductivity and a strong potential for absorption and for production of composites of high strength, energy conversion devices, fuel cells, field-emission devices, hydrogen storage devices, and semiconductor devices. The use of CNTs for wastewater treatment is a rapidly expanding area of research in the field of adsorption. Its high cost and non-renewable characteristics are the key problems with CNTs.

Currently, there are ongoing efforts to develop cost-effective preparation methods for CNTs. The article elaborates on the significant and potential uses of CNTs, as outlined in [21].

2.6.1 Carbon Nanotubes as Fillers

CNTs are widely utilized as fillers in various materials to produce nanocomposites, representing a highly advanced area of nanotechnology. Researchers in nanocomposites have utilized CNTs as fillers. The primary objective of integrating CNTs into various polymeric and other materials is to enhance their properties. This results in enhanced mechanical, electrical, and thermal properties that approach ideal levels. Garcia-Gutierrez et al. [40] produced PBT/SWCNT nanocomposites through melt processing and injection molding. Their findings indicate that SWCNTs influence polymer orientation under shear and also act as a template for PBT crystallization. Soichia et al. [41] observed an increase in tensile modulus and yield strength upon the incorporation of SWCNTs in a SWCNTs/polyimide nanocomposite [21].

Improved dispersion led to enhanced mechanical properties of polyimide. Bhattacharyya et al. [42] produced SMA-encapsulated SWCNTs with a PA12 matrix using a conical twin-screw extruder through melt-mixing. Encapsulation through SMA copolymer improves SWCNT dispersion and enhances interfacial adhesion between PA12 and SMA-modified SWCNT. This results in improved mechanical characteristics of the resultant product.

MWCNT/nylon nanocomposites were synthesized through in situ bulk polymerization by Saeed and Park [43]. The study examined the properties of pristine and acid-treated MWCNTs, which were utilized as reinforcing agents in nylon nanocomposites. The properties analyzed included mechanical, thermal, electrical, and rheological characteristics, as well as structural morphology and crystallization temperature. The properties of both types of nanocomposites were compared. The presence of functional groups on amino-modified multi-walled carbon nanotubes (A-MWCNTs) allows for better dispersion in nylon compared to P-MWCNTs, as concluded. The increase in the MWCNTs to nylon ratio resulted in an increase in the crystallization temperature. Prashantha et al. [44] investigated the rheological, mechanical, and morphological properties of MWCNTs/PP and MWCNTs/PP-g-MA nanocomposites with varying MWCNT compositions. The nanocomposites were prepared using MWCNTs and polypropylene or polypropylene-grafted maleic anhydride, and analyzed using multiple techniques. The authors observed superior dispersion of MWCNTs in PP-g-MA in comparison to PP. They also noted that MWCNTs and

PP-g-MA exhibit strong interfacial adhesion, resulting in high mechanical properties and an improved rheological percolation threshold, as opposed to MWCNTs/PP. PA66 and F-MWVNTs were fabricated by Zhang et al. [45].

A-MWCNTs were utilized in the manufacturing procedure. The dispersion of A-MWCNTs was enhanced in formic acid (HCOOH) after PA66 functionalization. The authors observed superior dispersion of MWCNTs in PP-g-MA in comparison to PP. They also noted that MWCNTs and PP-g-MA exhibit robust adhesion and interfacial strength, resulting in high mechanical properties and an enhanced rheological percolation threshold, as opposed to MWCNTs/PP. PA66 and F-MWCNTs were fabricated by Zhang et al. [45]. The fabrication process utilized A-MWCNTs, and their dispersion was enhanced by formic acid (HCOOH) after PA66 functionalization. A-MWCNTs were surface-grafted with PA66 materials. The study found that incorporating A-MWCNTs resulted in a decrease in the chain length of PA. Additionally, the thermal decomposition temperature of PA-MWCNTs was higher than that of pure PA66 composite, and the storage modulus was enhanced [21].

2.6.2 Field-Emission Sources

CNTs have potential applications as field emission sources in electronic devices. Application of potential between the CNT surface and anode enables this process. Electrons are emitted from CNT tips due to their curvature in the form of pentagons or oxidation. CNTs can be utilized to produce various electronic devices such as flat panel displays, intense light sources, bright lamps, and X-ray sources, based on this principle. CNTs exhibit good emission properties, however, nanocomposites containing CNTs demonstrate superior electron emission characteristics and are stable in vacuum conditions. CNTs offer numerous benefits as an electron emitters. The advantages of these components are extended lifetimes, sustained field emission, low emission thresholds, no requirement for ultra-high vacuum, and high current densities. Current densities up to 4 A/cm^2 have been achieved [21, 46].

2.6.3 Batteries (Lithium Ions Batteries)

Lithium (Li) possesses distinctive characteristics owing to its low electronegativity and high electron-donating capacity, rendering it a valuable element. Therefore, it is the optimal choice for producing batteries that are both lightweight and efficient. Despite its advantages, the high reactivity of lithium limits its applicability due to decreased efficiency. The problem can be resolved by intercalating Li ions within CNTs, utilizing their application. This facilitates the migration of Li+ ions from a graphitic anode to the cathode. A polyolefin separating medium is typically necessary to separate the anode and cathode. CNTs are expected to intercalate with Li and provide a theoretical storage capacity of 372 mAh/g. The Li+ intercalation and deintercalation rates control the charge and discharge phenomena in these batteries. Frackowiak and Beguin [47] demonstrated the applicability of CNTs in Li-ion batteries. The authors suggest that CNTs have the potential for a significant irreversible capacity. Li+ batteries' storage capacity and lifespan are being increased by a number of electronics businesses by using carbon nanofibers and nanotubes as electrodes [21].

2.6.4 Super Capacitors and Actuators

CNTs are suitable for electrochemical devices due to their extensive surface area and high electrical conductivity. High specific capacitances can be attained in individual cells of devices with 38 wt% H_2SO_4 electrolyte. The power densities of the cells surpassed 8,000 W/kg. Frackowiak and Beguin [47] conducted a comparable study and found that MWCNTs-polypyrrole composites achieved specific capacitances of 163 F/g. CNT supercapacitors are utilized in high-power and high-storage capacity

devices. According to [47], their power densities reach 20 kW/kg at energy densities of 7 Wh/kg. CNT-based supercapacitors have potential applications in hybrid electric vehicles for rapid acceleration and regenerative braking energy storage. Actuators are significant devices; however, their efficiency declines as the temperature rises. CNT-modified actuators have been prepared by various researchers. These operate at low voltages and high temperatures up to 350°C. The highest stress recorded in SWCNT actuators was 26 MPa. The that value was 100 times greater than that of natural muscle, indicating comparability [21].

2.6.5 Sensors

Sensors are widely utilized in various fields for detection purposes. CNTs can improve the effectiveness of biosensors and molecular sensors when attached to them. Wong et al. [48] demonstrated the ability to detect functional chemical groups on CNTs using chemical force microscopy techniques. Nanotube composite pellets can be utilized to create gas-sensitive sensors that are capable of detecting leaks in chemical plants. Collins et al. [49] observed significant fluctuations in the electrical resistance levels of their SWCNT samples, indicating the high sensitivity of SWCNTs to air and vacuum conditions. This finding is consistent with previous research in the field. The authors additionally stated that MWCNTs exhibit high sensitivity as sensors for NH_3, H_2O, CO_2, and CO. In 2002, microwave-resonant sensors with high sensitivity and fast response were developed for NH_3 detection, utilizing SWCNT or MWCNTs [50]. CNTs and their composites have potential applications as environmental pressure sensors, in addition to their gas-sensing capabilities. CNTs exhibit high sensitivity to liquid immersion or polymer embedding, causing slight deformation in the presence of various liquid media, as observed by Wood and Wagner [21, 51].

2.6.6 Gas and Hydrogen Storage

Due to their hollow cylindrical nature, CNTs can act as efficient gas and metal containers. It has been found that many important chemical species, such as metals, metal carbides, and oxides, can be introduced into CNT core by different methods, including chemical treatments, arc-discharge methods, solid-state reactions and electrochemical techniques. However, the major issues with these techniques are related to the fact that CNTs are not able to encapsulate gaseous substances. Recent studies have revealed that H_2 and Ar can be stored in SWCNTs [52, 53] and MWCNTs [54], respectively. Terrones et al. demonstrated experimentally that it is possible to introduce gaseous nitrogen inside MWCNTs using a single-step process. They also reported that MWCNTs can be loaded via the spray pyrolysis of ferrocene and benzylamine solutions. CNTs can store various chemical species, which is beneficial for developing fuel cells primarily for electric vehicle propulsion. Controversy surrounds the high-pressure storage of hydrogen. The hydrogen storage capacity of CNTs varies greatly between 0.1 to 66 wt %. [21]. Hirscher et al. [55] demonstrated that impurities from CNT synthesis methods may account for previously reported uptake levels of up to 7%. Density functional theory was employed to compute the H_2 storage capacity in CNTs from a theoretical perspective. Various mechanisms for hydrogen molecule adsorption on CNTs have been proposed, such as chemisorption, interstitial site adsorption, and nanotube array swelling.

Further experimentation and calculations are necessary to clarify whether CNTs are suitable for hydrogen storage, as the aforementioned situations suggest potential limitations. Tanaka et al. recently accomplished the adsorption of He, NH_3, N_2, and SF6 in both carbon nanotubes and carbon foams [21].

2.6.7 Scanning Probe Tips

Achieving greater imaging resolution requires improved scanning probe tips. When compared to earlier findings, using a MWCNTs-bound scanning probe can increase image resolution. The commercialization of these probes is now being done by Daiken Chemical Company and Seiko Instruments. Tips of chemically altered nanotubes are used as sensors to identify specific chemical and/or biological groups. These sensors are essential for finding unapproved or illegal substances. Nanotube tweezers can be fabricated by attaching two nanotubes to a probe tip, as determined by Kim and Lieber through experimentation. This tool functions based on the electrostatic interactions of two carbon cylinders. The aforementioned accomplishments demonstrate significant progress in the utilization of nanotubes in contemporary technologies. It is evident that additional advancements will be made in the foreseeable future [21].

2.6.8 Electronic Devices

CNTs are significant nanomaterials for enhancing the characteristics of electronic devices. Tans et al. [56] developed a three-terminal switchable device using SWCNT. The SWCNT exhibited semiconductor properties and was linked to metal nanoelectrodes. The low capacitance level demonstrated exceptional performance. Nanotubes pose a significant challenge in terms of manipulation. To address this issue, an alternative approach has been developed utilizing STM nanostructuring to regulate the length and electronic characteristics of individual nanotubes. AFM can be used to create bends and crossings in SWCNTs. The controlled application of voltages at the STM tips enables the cutting of nanotubes into shorter sections and the creation of small nanotube devices. The creation of molecular machinery, nanoscale circuits, and other nanoelectric materials could all benefit from the use of these devices. The current densities found in metals (105 A/cm^2) are much higher than those found in CNTs (109 A/cm^2), according to experimental findings.

In this study, field-effect transistors with high gain, a high on-off ratio, and room temperature operation are first demonstrated. The study showed that circuits with one, two, or three transistors were capable of carrying out digital logic operations. An inverter, a logic NOR, a static random-access memory cell, and an AC ring oscillator are examples. Crossed nanowire p-n junctions and junction arrays were made by a team from Harvard University, and they were configured as OR and NOR logic-gate architectures to show substantial amplification. In the near future, these results could be used to significantly advance computer technology.

CNTs have been shown to function as FETs. The study demonstrated that undamaged carbon nanotubes exhibit p-type transistor behavior, while doped nanotubes exhibit n-type behavior. Both types can be combined to produce voltage inverters. The study showed that p- and n-type nanotube FET arrays can produce logic rings, NOR and OR logic gates. The electronic properties are challenging to regulate due to the uncontrollable chirality of the tubes. The study revealed the feasibility of selectively removing the outer layers of MWCNTs produced through the arc-discharge method to achieve the desired electronic characteristics of the outer shell. Further research is necessary to explore and utilize controlled growth for achieving specific chiralities in electrical applications. A study was conducted to test the hypothesis that the electronic properties of CNTs can be applied to polymeric materials for specific electrical purposes. The results showed that this hypothesis was indeed valid [21].

2.6.9 Medical Applications

Due to the financial success of medical technology in gene therapy, cancer treatments, and cutting-edge treatments for life-threatening disorders, nanomedicine is currently the field characterized by the most rapid growth. CNTs have unique qualities that make it easier to explore brand-new areas of

nanomedicine. SWCNTs and MWCNTs have shown promise as less dangerous and more efficient substitutes for traditional medication delivery techniques. They facilitate the delivery of therapeutic drugs, vaccines, and nucleic acids to specific targets within cells by traversing membranes. They function as non-toxic vehicles that can enhance drug solubility, leading to improved efficacy and safety. Recent studies indicate a promising future for CNTs in medicine [21, 57].

2.7 Friction

The generally accepted definition nowadays is the resistance to motion which occurs when one solid body slides over another, [58] while the Kinetic friction is defined as a force that acts between moving surfaces. A body moving on a surface experiences a force in the opposite direction of its movement. The magnitude of the force will depend on the coefficient of kinetic friction between the two materials.

Friction is easily defined as the force that holds back a sliding object. The kinetic friction occurs in any moving system and it interferes in motion of two or more objects. The force acts in the opposite direction to the way an object wants to slide.

The friction is generally taken that the surfaces are in contact, directly (dry friction) or through a third body (lubricated friction). In the general case, however, it is justified to assume that friction, which is not itself yet defined, can take place between any two objects that are moving relative to each other when the motion has a sliding component (and find out afterward the values of proximity that make friction significant). Secondly, the "resistance" to tangential motion leads us to understand that friction is that part of the force, which is vectorially opposed to the said tangential relative motion. It definitely excludes the case in which that force would be in the same direction as sliding [59].

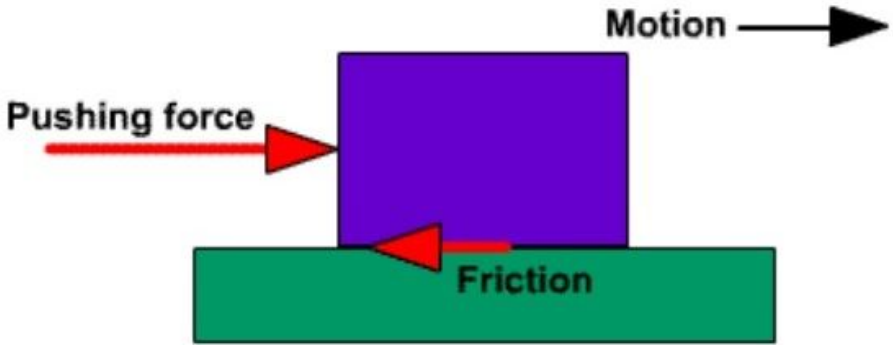

Fig. 2.6 A model for kinetic friction [59]

The symbol used to represent the coefficient of kinetic friction is μ_k, where μ is the Greek letter mu. The kinetic frictional force acting on an object is equal to the product of the coefficient of kinetic friction (μ_k) and the normal force exerted on the object. The unit of measurement is Newton (N). The equation for kinetic friction is expressed as [60]:

$$\boldsymbol{Force\ of\ Kinetic\ friction} = (\boldsymbol{coefficient\ of\ kinetic\ friction}) \times (\boldsymbol{normal\ force})$$

$$F_k = \mu_k \eta$$

Where,

- F_k = Force of Kinetic Friction
- μ_k = Coefficient of Kinetic Friction

- η = Normal Force (Greek Letter "eta")

Two primary categories of friction are outlined below.

- Static friction.
- Kinetic friction.

Static friction occurs between stationary objects. Viscosity is the term used to describe the frictional resistance between layers of a liquid in motion. When two solid objects are in motion, the resulting friction is referred to as kinetic or moving friction. Friction is a fraction of the perpendicular force between two bodies. The coefficient of friction is determined experimentally and represents the fraction of force required to initiate motion between two surfaces. The force is unaffected by the contact area and velocity of the objects. Static friction affects stationary objects. Friction is a resistive force that opposes motion between two objects that are in contact. All objects have microscopic irregularities on their surfaces. The surface roughness of two objects causes interlocking when in relative motion. In addition to mechanical forces, chemical bonding and electrical interactions also play a role.

The coefficient of friction, μ, is a numerical parameter that is frequently used to characterize friction. Experiments have shown that the friction force is frequently linearly proportional to the force of the body's normal load. This phenomenon is known as coulomb friction. The ratio of the tangential friction force (F_T) to the normal load force (F_N), often known as the coefficient of friction or friction coefficient, is a dimensionless scalar value [61].

$$\mu = \frac{F_T}{F_N}$$

A tangential force (F) is needed to move the upper body over the stationary counterface. As explained above, the ratio between these two forces is known as the coefficient of friction.

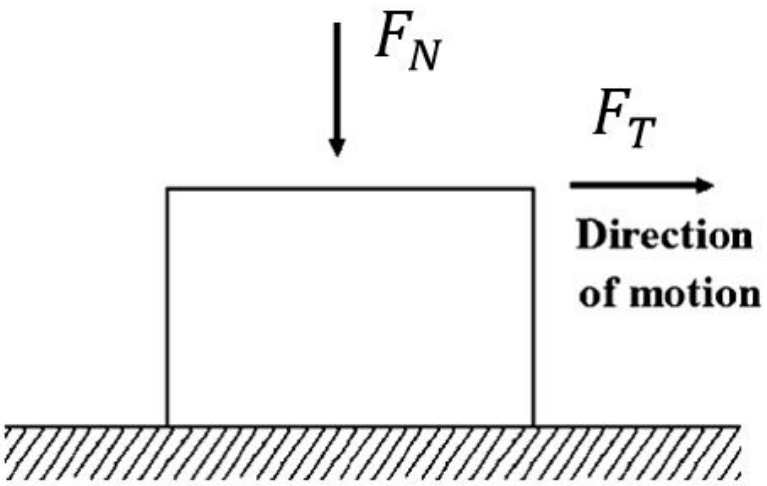

Fig. 2.7 Diagram depicting body sliding on a surface [61]

The friction force, also known as tangential force, is a resistive force that acts in the opposite direction of motion. The normal force is the resultant force that presses two parallel surfaces against each other, oriented perpendicularly to the surfaces. For a stationary mass on a level surface, the normal force is solely comprised of the gravitational weight force.

The friction force's maximum magnitude is equal to the product of the object's mass, acceleration due to gravity, and its coefficient of friction.

The materials used and the testing conditions alone can be used to define the coefficient of friction, which is independent of parameters like mass and volume. The coefficient of friction between a large aluminum block and steel is the same as that between a tiny aluminum block and steel. The normal force and the mass of the block both influence how much friction there is.

Calculations cannot be used to determine the coefficient of friction because it is an empirical characteristic that requires experimental measurement. The coefficient of friction has a wide range of values, from 0.001 in a rolling bearing that is barely loaded to over 10 when metals are sliding against one another in a vacuum. Common materials sliding in air typically have coefficients of friction between 0.1 and 1[61].

2.8 Adding Nanostructured Carbon to the Lubricating Oil

Numerous independent studies have reported that the addition of nanostructured carbon, particularly CNTs, to lubricating oil, can significantly decrease friction losses. However, this benefit is short-lived, due to the tendency of carbon nanotubes to re-agglomerate when added in large concentrations to the oil. It is important to note that most of these studies were conducted under idealized tribometer conditions [1, 4, 12, 15, 62-71].

Through various engine tests, it has been shown that CNTs exhibited favorable tribological behavior. In the beginning, MWCNTs were applied as a coating on the piston skirt, which resulted in a decrease of up to 16% in the overall friction of the engine being, tested [6, 72]. These results led to the hypothesis that during the engine operation, the CNTs gradually abraded from the piston side surface due to the process of friction and then dispersed in the lubricating oil, which delivered it to all of the engine components. This hypothesis was tested by a study in which CNTs were added to the lubricating oil, rather than using a coating on the pistons as in [8]. During the experiments, CNTs were added to the oil with a constant concentration of at least 0.5 wt%. However, the results showed a friction reduction of only up to 6%, which was lower than the reduction achieved in the previous experiments where the CNTs were introduced in situ during the abrasion process.

Based on these results, a hypothesis was redrawn that the critical factor for any tribological function is the dispersion quality of CNTs in lubricating oil. Regarding tribological mechanisms, it is important to note that if CNTs are not adequately dispersed, they will not be able to provide any benefits and cannot be classified as a nanomaterial addition [3]. Moreover, the existence of CNT agglomerates that are micrometer-sized appearing in the oil can have a negative impact by impeding the oil flow in the converging lubrication gap, leading to a decline in lubrication conditions [63, 64].

Kałużny et al. in their experiments, attempted to enhance lubricating oil by adding a 1% wt % concentration of CNTs. Despite using an ultrasound disintegrator for several hours, they were unable to achieve optimal dispersion. However, after a few minutes of engine operation, the CNTs were surprisingly well dispersed, causing the oil to turn into grease, making it difficult to pump.

It is significant to note that the grease produced by Kałużny et al. had a uniform CNT scaffold that resembled the typical fibrous matrix of lithium or calcium soap in commercial greases. This was due to the effective separation of CNT agglomerates caused by shear stress in the oil film, as observed by Kałużny et al. [8]. Other studies also support the positive outcome of shear stress mixing in liquids with high viscosity [73]. Therefore, the idea was to reduce the concentration of CNTs by weight added to the lubricating oil to inhibit the re-agglomeration process. Several authors have recently reported a trend of decreasing CNT concentrations in their research, these authors include those cited in the references [62, 74, 75].

The research was focused on the impact of the MWCNTs added to the lubricating oil on friction and vibrations generated in the actual operating conditions of machines assuming that, in the background, various CNT mechanisms in tribological processes occur simultaneously [63, 64, 68, 76-78].

2.9 Carbon Nanotubes Effect According to the Friction-Induced Vibrations Theory

Engine oil may have ordered molecular configurations inside its volume when subjected to high pressure and shear conditions. In a review paper that appeared in the journal Nature, Bushan et al. (1995) provided information on the shear-induced ordering transition. This phenomenon has been supported by experiments and simulations, as referenced in their work [3, 79].

Under specific pressure and entrainment speed conditions during shearing, the lubricant may undergo periodic solidification and melting. The mechanism involves the deformation of a solid lubricant under a specific stress limit, followed by rapid melting of the entire substance, and subsequent solidification of the lubricant. The process entails intermittent shifts of the lubricant molecules' systems between static and kinetic friction. Stick-slip vibrations are caused by friction and can be considered a specific type of vibration [3].

The features of stationary states in one-atom lubricants under external load and shear conditions were examined in [80-82]. Frictional vibrations in the system were absent because of the asymmetry. By preserving a straightforward asymmetry in the form of rough walls, it was possible to exclude frictional vibrations from the stationary state diagram [82]. The presence of particles that are larger or smaller than the original lubricant has been shown in [81] to drastically modify the stationary states diagram and obstruct the ordering of lubricant molecules. Instead of pure oil, a lubricated oil system with nanotubes exhibits less vibration, which may be explained by the nanotubes' ability to prevent ordered groupings of oil particles [3].

2.10 The Indirect Tribological Role of Carbon Nanotubes

Experimental investigations have demonstrated that when both zinc dialkyl dithiophosphates (ZDDPs) and MWCNTs were introduced simultaneously into a poly-alpha-olefin base oil, they exhibited a significant reduction in wear. This reduction was attributed to their ability to form an anti-wear (AW) layer on the metal surface, even when used as standalone additives.

For several decades, researchers have extensively investigated two mechanisms responsible for the formation of boundary layers by lubricating additives. These mechanisms have been extensively documented in numerous tribochemistry publications [83, 84], particularly in the context of carbon-based ternary films [65, 66, 68, 77], the first mechanism involves the adsorption, or more precisely, chemisorption of additive molecules onto lubricated surfaces, leading to the creation of an AW film. The second mechanism entails a chemical reaction between the additive and the material surface, resulting in the development of an extreme pressure (EP) layer.

Under specific conditions, carbon nanostructures exhibit a phenomenon known as superlubricity, which results in an almost complete elimination of friction between two sliding surfaces [85]. Carbon nanomaterials play a significant role in tribological processes, particularly in their interactions with oil molecules and additives, such as ionic liquids [86-89]. The majority of experiments conducted to gain insights into these tribological mechanisms involved characterizing lubricated surfaces. This characterization can only occur after the mechanical and thermal loads in tribometers have been released. Various analytical techniques were employed to study the enduring reaction products formed by lubricating additives deposited on the metal surfaces of friction components. Both the chemical

composition and the thickness of the deposited AW film are crucial parameters for safeguarding lubricated surfaces against direct contact, preventing wear or seizing.

ZDDPs are common oil additives found in nearly all commercial lubricating oils, enabling the effective formation of AW films. The mechanism underlying ZDDP film formation has been explained in numerous papers [90-92]. This mechanism can be significantly enhanced and modified in the presence of various chemical compounds added to the lubricating oil. Moreover, the addition of nanomaterials to oils may result in new synergistic interactions with ZDDPs [66, 93-95].

Kajdas et al. and Kulczycki et al. [78, 96] have proposed a mathematical model of heat-induced triboreactions and mechanical forces in papers. This model was developed to assess the efficacy of different lubricating additives and investigate the influence of base oil types on these additives' performance. The model assumes that lubricated metal surfaces act as solid tribocatalysts, releasing electrons during friction on individual asperities. These electrons facilitate an endothermic decomposition reaction of ZDDP molecules present in the oil, leading to the formation of durable deposits on the metal surface, i.e., the AW layer. In conventional oil, electrons emitted from the metal surface have limited penetration into the oil volume, limiting the efficiency of AW layer formation. However, the unique properties of MWCNTs, including their elongated shape and electrical conductivity, enable electrons emitted from rubbing surfaces to penetrate deeply into the oil volume, thereby expanding the area where ZDDP reactions occur. In this indirect mechanism of tribological action, MWCNTs actively support the formation of a robust AW film.

Until recently, it was hypothesized that carbon nanomaterials dispersed in the lubricating oil serve three primary functions:

1- Purely mechanical actions such as rolling and localized lifting of lubricated surfaces.
2- Promoting the formation of tribofilms on the lubricated metal surface (e.g., through CNT exfoliation).
3- Contributing to metal surface polishing and mending [22].

However, based on previous studies and the experiments presented in this research, it is evident that the role of MWCNTs in the friction process extends beyond these mechanisms alone.

2.11 Wear

Wear is the damaging, gradual removal or deformation of material at solid surfaces. Causes of wear can be mechanical (erosion) or chemical (corrosion). The study of wear and related processes is referred to as tribology.

Wear of metals occurs by plastic displacement of surface and near-surface material and by detachment of particles that form wear debris. The particle size may vary from millimeters to nanometers [97]. This process may occur by contact with other metals, nonmetallic solids, flowing liquids, solid particles or liquid droplets entrained in flowing gasses.

The wear rate is affected by factors such as type of loading (impact, static, dynamic), type of motion (sliding, rolling), temperature, and lubrication, in particular by the process of deposition and wearing out of the boundary lubrication layer [98]. Depending on the tribosystem, different wear types and wear mechanisms can be observed, of which the abrasion, adhesion, and corrosion being the three main types of wear. Each form has inherent problems and advantages that materials, lubrication, and surface finish can affect. Two different forms exist: two-body abrasion and three-body abrasion.

2.12 Diesel Engine

The diesel engine, named after Rudolf Diesel, is an internal combustion engine in which ignition of the fuel is caused by the elevated temperature of the air in the cylinder due to the mechanical compression (adiabatic compression), thus, the diesel engine is a so-called compression-ignition engine (CI engine). This contrasts with engines using spark plug-ignition of the air-fuel mixture, such as a petrol engine (gasoline engine) or a gas engine (using a gaseous fuel like natural gas or liquefied petroleum gas).

Diesel engines work by compressing only the air. This increases the air temperature inside the cylinder to such a high degree that atomized diesel fuel injected into the combustion chamber ignites spontaneously. With the fuel being injected into the air just before combustion, the dispersion of the fuel is uneven, this is called a heterogeneous air-fuel mixture. The torque a diesel engine produces is controlled by manipulating the air-fuel ratio (λ) instead of throttling the intake air, the diesel engine relies on altering the fuel dose that is injected, and the air-fuel ratio is usually kept high [99] Fig. 2.8.

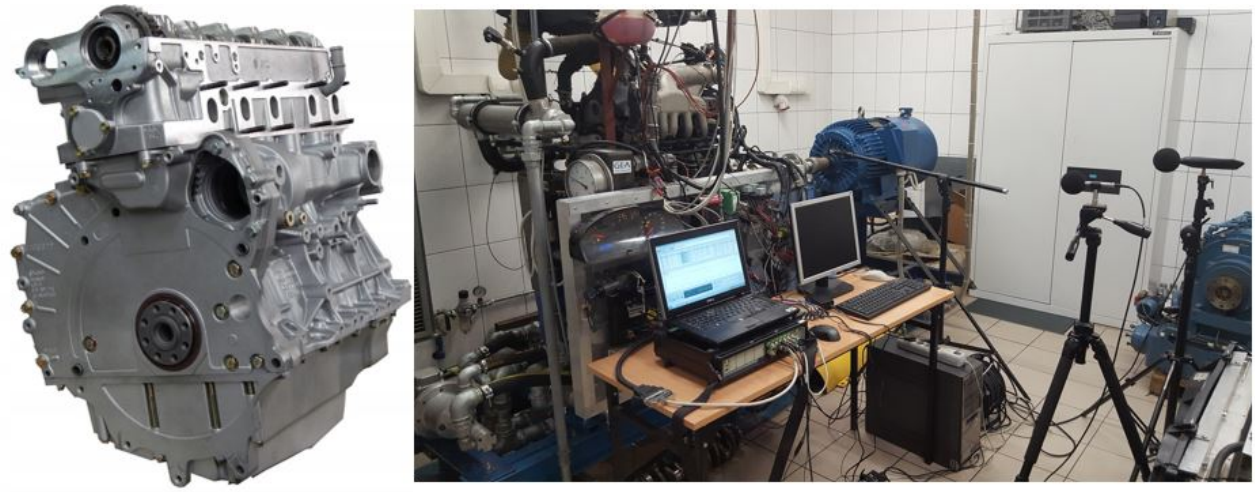

Fig. 2.8 Volkswagen 2.5 I R5 TDI diesel engine type AXD [100];
5-cylinder aluminum-block core engine on the left and fully equipped engine
running on the test bench during vibration tests for CNTs enriched oil – on the right

A medium or high-speed diesel engine has components and parts that include: the engine body, crankshaft, connecting rod, piston, cylinder liner, heat exchanger, cylinder cover, high-pressure fuel pipe and alarm, connecting rod bolt, supercharger, and fuel injection pump assembly.

The moving parts of an engine serve an important function turning heat energy into mechanical motion. The principal moving parts to be considered for the topic of this research are:

- The piston assembly and connecting rods,
- The crankshaft assembly,
- The camshaft assembly,
- Ball bearing.

The piston is the part of the engine that converts heat and pressure energy liberated by fuel combustion into mechanical works. Engine piston is the most complex component in vehicles equipped with combustion engines [101].

In every engine, piston plays an important role in working and producing results. Piston forms a guide and bearing for the small end of the connecting rod and also transmits the force of the explosion in the cylinder, to the crankshaft through the connecting rod. The piston is the single, most active and very critical component of the automotive engine [102].

In a reciprocating piston engine, the connecting rod connects the piston to the crankshaft. The small end attaches to the piston pin, gudgeon pin or wrist pin and the larger end connects to the journal bearing on the crank throw, running on replaceable bearing shells accessible via the connecting rod bolts, which hold the bearing "cap" onto the big end. Typically there is a pinhole bored through the bearing and the big end of the con rod so that pressurized lubricating motor oil squirts out onto the thrust side of the cylinder wall to lubricate the travel of the pistons and piston rings Fig. 2.9.

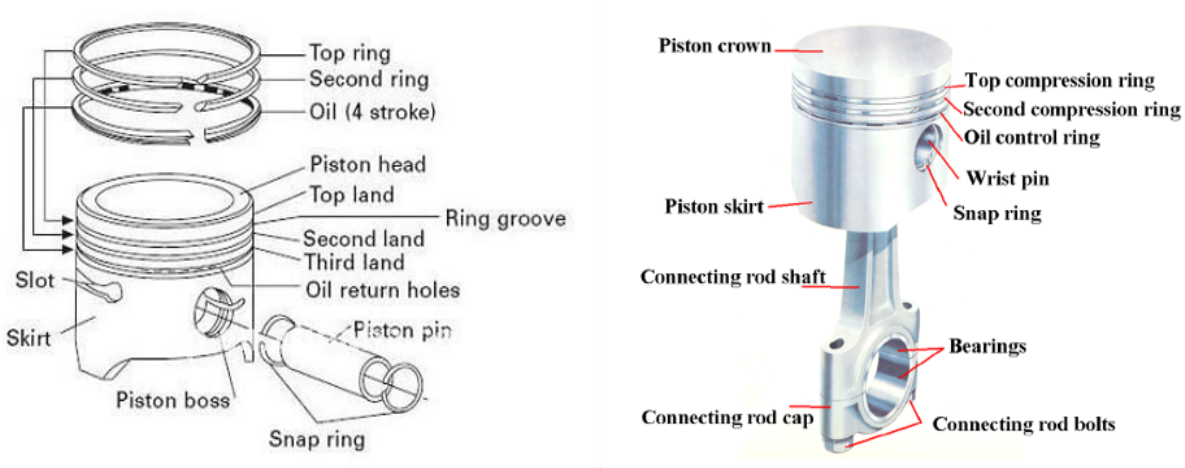

Fig. 2.9 The piston assembly and connecting rods [103]

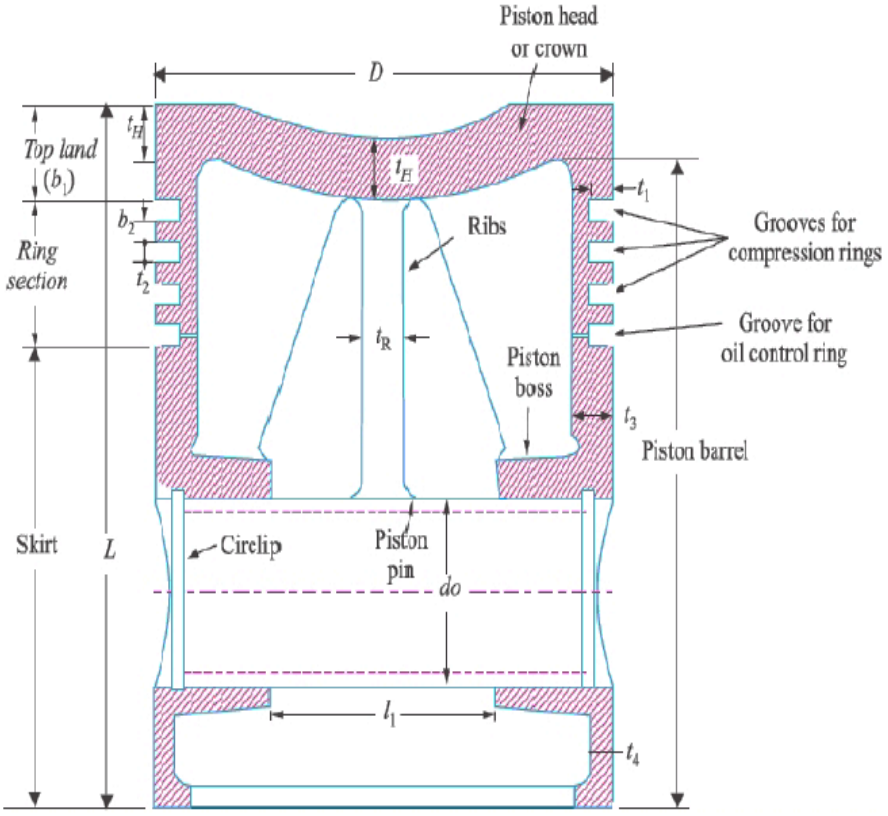

Fig. 2.10 Nomenclature of piston [104]

The design of the piston head or crown is based on two main considerations:
1. The component must possess sufficient strength to endure the force exerted by the explosion pressure within the engine cylinder and
2. Efficient heat dissipation to the cylinder walls is desirable.

The thickness of the piston head is determined based on its straining action. It is treated as a flat circular plate with uniform thickness, fixed at the outer edges, and subjected to a uniformly distributed load caused by gas pressure across the entire cross-section. Piston rings maintain the seal between the piston and cylinder bore through radial pressure. Typically, grey cast iron or alloy cast iron is utilized due to its favorable wear properties and ability to maintain spring characteristics under elevated temperatures. There are two types of piston rings:

1) Compression rings or pressure rings.
2) Oil control rings or oil scraper.

Compression rings, also known as pressure rings, are typically installed in the upper grooves of the piston. The number of rings may range from three to seven depending on the piston. The rings facilitate heat transfer from the piston to the cylinder liner and mitigate piston fluctuation resulting from side thrust. The oil control rings, also known as oil scrapers, are located beneath the compression rings. The rings facilitate the lubrication of the liner by enabling upward oil movement during the upstroke and simultaneously removing lubricating oil from the liner surface to reduce oil flow to the combustion chamber during downstroke.

Compression rings are typically rectangular in shape and have a diameter slightly larger than the cylinder bore. A section of the ring is removed to facilitate its insertion into the cylinder against the liner wall. To prevent buckling of the ring or other damage, one must ensure that the gap between the ends is large enough when the ring is cold to accommodate expansion at high temperatures without contact between the ends.

The lower section of the piston, situated beneath the ring area, is referred to as the **Piston skirt,** which serves as a support for the lateral force exerted by the connecting rod. The piston skirt length must limit the bearing pressure on the piston barrel caused by side thrust to 0.25 N/mm^2 for low-speed engines and 0.5 N/mm^2 for high-speed engines. The expansion stroke yields the highest thrust. The side thrust (R) of the cylinder liner is typically assumed to be 1/10 of the maximum gas load acting on the piston.

The piston pin, also known as the gudgeon pin or wrist pin, serves to link the piston and connecting rod. Typically, the pin is hollow and tapered inwardly, with the smallest inner diameter located at its center. The piston pin traverses the bosses on the interior of the piston skirt and the bush of the connecting rod's small end. To achieve a uniform distribution of pressure between the piston and cylinder liner and counteract the turning effect of friction, it is recommended that the center of the piston pin be positioned 0.02 D to 0.04 D above the center of the skirt. Piston pins are typically made of case-hardened steel alloys that contain nickel, chromium, molybdenum, or vanadium. These alloys have a tensile strength ranging from 710 MPa to 910 MPa [101].

The crankshaft is one of the critical components for the effective and precise working of the internal combustion engine [105] it is also one of the most critical elements because it is subject to very high loads, that cyclically vary in modulus and direction. The crankshaft has a complex geometry and its dimensions vary according to the type of application. It is often called crankshaft or, less frequently, "goose-neck" [106].

The crankshaft, sometimes casually abbreviated to crank, is the part of an engine that translates reciprocating linear piston motion into rotation. To convert the reciprocating motion into rotation, the crankshaft has "crank throws" or "crankpins", additional bearing surfaces whose axis is offset from that of the crank, to which the "big ends" of the connecting rods from each cylinder attach. It typically connects to a flywheel, to reduce the pulsation characteristic of the four-stroke cycle, and sometimes a torsional or vibrational damper at the opposite end, to reduce the torsion vibrations often caused along the length of

the crankshaft by the cylinders farthest from the output end acting on the torsional elasticity of the metal Fig. 2.11 [102].

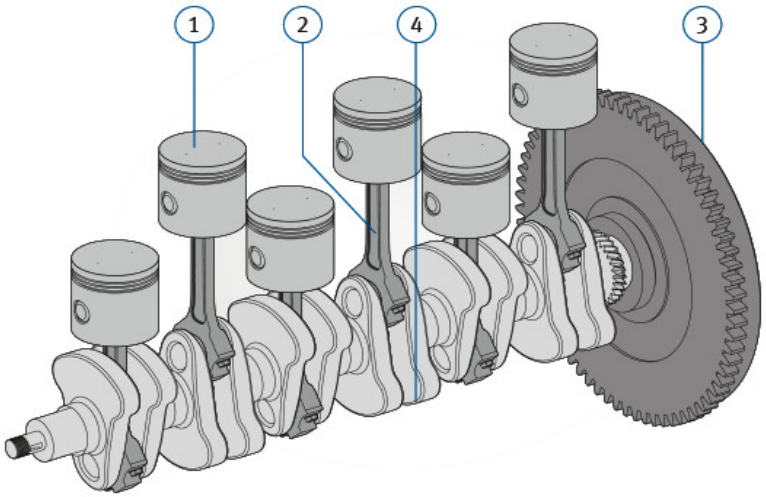

Fig. 2.11 1. Piston 2. Connecting rod 3. Flywheel 4. Crankshaft balance masses

The crankshaft is fitted with a series of pins of coaxial bench that lean, by the interposition of bearings, on suitable supports in the crankcase. In order to function properly, the bearings need a continuous and adequate flow of oil that realizes the minimum thickness of the meatus necessary for the sustenance of the pin and avoids contact between the working surfaces. The bearings are oil supplied directly from the lubrication circuit, while those of the connecting rod receive the oil by suitable channels, drilled in the crankshaft, which connects the crankshaft with those of the connecting rod Fig. 2.12.

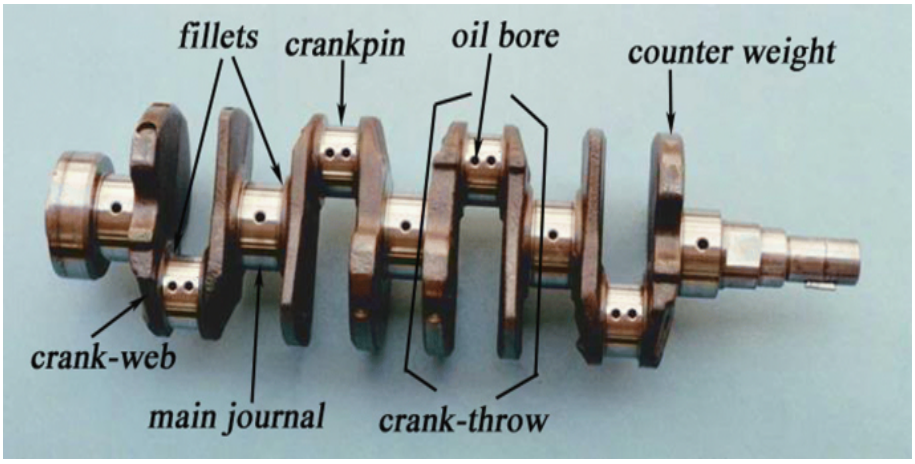

Fig. 2.12 Lubrication channels of the crankshaft

The design process for a crankshaft is non-linear. The procedure necessitates multiple iterations and analyses. The iterative process can be summarized as follows [107]:

1. Engine Configuration Data: The initial stage of crankshaft design involves identifying the engine for which the crankshaft is intended:

a) Bore and stroke of the engine
b) Number of cylinders and their arrangement

c) Component masses such as piston and connecting rod as well as connecting rod length.

2. Engine Output Data: The engine's intended use and desired power output significantly impact stress calculations, thereby influencing the design.

a) Maximum Torque at RPM
b) Maximum Power at RPM
c) Maximum engine angular velocity
d) Expected cylinder pressure pattern

3. Initial Dimensional Values: Crankshaft characteristic parts' initial dimensional values are selected based on prior experiments or available comparisons. Key components comprise the diameter of the primary journal bearing, the diameter of the crank throw, the fillet radius, and the thickness of the web.

4. Calculation of Reciprocating and Rotating Masses: The crankshaft assembly masses can be calculated using the previously obtained dimensions. The connecting rod exhibits reciprocating and rotating motion. This step involves calculating the reciprocating and rotating portions of the connecting rod. Additional calculated masses include the crank throw and counterweight for rotational motion, as well as the piston assembly for reciprocating motion.

5. Calculation of Pressure and Inertia Forces: Pressure and inertia forces are computed across the engine's complete RPM range. The pressure and inertia forces are computed at the points of maximum power and torque, as these are the locations where the stresses will be highest.

6. Reaction Forces: The reaction forces on the main journal bearings are computed. This provides the criteria for appropriately selecting primary journal bearings.

7. Bending Moments: Bending moments are computed to assess the need for balancing shafts and the significance of the stresses resulting from them in the crankshaft design.

8. Failure Criteria: Failure criteria are used to assess the effectiveness of design considerations. The design margin and safety coefficient are determined based on the fatigue of the material under consideration.

9. Iteration: The process is then iterated until satisfactory preliminary calculations are achieved.

A camshaft is a shaft to which a cam is fastened or of which a cam forms an integral part that turns at half the speed of the crankshaft. It is a rotating object usually made of metal that contains pointed cams, which convert rotational motion to reciprocal motion. The camshaft is used in internal combustion engines (to operate the intake and exhaust valves) mechanically controlled ignition systems and early electric motor speed controllers. Camshaft in automobiles is made from steel or cast iron and is a key factor in determining the RPM range of an engine's power band Fig 2.13.

Fig. 2.13 Engine camshaft

The associated parts are push rods, rocker arms, valve springs and tappets. The camshaft also provides the drive to the ignition system. It is driven by the crankshaft through timing gears. Cams are made as integral parts of the camshaft and are designed in such a way to open the valves at the correct timing and to keep them open for the necessary duration Fig. 2.14 [108].

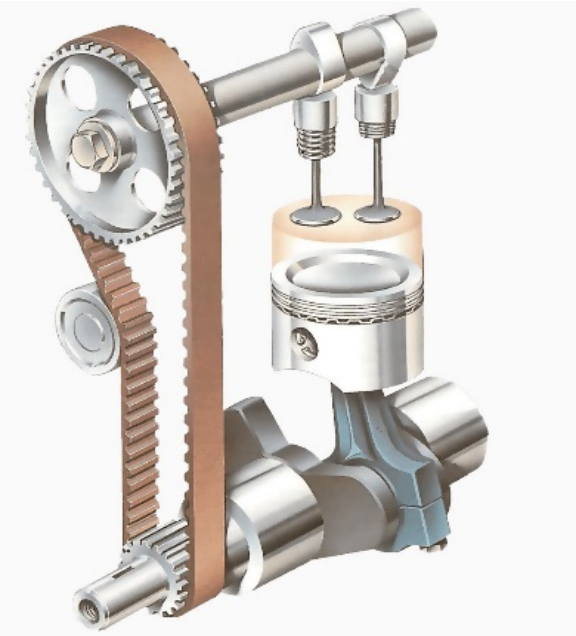

Fig. 2.14 Camshaft and valve lifters

When speaking about engine bearings, most commonly, the focus is on main and connecting rod bearings and the roles they play in crankshaft operation. Camshaft bearings are less loaded and generally have fewer problems. Therefore, innovative bearing materials and new designs are mostly focused on crankshaft bearings, where the probability of failure is higher [109].

However, camshaft bearings are also hydrodynamic bearings. They suffer from the same operational conditions as do crankshaft bearings: overloading, oil starvation, the minimum oil film being too thin, misalignment, and oil contamination. The possible failures are also similar: material fatigue, excessive wear, seizure, and corrosion Fig 2.15.

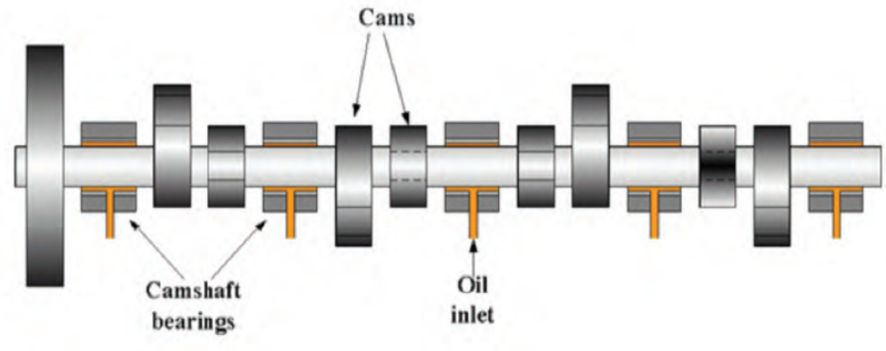

Fig. 2.15 Camshaft assembly

Engines with high performance, diesel direct injection, turbo, and supercharging exhibit greater loads on their bearings. Cylinder pressures and valve spring strength are higher. Consequently, the

camshaft bearings experience greater loads compared to those in typical gasoline engines. Excessive load can result in two forms of bearing malfunction:

1) Fatigue of the Lining (or Overlay). Fatigue cracks may develop on the lining surface when the load surpasses its fatigue strength after a certain number of load cycles. The cracks propagate through the lining and advance along the steel-lining interface. Fragments of the lining detach from the steel surface. Thick and soft linings are susceptible to fatigue.

The load capacity of camshaft bearings can be further reduced by the presence of a circumferential oil groove in the bearing housing of certain engines. The groove reduces the bearing-housing contact area. The unsupported bearing material below the groove experiences strain from the cyclic load and may experience fatigue damage.

2) Excessive Wear. The thickness of the oil film decreases under high load. Failure to maintain the minimum oil film thickness relative to micro-asperities on bearing and journal surfaces results in compromised hydrodynamic lubrication and establishes metal-to-metal contact between the surfaces. Friction causes rapid wear of the bearing material.

Misalignment is a contributing factor to camshaft bearing failure. Proper alignment of the bearing and camshaft surfaces is necessary during camshaft installation in the engine. Thermal or mechanical stresses can cause bearing misalignments due to block distortions. Subsequently, certain camshaft bearings engage in perpetual metal-to-metal interaction with the journal surface, resulting in rapid lining erosion. The realignment of the deformed camshaft-bearing housings can be achieved through the process of oversize boring. Engines of this type require the use of oversized OD camshaft bearings.

Camshaft bearing wear can result from insufficient oil supply during engine cold start. Some engines have a lengthy oil path to their camshaft bearings. Cold oil requires time to reach the bearing surface. During cold starts, the camshaft bearings experience metal-to-metal contact due to the delay in oil delivery and thus lack of oil lubrication.

Excessive bearing clearance can cause oil leakage and subsequent oil starvation. Oil pump pressure reduction due to leakage is more common in hot low-viscosity oils, as opposed to cold start.

The standard oil clearance range for camshaft bearings is 0.0015-0.002” *D, where *D represents the bearing diameter [109].

Fig. 2.16 Camshaft bearings with aluminum lining

Bearing is a mechanical element that limits relative motion to only the desired motion direction and at the same time it serves to reduce the frictional resistance to the desired motion direction. Depending of the design of the bearing, it may allow free rotation around a fixed axis (such as the case of shafts or free linear movement, or both in some cases).

Bearings may be categorized according to the type of operation it performs, the motions allowed, or to the directions of the loads applied to the parts. The most broad classification of bearings is according to the type of operation where they are classified into two groups;

- ✓ Rolling-contact bearings
- ✓ Sliding-contact bearings

Rolling-contact bearings, also called "rolling bearings" or "antifriction bearings", have rolling elements (balls or rollers) that supports the loads and allow connected parts to move freely in the desired direction. Unlike sliding-contact bearings, rolling bearings have very small frictional resistance at both starting and running conditions (the starting friction is about twice the running friction).
In general, rolling-contact bearings consist of four main parts, as seen in the Fig 2.17.

1) Inner ring
2) Outer ring
3) Balls or Rollers
4) Separator (also called retainer or cage)

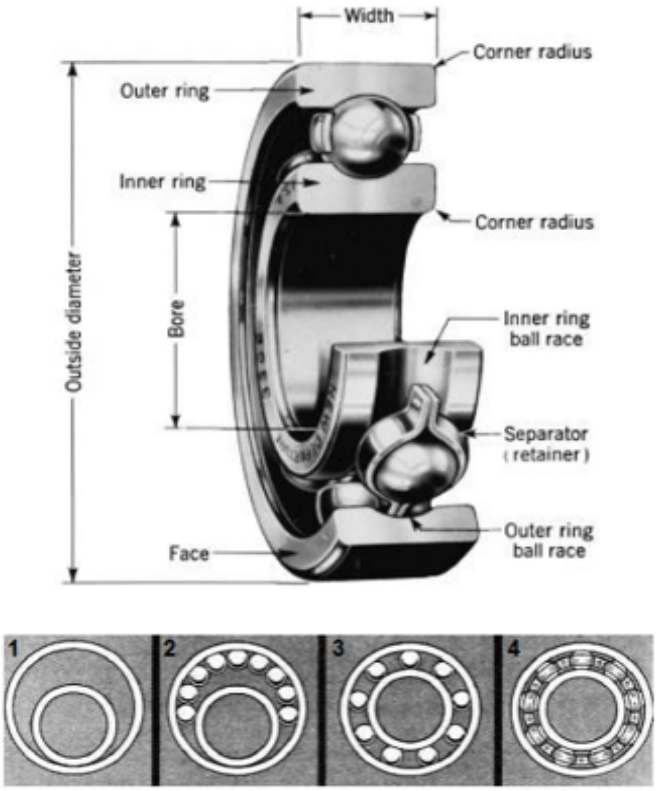

Fig. 2.17 Rolling-contact bearings [110]

The sliding-contact bearings may be considered the simplest kind of bearings in terms of construction where it could simply consist of a shaft rotating inside a hole (with appropriate clearance between them) Fig. 2.18. Unlike rolling contact bearings which generally have a limited life, sliding contact bearings could have a very long life if they are well designed, lubricated and working under reasonable operating conditions. Sliding contact bearings are generally more applicable for extreme operational conditions (high loads and rotational speeds). Also, they are used for not demanding applications (without external lubrication) because they are more cost effective than antifriction bearings [110].

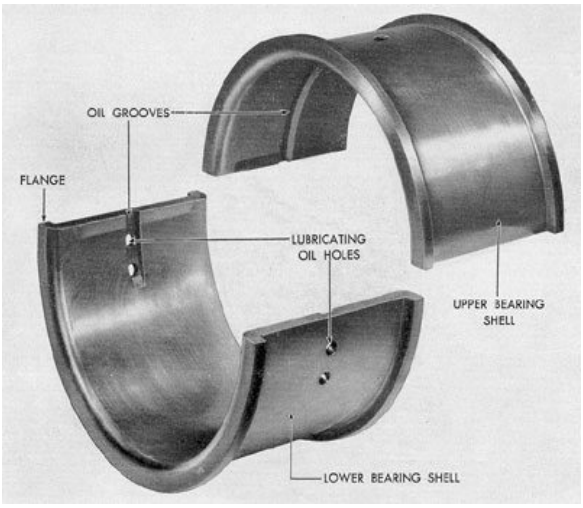

Fig. 2.18 Sliding contact bearings

Bearings can be classified into the following types:

- Ball bearings;
- Cylindrical roller bearings;
- Roller cone bearings;
- Double-row self-aligning ball bearings;
- Needle bearings;
- Thrust Ball bearings;
- Thrust roller bearings.

Furthermore the ball bearings can be classified into:

- Radial - accommodate mainly radial forces;
- Thrust-radial - accommodate the radial and axial efforts;
- Thrust - accommodate only the axial force;
- A four-point contact - axial load in both directions, or a combined radial load at simultaneous axial movement [110].

3
Methodology

3.1 Simulation

Simulation, according to Shannon (1975), is “the process of designing a model of a real system and conducting experiments with this model for the purpose either of understanding the behavior of the system or of evaluating various strategies (within the limits imposed by a criterion or set of criteria) for the operation of the system.” [111].

Simulation is the imitation of the operation of a real-world process or system in time [112]. In addition, it is a powerful tool if understood and used properly [111]. Simulation involves the generation of an artificial history of the system, and the observation of that artificial history to draw inferences concerning the operating characteristics of the real system that is represented. Simulation is an indispensable problem-solving methodology for the solution of many real-world problems. It is used to describe and analyze the behavior of a system, ask "what if" questions about the real system, and aid in the design of real systems. Both existing and conceptual systems can be modeled with a simulation [112].

Simulation involves modeling and experimentation. The model mimics a notable aspect of the system's behavior, and the user conducts experiments with the model to deduce this behavior. The framework mentioned has been found to be effective in enhancing learning, problem-solving, and design [112].

Most simulation software packages utilize a basic structure for discrete-event simulation, despite the existence of various paradigms. Discrete-event simulation packages typically comprise fundamental structural components as outlined in section [112] , despite their level of complexity.

The inputs to a system refer to the environmental actions upon it. The inputs induce changes in the system's internal state, which is referred to as the system state. The system outputs are the measured quantities derived from the system state necessary to answer the simulation study questions. The inputs induce modifications in the system state, which are manifested by resulting changes in the output [112].

3.2 Material Preparation

The materials used in the experiments are CNTs, engine lubricating oils and surfactants, presented in the figure 3.1.

Fig. 3.1 Carbon nanotubes (CNTs), engine lubricating oil, surfactant and experimental grease as a product, examples from the own experiment

Preparation of the test lubricants can be divided into steps characterized below.

- Homogenization

Homogenization is defined as the process of converting two immiscible liquids (i.e. liquids that are not soluble, in all proportions, one in another) into an emulsion [113] (mixture of two or more liquids that are generally immiscible). Sometimes two types of homogenization can be distinguished: primary homogenization, when the emulsion is created directly from separate liquids and secondary homogenization, when the emulsion is created by the reduction in the size of droplets in an existing emulsion [113]. A mechanical device called a homogenizer is used to achieve homogenization [114, 115]

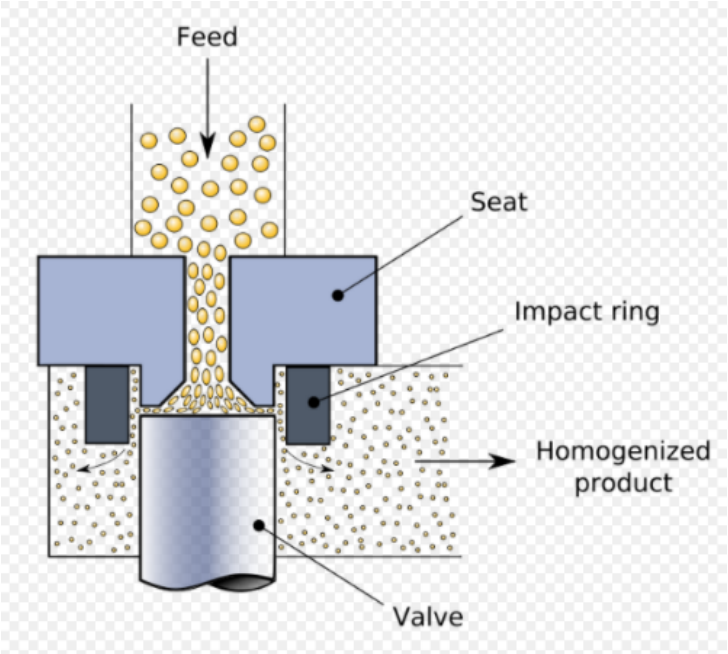

Fig. 3.2 Homogenizing valve, a method to homogenize at high pressure

- **High Shear Mixing**

High shear mixers (HSMs), Fig. 3.3, are also known as high shear reactors (HSRs). Rotor-stator mixers, and high shear homogenizers, are characteristic of high rotor tip speeds (ranging from 10 to 50 m/s).

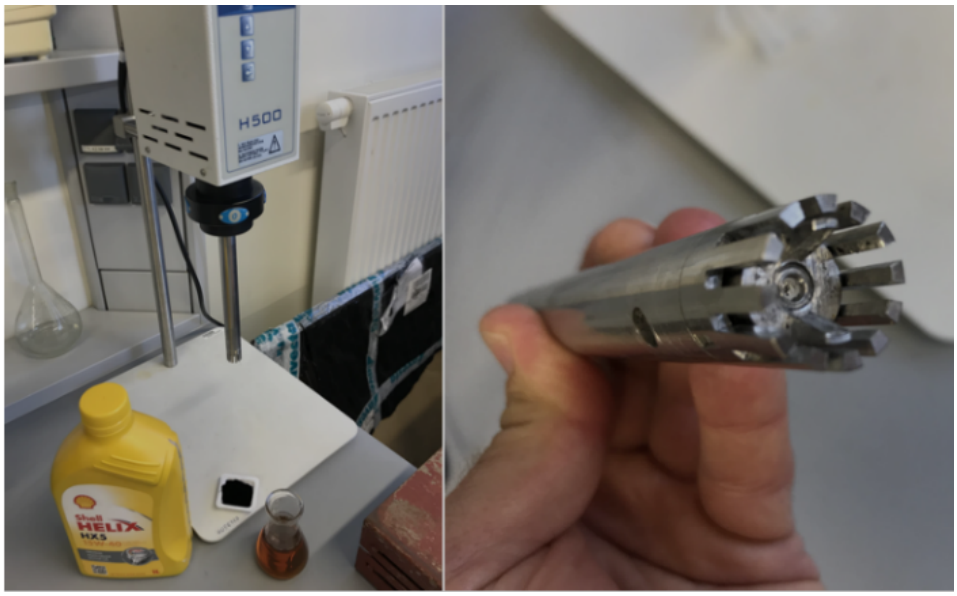

Fig. 3.3 High shear mixer H 500 & probe

Very high shear rates (ranging from 20,000 to 100,000 s^{-1}), highly localized energy dissipation rates near the mixing head, and relatively higher power consumptions than conventional mechanically stirred vessels are characteristic of HSMs [4], which are attributed to the centrifugal forces generated from the relative motion between the rotor and the stator equipped with narrow spacing (ranging from 100 to 3000 µm). HSMs have been widely used in energy-intensive processes such as homogenization, dispersion,

emulsification, grinding, dissolving, and cell disruption in the fields of agricultural and food-manufacturing, and chemical reaction processes, etc. [116].

A high-shear mixer facilitates the dispersion or transportation of one phase or ingredient (liquid, solid, gas) into a main continuous phase (liquid) that is typically immiscible. A rotor or impeller, along with a stationary stator or a set of rotors and stators, is utilized to induce shear either in a tank containing the solution to be mixed or in a pipe through which the solution flows. A high-shear mixer is capable of producing emulsions, suspensions, lyosols, and granular products. This substance finds application in various industries including adhesives, chemicals, cosmetics, food, pharmaceuticals, and plastics for purposes such as emulsification, homogenization, particle size reduction, and dispersion [117].

- **Sonication (Ultrasound)**

Sonication is the application of sound energy to agitate particles or fibers in a liquid. Ultrasonication, also referred to as the use of ultrasonic frequencies (>20 kHz). Sonication can be performed with an ultrasonic bath or an ultrasonic probe (called a sonicator) (see Fig. 3.4).

Adequate dispersion of short carbon fiber in a cement slurry can be achieved without sonication. However, due to the clinginess of CNTs or CNFs, the degree of dispersion of CNTs or CNFs in a cement slurry can be improved by sonicating a suspension of the CNTs or CNFs in water prior to incorporation in the cement mix. The MWCNTs increase the viscosity of a cement mix, but sonication decreases the viscosity of the MWCNTs cement mix [117].

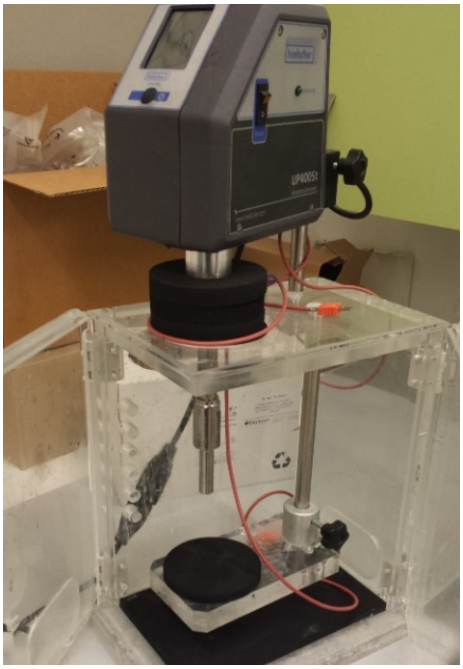

Fig. 3.4 Sonicator Hielscher UP400St

- **CVD Process (CNT growth)**

The CNTs formation by catalytic chemical vapor deposition is initiated by precursor decomposition to form a multitude of reactive species Fig 3.5. During large-scale CNTs self-assembly, these species vary with residence time leading to a non-uniform CNT growth [118].

The synthesis of CNTs (single- or multiple-walled) by CVD involves the catalytic decomposition of a carbon precursor (e.g., CO, hydrocarbons, or alcohol) on nanostructured transition metal catalysts like Co, Ni, or Fe. Typical CVD temperatures vary between 600 and 1000 ^{o}C. The process is sensitive to the catalyst structuring, as well as to the reaction conditions. Nanotubes synthesized by CVD are known to be longer than those obtained by other processes. It is also possible to grow dense arrays of aligned CNTs by using the CVD method [118].

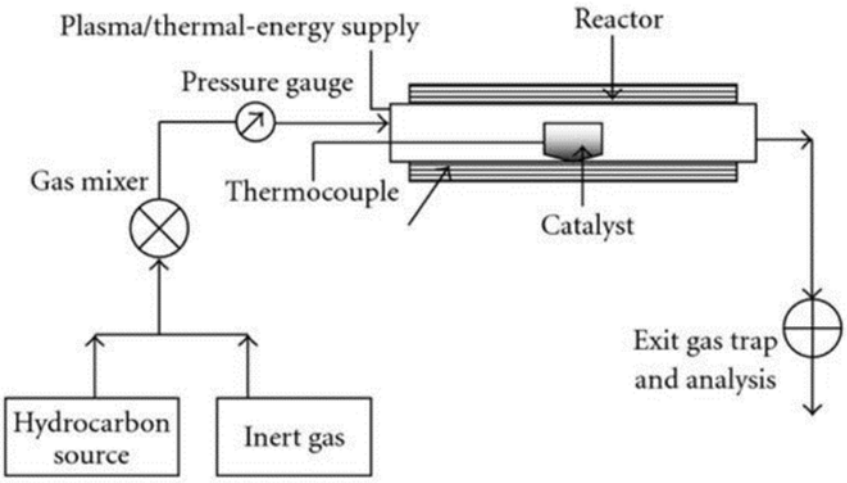

Fig. 3.5 Schematic diagram of a CVD process for CNTs synthesis

- Wet Chemistry

Wet chemistry is a form of analytical chemistry that uses classical methods such as observation to analyze materials. It is called wet chemistry since most analysis is done in the liquid phase. Wet chemistry is also called bench chemistry since many tests are performed at lab benches [119].

CNTs are commonly produced with impurities such as non-nanotube or amorphous carbons, ash, and metal catalysts that exhibit high hydrophobicity. Current methods for synthesizing CNTs involve the addition of metal catalysts to enhance yield and decrease expenses, resulting in these impurities [120].

The quantity of undesired substances is contingent upon the particular technique employed for the synthesis of CNTs. Impurities can impede the CNTs performance and obscure their original functions, thereby restricting their utility in various significant domains, regardless of the chosen methodology. CNTs aggregation in polymers can also reduce their mechanical strength and electrical conductivity [120].

Three categories of purification methods for pristine CNTs have been developed, this includes chemical, physical, and hybrid methods. The chemical purification method exhibited efficacy due to its selectivity, sensitivity, accelerated oxidation kinetics of carbonaceous impurities, and dissolution of metal catalysts from the original CNTs. Chemical agents are readily available, cost-effective, and require only basic laboratory facilities. The physical approach was utilized to eliminate graphitic sheets and carbon nanospheres from CNTs. The method's inefficacy in removing carbon impurities is often attributed to its complexity and time-consuming nature. One can choose chemical, physical, or a combination of both methods to obtain pure CNTs with desired properties, based on the impurities present in pristine CNTs [120].

HCl, H_2O_2, and KOH are readily available chemical substances and commonly found in most laboratories. HCl can serve as a reference treatment for MWCNTs, but HCl may not fully eliminate impurities that are not nanotubes. The oxidation and purification of pristine few-walled carbon nanotubes (FWCNTs) was carried out using H_2O_2 [120].

3.3 Material Characterization

3.3.1 Microscopy

Microscopy is the technical field of using microscopes to view objects and areas of objects that cannot be seen with the naked eye (objects that are not within the resolution range of the human eye). There are three well-known branches of microscopy: optical, electron, and scanning probe microscopy, along with the emerging field of X-ray microscopy [121].

The microscopy and spectroscopy data used to support the findings of this study is available from the corresponding experiment results, for example: characterization, morphology, and microstructural characterization of the CNTs are observed by Scanning Electron Microscopy (SEM) instrument and by transmission electron microscope (TEM), Environmental Scanning Electron Microscope (ESEM), and Atomic Force Microscope (AFM) [122].

Microscopy studies the enlargement of the image of objects too small to be properly seen by the unaided eye. Microscopy accomplishes its task by making use of the radiation emitted, absorbed, transmitted, or reflected by the observed specimen. The nature of the radiation specifies the type of microscopy: electron microscopy, x-ray microscopy, acoustic microscopy, etc. The visible part of the electromagnetic spectrum is the type of radiation used by optical microscopy [123].

Fig. 3.6 Optical microscope

An electron microscope is a microscope that uses a beam of accelerated electrons as a source of illumination. As the wavelength of an electron can be up to 100,000 times shorter than that of visible light photons, electron microscopes have a higher resolving power than light microscopes and can reveal the structure of smaller objects [124].

SEM provides a valuable combination of high-resolution imaging, elemental analysis, and recently, crystallographic analysis. It is used for inspecting topographies of specimens at very high magnifications using a piece of equipment called the scanning electron microscope. Furthermore, it is often used in the

analysis of die/package cracks and fracture surfaces, bond failures, and physical defects on the die or package surface [125].

SEM with a high resolution is a powerful instrument for the imaging of fine structures of materials and nanoparticles fabricated by nanotechnology. For SWCNTs observation and their morphological analysis the Field Emission Scanning Electron Microscope QUANTA FEG 250 was used [126]. Due to the need to accurately assess the diameter of bundles, SEM (Fig. 3.7) method was used. This method gives information mainly about surface morphology of the sample [126].

Fig. 3.7 Quanta FEG 250 used for most SEM microscopy and EDS spectroscopy tasks in this thesis, picture of the microscope column and close view to the microscope chamber with detectors

TEM is the original form of electron microscopy and the analogue to the optical microscope. It can achieve a resolution of ~0.1 nm, which is a thousand times better resolution than its optical counterpart, due to the wavelength range of visible light. The beam of electrons passes through the specimen and analyzes the internal structure of the specimen in the form of images. The electron has a poor penetrating capability and gets absorbed by the thick parts of the specimen. Therefore, the thickness of the specimen should not be more than few hundred Angstroms (one angstrom = 10^{-10} m) However sometimes, slightly thicker samples are used in High Voltage Electron Microscope.

The situ TEM is used to examine the dynamic behavior of field-emitting CNTs [127]. The reason for the usage of TEM for nanotubes analysis is very simple. TEM has been traditionally applied to characterizing the interior structures of nanomaterials. It is due to this method, that atomic planes of nanoparticles can be observed [126].

AFM, a form of SPM, has a resolution of fractions of a nanometer, exceeding the optical diffraction limit by over 1000 times. The data in this device is obtained through tactile exploration using a mechanical probe. Piezoelectric elements enable precise scanning through accurate and precise movements using an electronic control system [128].

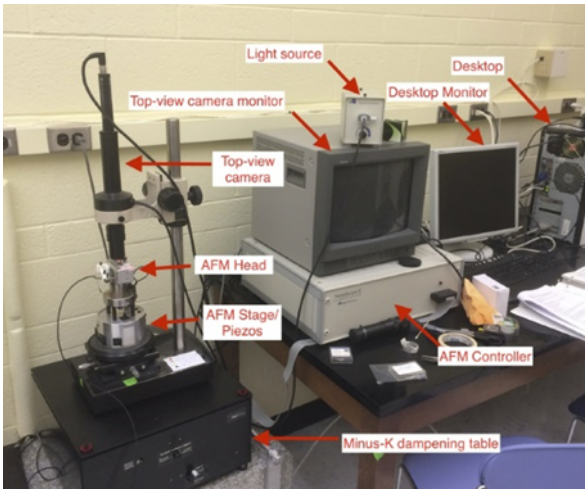

Fig. 3.8 Atomic force microscope (AFM)

The reason why AFM can be used (Fig. 3.8) for nanotubes analysis is very simple. Because AFM is a powerful tool in manipulating and characterizing the properties of nanostructures [126]. The images demonstrated with carbon nanotube atomic force microscopy (CNTs-AFM) probes imaging mode shows great promise for providing simple, stable imaging with CNTs-AFM probes. The use of CNTs-AFM probes to demonstrate high-resolution imaging on samples with features in the nanometer range, in order to demonstrate the modes imaging effectiveness and to also aid in determining the diameter of very thin CNTs-AFM probes [129].

3.3.2 Spectroscopy

Spectroscopy is the study of the interaction of electromagnetic radiation with atoms or molecules to determine their structures. Electromagnetic Radiation: A propagating wave of electrical energy with an orthogonal magnetic component oscillating with exactly the same frequency [130].

X-Ray Diffraction (XRD) is a characterization technique used for examining the fine structure of matter. It is used in the determination of crystal structure, qualitative phase identification, quantitative phase analysis, particle size and strain measurements, and the study of preferred orientation in crystals.

Most of the characterization tools such as scanning electron microscopy, transmission electron microscopy, scanning tunneling microscopy, and atomic force microscopy probes only for characterizing the local features of CNTs. However, X-ray powder diffraction can reveal the local and global features of microstructure's lattice and crystalline phases, domain sizes, and impurities [131].

This technique can be used to unravel the structural details of CNTs. Where XRD (Fig. 3.9) possesses unique advantages is because it simultaneously reveals most of the physicochemical aspects of CNTs both at the local and global scales. Thus it is worthwhile to use this technique for better understanding and utilization of its benefit to unravel the CNT ambiguities [131].

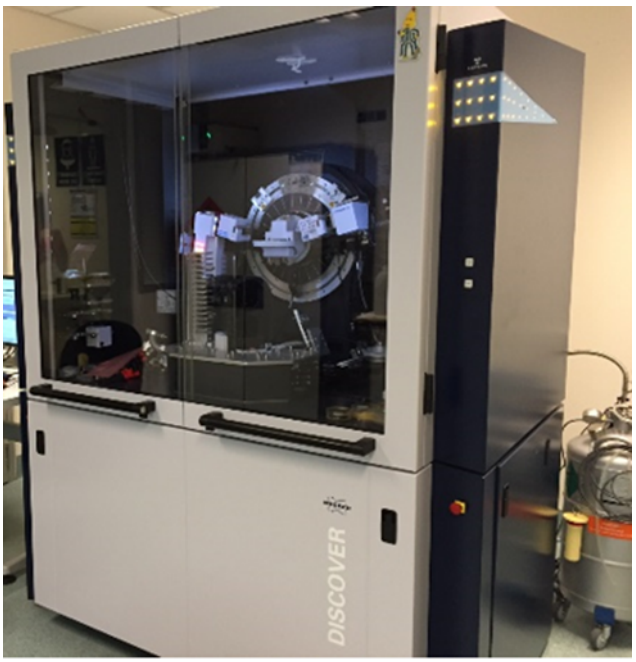

Fig. 3.9 X-ray diffraction (XRD)

Energy Dispersive X-Ray Spectroscopy (EDS or EDX) is a chemical microanalysis technique used in conjunction with SEM. The EDS technique detects x-rays emitted from the sample during bombardment by an electron beam to characterize the elemental composition of the analyzed sample [132].

Functionalization is a key technique for improving the dispersibility of CNTs in solvents and polymer matrices for producing versatile CNTs-based materials. Therefore, a robust and efficient characterization method is required to confirm that the functionalization on the CNTs surface is indeed spatially uniform. Although several imaging techniques for TEMs can characterize the spatial localization of elements chemically bound to an isolated CNTs surface, they are unsuitable for examinations on a practical scale because of their limited scanning area. High spatially resolved EDS imaging of functionalized CNTs can be done in SEM. Highly sensitive EDS detection and drift-free operation enables this technique to image the light elements of CNTs with sufficient spatial resolution (<10 nm). EDS analysis (Fig. 3.10) describes an experimental visualization of the spatial distribution of the functionalization on individual CNTs bundle structures and discusses the CNTs de-bundling mechanism via surface modification and the uniformity of the CNTs dispersion state [133].

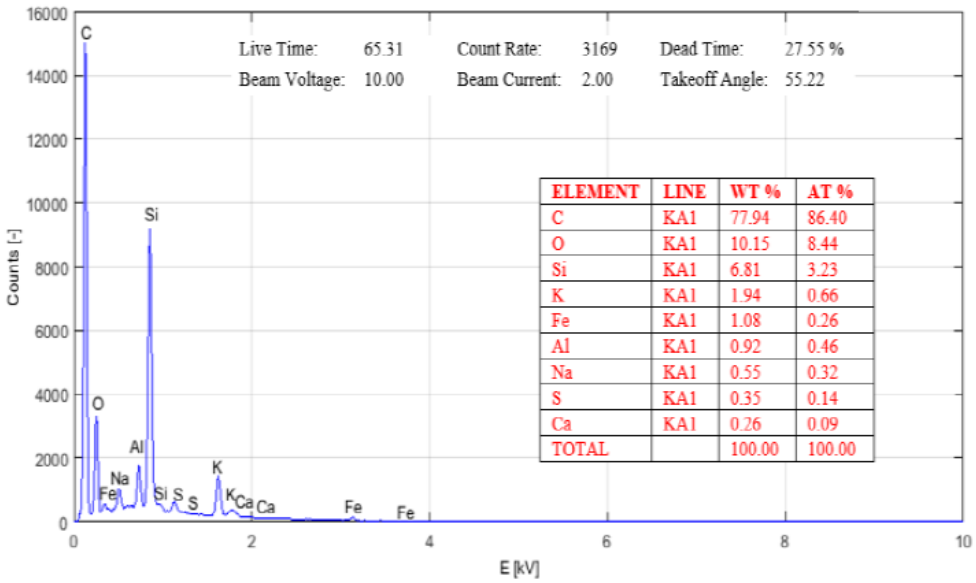

ELEMENT	LINE	WT %	AT %
C	KA1	77.94	86.40
O	KA1	10.15	8.44
Si	KA1	6.81	3.23
K	KA1	1.94	0.66
Fe	KA1	1.08	0.26
Al	KA1	0.92	0.46
Na	KA1	0.55	0.32
S	KA1	0.35	0.14
Ca	KA1	0.26	0.09
TOTAL		100.00	100.00

Fig. 3.10 EDS spectroscopy for the surface of the CNT layer on the piston dismounted after completing the engine tests

Raman spectroscopy is a spectroscopic method commonly employed to identify the vibrational modes of molecules, although it can also detect rotational and other low-frequency modes of systems. Raman spectroscopy is a prevalent tool in chemistry for identifying molecules based on their structural fingerprint [134].

Raman spectroscopy (Fig. 3.11) can be used for the extensive characterization of MWCNTs. Furthermore, could be also measured the Raman spectra of bundled and dispersed multiwall carbon nanotubes. All the Raman bands of the CNTs are seen to shift to higher wavenumbers upon debundling on account of fewer intertube interactions [135].

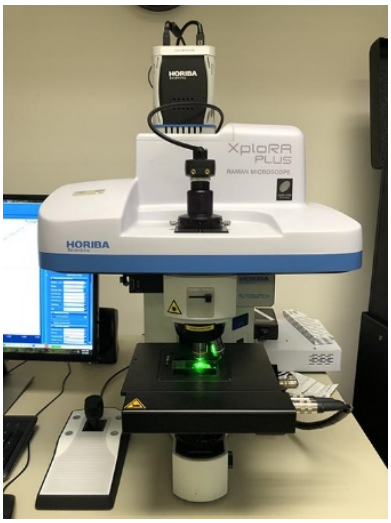

Fig. 3.11 Raman spectroscope, a with sample in the optical microscope, green laser incident light for Raman scattering and motorized sample table visible

3.3.3 Rheology

Rheology is the study of the flow of matter, primarily in a liquid or gas state, but also as "soft solids" or solids under conditions in which they respond with the plastic flow rather than deforming elastically in response to an applied force. Rheology is a branch of physics, and it's the science that deals with the deformation and flow of materials in both solids and liquids [136].

In order to achieve optimal CNTs properties enhancement with other materials (CNTs plus liquid), two key issues need to be considered: homogeneous dispersion of CNTs in the liquids and strong interfacial bonding between the CNTs and the other materials matrix. Measurement of the rheological property is useful to examine the changes in dispersion state and interfacial bonding affected by surface modification. There are a few reports on the rheological behavior of CNTs/polymer composites [137].

3.4 Tribometer Research

The tribometer is a device used in the field of tribology, the science that studies lubrication in general. The mechanical system of tribometer comprises basically a relative motion between two surfaces, which are evaluated in terms of the measurement of the frictional force between them. The tribometer has a simple concept that consists of a counterface, which may contain different quantities of lubricating oil and slides in a reciprocating mode in contact with a specimen attached to a force transducer. During the tests, the speed of sliding of the counterface and the contact force between the samples can be changed, allowing the accomplishment of a large variety of tests. Moreover, a large number of cycles can be done reasonably quickly in order to evaluate the rate of wear of materials. The force transducer uses strain gauges, which depending on its configuration, allows the measurement of a wide range of magnitudes of normal forces and friction. This equipment was used in the characterization of oils that have not been evaluated in terms of lubrication [138]. Tribometer test can be performed to evaluate the friction and wear behavior of the CNTs composite [139].

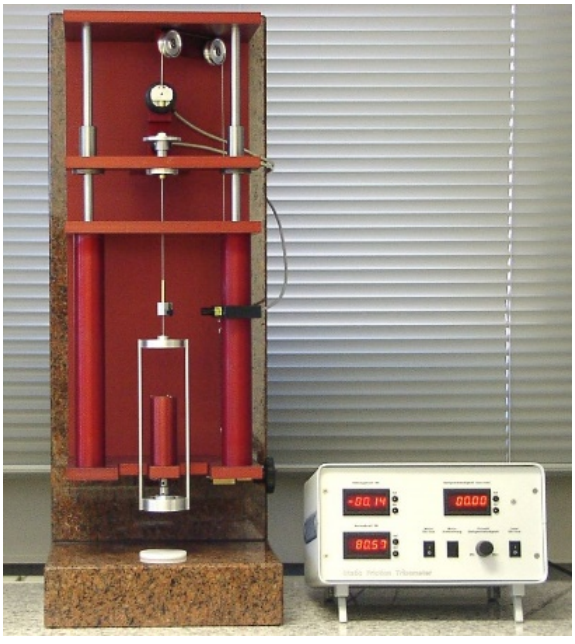

Fig. 3.12 Static friction tribometer

A simple tribometer is described by a hanging mass and a resting mass on a horizontal surface connected to each other via a string and pulley. The coefficient of friction, μ, when the system is

stationary, is determined by increasing the hanging mass until the moment that the resting mass begins to slide. Then using the general equation for friction force [140]:

$$F = \mu N$$

Where:

N is the normal force and equal to the weight (mass x gravity) of the sitting mass (m_T)

F is the loading force and equal to the weight (mass x gravity) of the hanging mass (m_H).

To determine the kinetic coefficient of friction the hanging mass is increased or decreased until the mass system moves at a constant speed. In both cases, the coefficient of friction is simplified to the ratio of the two masses:

$$\mu = \frac{m_H}{m_T}$$

In most test applications using tribometers, wear is measured by comparing the mass or surfaces of test specimens before and after testing. Equipment and methods used to examine the worn surfaces include optical microscopes, scanning electron microscopes, optical interferometry, and mechanical surface roughness testing devices [140].

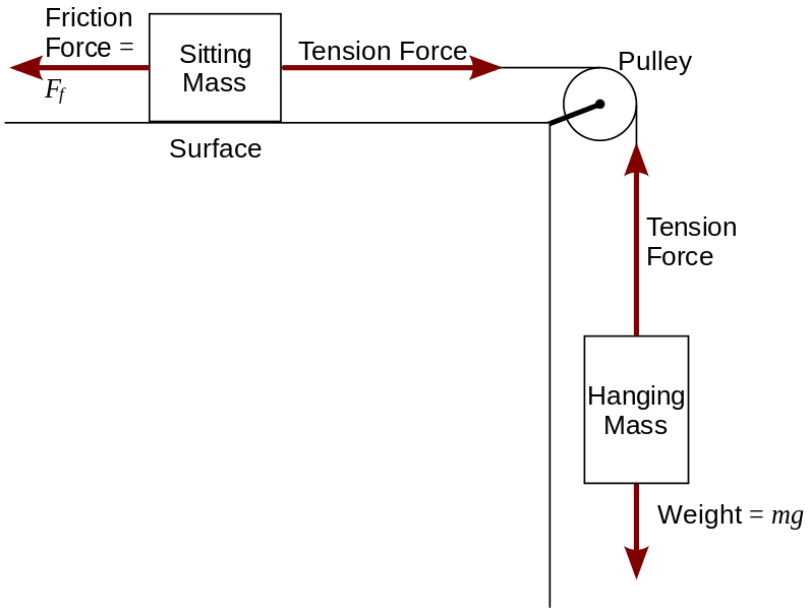

Fig. 3.13 Diagram of a pulley system

Different types of tribometers include:

- Amsler Tribometer
- Four Ball Tribometer
- T5 Tribometer

CNTs have demonstrated favorable tribological qualities in various studies. Although these studies were conducted under idealized tribometer conditions, recent engine tests have confirmed that the addition of CNTs to lubricating oil has a potential to significantly reduce friction. However, it has been observed that the concentration of CNTs in the oil must be kept very low for effective engine application. Increasing the CNT concentration beyond a certain level can result in a rapid increase in oil viscosity, leading to the formation of a greasy substance that is unsuitable for engine lubrication. In this experiment, a comparison between the tribological properties of a high-viscosity lubricant containing CNTs and a high-quality commercially available lithium grease was conducted, using an Amsler tribometer.

In this experiment, an Amsler tribometer was used featuring a rotating steel ring that exerted pressure on samples composed of cast iron, brass, aluminum, and polymer. These samples formed friction pairs lubricated with various formulations of CNT-based lubricants, whereas a high-quality commercially available grease was used as reference. The polymer selected for the experiments is commonly used as a material for friction components due to its cost-effectiveness, favorable mechanical properties, low friction coefficient, and ease of manufacturing.

High-viscosity lubricants formulated using CNTs as thickeners were subjected to testing in a tribometer, and their performance was evaluated against a standard lithium grease, a commercially available top-quality product consisting of PAO synthetic oil thickened with lithium soap (referred to as S1). The complete list of lubricants examined as part of this research can be found in Table 3.1.

Table 3.1. Formulation of lubricants

Lubricant	OIL	Thickener
S0	Mobil 1 0W/40	1% MWCNTs
S1	Synthetic, PAO + additives	Lithium complex
S2	Synthetic, PAO + additives	Lithium complex / 0.5 MWCNTs short
S4	Orlen Platinum 5W/30	3% MWCNTs short
S5	VW Oil 5W/30	2% MWCNTs short[1]
S6	Castrol RS 10W/60	1% MWCNTs short[1] / 0.2% MWCNTs long[2] / 0.2% Graphene
[1] outer diameter 9.5 nm, length 1.5 μm [2] outer diameter > 50 nm, length 10…20 μm		

Lubricant S0 was inadvertently generated during the engine tests detailed in [8], whereas lubricants S4, S5, and S6 were intentionally prepared using an ultrasound disintegrator. Lubricant S2, on the other hand, is essentially standard S1 grease with the addition of CNTs.

For the comparative assessments, the Amsler A-135 friction machine was used. The friction interface featured a rotating cylindrical ring against which a rectangular sample was applied, directed toward the frictional surface. The rings employed in these tests possessed an outer diameter of 40 mm and a thickness of 10 mm. They were crafted from hardened steel with a surface hardness of 60 ±2 HRC. The samples used were rectangular elements measuring 15×10×5 mm, composed of various metal and polymer materials, as depicted in Figure 3.14.

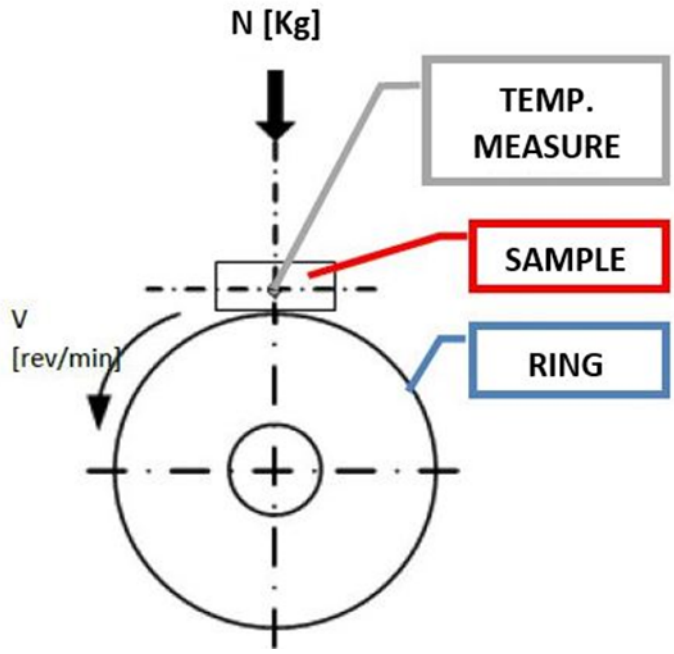

Fig. 3.14 Kinematics of the Amsler Tribometer, which involves applying a controlled load to a tested sample and pressing it against a rotating ring

Both before and after the tests, surface profilometry of the samples and rings was performed using a ZEISS contact profilometer equipped with inductive transducer heads and SAJD METROLOGIA software known as SUFORM. This software enabled the measurement and analysis of the uniformity and deviations in surface roughness. The measurements were conducted using a measuring arm with a diamond contact tip, shaped like a pyramid with a rounded tip. The vertical measurement range when using the induction head was ±200 μm. The measuring tip traveled at a speed of 0.1 mm/s, within the device's range of capabilities (0.01 mm/s to 1 mm/s). Measurements were carried out with a defined segment size of λc = 0.25 mm, and the measuring section (L_n) spanned 4 mm. Cut-off filtration was applied in the analysis of the surface roughness results.

Subsequent to the friction tests, the samples were once again used to generate four additional profiles for each sample. Three of these profiles were conducted perpendicular to the friction groove, while one profile was executed along the groove at the point exhibiting the greatest depth change. By generating profilograms across the groove, it became possible to ascertain the average groove depth for a particular sample group, serving as an indicator of wear. The results were also statistically analyzed, with confidence intervals specified for the average value at a significance level of 0.1.

3.5 Engine Research

3.5.1 Engine Test Introduction

The piston ring and cylinder liner (PRCL) is a key tribosystem in an automotive engine. The friction and wear properties of the PRCL directly relate to automotive engine performance. Meanwhile, the never-ending evolution of energy conservation and emissions reduction regulations for vehicles has driven the

auto industry to continuously attempt to reduce friction losses in engine components in order to meet such regulations and maintain a competitive edge in the market [71, 141].

The tribological problems regarding the PRCL system remain; however, they must be overcome in order to keep adapting to the development of auto engines [71, 142].

Researchers have developed or improved various models of engine motion to understand the detailed interactions between the piston ring and cylinder liner. Numerous methods have been proposed for reducing the friction and wear of the PRCL tribosystem, those methods include: surface modification, lubrication improvement, and mechanical design. Currently, research on lubricating oil additives has gained a considerable amount of interest.

CNTs have attracted much attention for their possible industrial applications, mostly owing to their outstanding mechanical properties, such as their high elastic modulus, high tensile strength, and good thermal conductivity. Although CNTs provide excellently performance, whether they are a viable lubricating oil additive for the PRCL system is yet to be determined [71].

3.5.2 Carbon Nanotubes Layer-Coated Engine Piston

The objective of the conducted experiments was to examine the viability of CNTs applied onto the piston skirt as a means to effectively reduce internal friction losses in a combustion engine. This investigation aimed to explore the potential application of CNTs in reducing the friction losses within internal combustion engines.

The tests were performed using experimental pistons, constructed from standard aluminum alloys, and were fabricated by NanoLab Inc. using a proprietary process developed by the company. These pistons were subsequently coated with a layer of MWCNTs with a diameter of approximately 15 nanometers and lengths ranging from 5 to 20 micrometers. The nanotubes were applied onto the surface by spraying them with an aqueous solution which contained a binding agent. It is noteworthy that this technology has the potential for practical implementation on an industrial scale.

The experimental approach employed in this study to quantify engine friction losses involved a comparative analysis of the engine torque. Specifically, the torque output of the engine equipped with standard pistons was compared with the respective values obtained for the engine utilizing experimental pistons coated with a layer of MWCNTs on the piston skirt, as illustrated in Figure 3.15. The solution was formulated by combining four distinct components, which were detailed in Table 3.2.

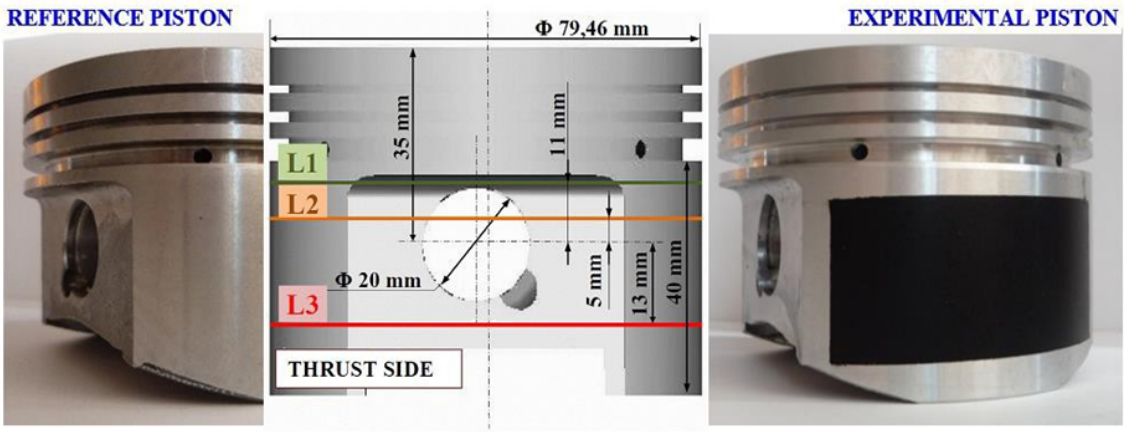

Fig. 3.15 CNTs-coated aluminum alloy pistons used,
the focus is the horizontal level of L1-L3 where wear will be assessed

Table 3.2. Properties of the solutions for the layer

Distilled water	100 ml
Dodecylbenzensulfonic Acid (DBS)	300 mg
MWCNT PD15L5-20	300 mg
Potassium Silicate	5 ml (KASIL 1, 2.50 weight ratio potassium silicate, 29.1% K_4SiO_4 solution in water

The process began by subjecting a mixture of distilled water, MWCNTs, and DBS to 10 minutes of sonication using a horn sonicator. Next, potassium silicate was introduced, and the entire solution was stirred for an additional minute.

To apply the aqueous CNT solution, it was sprayed onto the pre-heated piston's surface at 95°C in multiple successive passes. A quantity of several tens of milliliters of the solution was used to coat the skirt surface of a single piston as illustrated in Figure 3.20. The process was then brought to completion by maintaining the piston at a temperature of 300°C for 1 hour.

This experiment employed the original test bench depicted in Figure 3.16, initially developed as a component of a PhD thesis [143] and comprehensively documented in a subsequent study [72].

This test bench contained a modified two-cylinder in-line internal combustion engine, which was powered by an electric motor. To ensure precise torque measurements, a transmission shaft equipped with a T5-type HBM torque meter, offering a torque range of 50 Nm and a remarkably low relative standard deviation of repeatability (±0.025 Nm) according to DIN 1319, was employed for torque transmission. The PID controller enabled precise maintenance of the target oil temperature with an accuracy of ±0.2°C, ensuring consistent and reproducible measurements.

The measurement signal was recorded using the HBM Spider 8 device. Each torque value presented in this experiment represents an average derived from 20,000 consecutive measurements recorded at a frequency of 9.6 kHz, with a negligible deviation of the average torque value not exceeding 0.05 Nm.

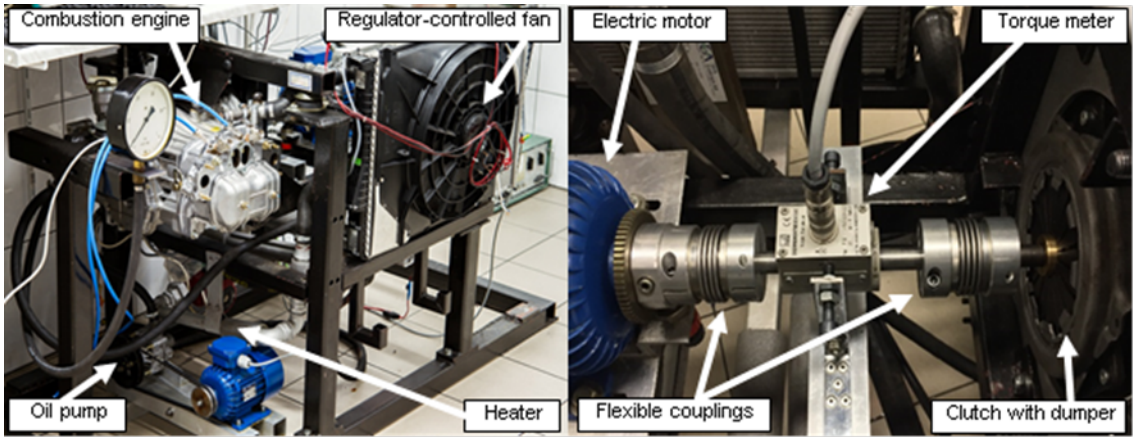

Fig. 3.16 The test bench for measuring the friction losses in the crank mechanism;
general view on the left and a method for measuring the torque of the motoring torque on the right

To replicate an overload scenario within a real engine, a specific method was employed. This method involved implementing modifications, including immobilizing the engine's camshaft to keep all valves closed and replacing the crankshaft-driven water and oil pumps with external units, each driven by an individual electric motor.

These modifications resulted in a unique condition where, during each crankshaft revolution, the piston was responsible for compressing and decompressing the contents within the cylinder. A portion of

this cylinder gas leaked into the crankcase. With the engine valves sealed shut, any blow-back gases were managed by the introduction of additional one-way valves, referred to as load refill valves, placed in lieu of the spark plugs. The test bench design allowed for the controlled opening and closing of these valves, enabling the intake of free air, either from the ambient surroundings or from air supplied at a specific overpressure level. This facilitated an increase in the maximum cylinder pressure by directing additional air into the cylinder at the start of the compression stroke under increased pressure.

To filter out pistons that couldn't maintain stable operating conditions, a preliminary test was conducted, lasting 100 minutes. This test was conducted at a constant oil temperature of 80°C and a fixed speed of 1000 rpm, immediately after the experimental pistons were installed in the engine. Figure 3.17 provides a comparison of the results obtained from the preliminary engine test on one of the test piston versions with the final piston version.

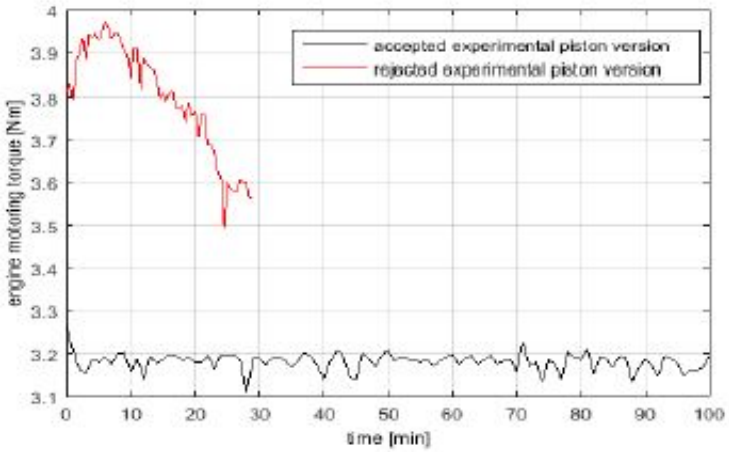

Fig. 3.17 Preliminary engine test of two CNT-coated experimental piston versions representing early and final development stages; comparing the stability of the engine motoring torque over time

The testing of the final piston version was discontinued due to the instability in friction losses between the engine pistons and experimental pistons. Ultimately, only pistons that successfully passed the preliminary engine test were chosen to be used in the main friction tests.

For the main friction tests, the pistons that had previously passed the preliminary engine test were used, both for the experimental pistons and the reference pistons. These tests encompassed 96 different combinations of engine operating conditions, which varied in terms of oil temperatures (50°C, 80°C, and 110°C), crankshaft rotational speeds (set in increments of 250 rpm, ranging from 500 rpm to 3000 rpm), and load conditions, simulated by adjusting the air pressure supplied to the cylinder (0 bar, 1 bar, and 1.5 bar). The experimental pistons that successfully completed all stages of engine research accumulated a total engine runtime of approximately 10 hours.

Before using the experimental pistons, a series of tests had to be performed to characterize the nanotube layer, the pistons' surface (references and experimental), and the cylinder walls. Most of these tests were repeated immediately after the engine test was completed and the pistons were removed from the engine. These tests included:

1. **Surface Roughness Measurement:** The surface roughness of both reference and experimental pistons was measured before and after the application of CNTs on the surface, as well as after the engine tests. This assessment was carried out using the Mahr Perthen Perthometer S8P profiler, utilizing the RHT6-50 contact measuring tip. The applied pressure force ranged from 0.8 to 1.2 mN, and the stylus tip radius was 5 µm.
2. **Surface Shape Analysis:** The surface shape of reference and experimental pistons was analyzed before and after CNT application, as well as after the engine tests. This analysis was performed

using the DEA Global Image 7.7.5 Coordinate measuring machine, which was equipped with the Renishaw SP25M probe head and SM25-2 module. The measuring tip had a length of 62 mm and featured a measuring ball with a diameter of 6 mm.

3. **Measurement of CNT Layer Wear:** The wear of the CNT layers was quantified using the Hommel etamic roundscan 535 Formtester.
4. **Cylinder Wall Shape Analysis:** The shape of the cylinder walls was assessed before and after the engine tests. A Mitutoyo 511-501 digital bore gauge was used to determine the wear on the cylinder running surfaces.
5. **Detection of Hidden Piston Material Defects:** Hidden defects within the piston materials were revealed through computer tomography using the GE v|tome|x s 240.
6. **Examination of CNT Layer Structure:** The structure of the CNT layer was examined using SEM devices such as the Mira 3 Tescan and the Jeol JSM-7001F.
7. **EDS (Energy-Dispersive X-ray Spectroscopy):** EDS analysis was conducted using equipment from Princeton Gamma-Tech, Inc. to provide insights into the elemental composition of the tested materials.

3.5.3 Adding Nanostructured Carbon to the Lubricating Oil

The objective of this experiment was to showcase the enhancement of lubricating properties in oils through the incorporation of CNTs. The introduction of CNTs into the lubricating oil allowed for their dispersion throughout the oil, facilitating distribution to all engine components. However, these advantages tend to be short-lived due to the propensity of carbon nanotubes to re-agglomerate when added to the oil in high enough concentrations.

In previous tests, a 1wt % concentration of CNTs was introduced into the oil. Despite using an ultrasound disintegrator for several hours, achieving optimal dispersion proved challenging. Surprisingly, the carbon nanotubes dispersed so well in the oil that after just a few minutes of engine operation, the oil thickened, impeding its pumpability. Consequently, in subsequent experimental attempts, CNTs were blended with the oil to maintain a minimum concentration of 0.5%. However, the observed reduction in friction was limited to 6%, which is significantly lower than the reduction seen in the initial tests where CNTs were introduced into the oil through an in-situ abrasion process.

When analyzing this outcome, Kałużny et al. suggested that the quality of the CNTs dispersion is a critical factor in achieving effective tribological performance. Inadequate dispersion hinders the potential benefits of CNTs, and they should not be regarded as a nano-addition under such circumstances. Furthermore, the presence of micrometer-sized CNT agglomerates in the oil can obstruct oil flow in the narrowing lubrication gap, adversely affecting lubrication conditions.

Therefore, Kałużny et al. opted to explore the frictional effects at trace levels of CNTs by introducing minute amounts (as low as 0.03%) in their experiment. This concentration level efficiently mitigates the re-agglomeration effects. Surprisingly, even at such low CNT concentrations, engine friction could be reduced by up to 6%. Additionally, during rigorous driving tests, a noticeable reduction in vibration of up to 30% was observed.

In this particular experiment, various nanocarbon structures were used as additives to augment a commercially available engine lubricating oil, which belonged to the 5W/30 viscosity class. The chosen reference oil adhered to ACEA C3 requirements and possessed approvals from Volkswagen under the designations 504 00 and 507 00.

To ensure the effectiveness of these additives, each oil sample, including the reference oil, was subjected to an engine flush using Liqui Moly. A consistent concentration of 40 ml of engine flush per

liter of oil was maintained throughout the experiment. Notably, the results underscored the efficacy of the engine flush as a potent surfactant. Figure 3.18 shows a comparative illustration of the outcomes for the reference oil and the same oil supplemented with carbon nanomaterial additives. Throughout the experiment, several preliminary tests were conducted using a rheometer to evaluate various forms of nanocarbon as potential oil additives. The primary objective was to gain insights into the pivotal role of CNT dispersion within lubricating oil. The viscosity of the oil was measured at different shear rates.

A comparative analysis of the results obtained for the reference oil and the same oil augmented with carbon nanomaterial additives was performed (Figure 3.18). Notably, it was observed that the high aspect ratio characteristic of CNTs could elevate the oil's viscosity, even when present at concentrations as low as 0.03% of MWCNTs. This viscosity increase serves as a reliable indicator for assessing the nanotubes dispersion quality. Specifically, only the well-dispersed fractions of CNTs exhibited a significant impact on altering the oil's viscosity. Importantly, this particular effect was not observed for other forms of carbon allotropes.

Consequently, OIL 1, containing the MWCNTs NC 7000 in its original form, was selected for the engine tests. During these tests, it was found that minor fluctuations in oil viscosity had minimal direct impact on the measured friction. This was mainly because the changes induced by oil temperature variations during engine warm-up were considerably more significant in comparison. The behavior of oil with dispersed CNTs exhibited a non-Newtonian nature, which was quite intriguing. This unique characteristic enables lubrication to effectively support a wide range of contact pressures and entrainment speeds, making it particularly suitable for intricate tribological systems like engines.

The experiment involved a comparison of the performance between regular oil and oils enriched with nanotubes. The primary parameter assessed in this experiment was engine torque, which serves as an indicator of power loss due to friction as well as the vibration signal emanating from the engine block. The test setup was meticulously designed, with the vehicle's engine connected to an electric machine. This setup allowed for the operation of an un-ignited engine at a constant speed to measure internal engine friction or to act as a brake for a working engine. Additionally, the engine coolant was electrically heated, gradually increasing its temperature from around 20°C to 90°C during testing.

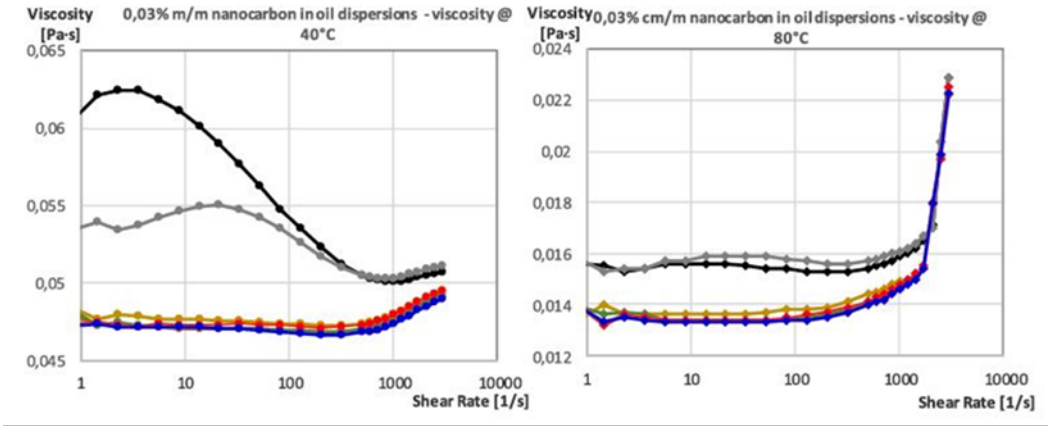

SAMPLE	ALLOTROPES	MANUF.	CODE	DIAMETER [nm]	LENGTH [μm]
OIL 1	MWCNTs	Nanocyl	NC7000	9.5	1.5
OIL 2	MWCNTs	Nanocyl	NC7000 functionalized c12 alkane	9.5	1.5
OIL 3	MWCNTs	NanoLab		15	1...3
OIL 4	MWCNTs	NanoLab		15	5…20
OIL 5	amorphous				
OIL 6	graphene		G3		
OIL 7	reference oil	Orlen Oil	Platinum 5W/30		

Fig. 3.18 Oil viscosity curves for the reference oil
and the impact of the nanocarbon additives of various morphologies

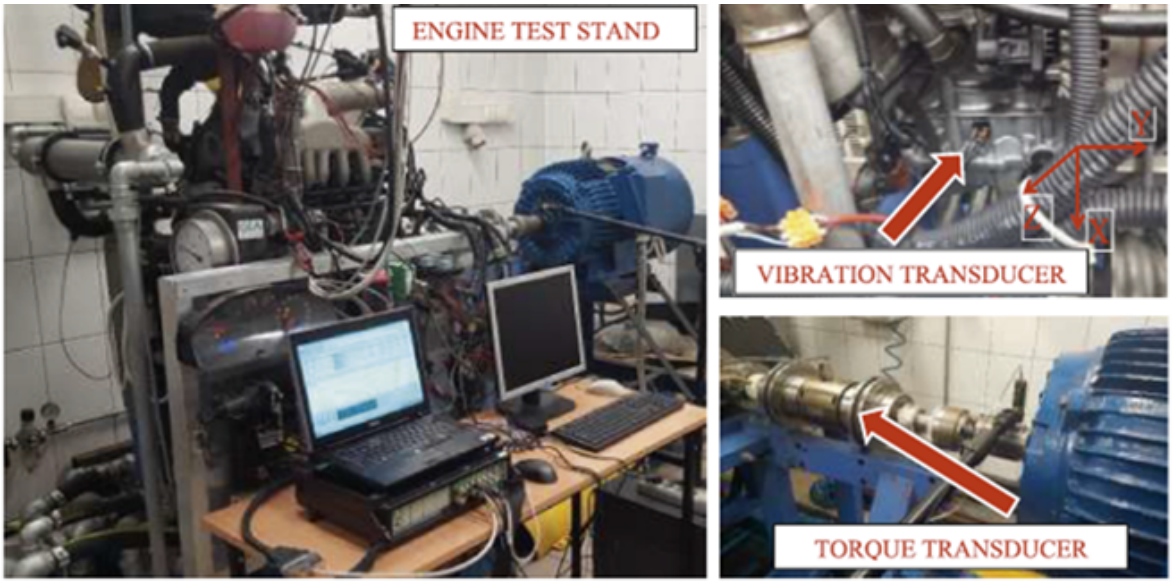

Fig. 3.19 Engine test stand

In the context of vibration analyses, the axes were designated as follows:
X-axis: Aligned parallel to the cylinder axis.
Y-axis: Aligned parallel to the engine crankshaft axis.
Z-axis: Aligned parallel to the cylinder bore diameter and perpendicular to the Y-axis.

These tests, outlined in experiments 1 through 4 and visually represented in Figure 3.19, were detailed in Table 5.3. It's important to emphasize that, in the case of the oil blended with nanotubes, the tests commenced promptly after pouring the oil into the engine, without any pre-distribution of the oil within the engine's lubrication system.

Table 3.3. The test procedures

	Experiment 1	Experiment 2	Experiment 3	Experiment 4
Operating condition	motoring	motoring	fired	fired
Engine speed[rpm]	1200	2500	1200	2500
Fuel dose[1]	0	0	11	25
Torque[2,3][Nm]	70…-50[4]	50	50	160
Oil temperature[°C]	Warm-up[4]	95	100	130
Test time[minutes]	30	10	10	10

[1]in all experiments the engine load was precisely controlled by setting the fuel dose [2]approximate values, actual values depending on the oil type, discussed in results. [3]absolute values [4]values change due to the oil.

The measurements were conducted under specific research conditions, which can be outlined as follows:

1. **Ambient Conditions at the Engine Test Stand:**
   - Temperature: 20 degrees Celsius (20°C)
   - Pressure: 1013 hectopascals (hPa)
2. **Engine Operating Conditions:**
   - The engine was in a stationary state during the measurements.
   - Separate measurements were taken for defined engine operating conditions, denoted as experiment 1 to experiment 4. These experiments likely represent different scenarios or settings for the engine under study.
3. **Vibroacoustic Measurement Conditions:**
   - Vibration Acceleration Frequency Range: Measurements were performed in a frequency range spanning from 1 Hz to 10,000 Hz. This range is often referred to as the "signal pass band" and indicates the frequencies of vibration acceleration that were monitored.
   - Sampling Rate: A sampling rate of 25.6 kilohertz (kHz) was used for data acquisition. This means that measurements were taken 25,600 times per second, providing high-resolution data.
   - Location of the Vibration Transducer: The vibration transducer was positioned on the engine block, as indicated in Figure 3.23. This placement likely allowed for the measurement of vibrations directly on the engine structure.
   - Measurement in 3 Perpendicular Geometrical Axes: Measurements were taken along three perpendicular axes. This means that vibrations in the X, Y, and Z directions were likely recorded, providing a comprehensive view of the engine's vibrational behavior.

These detailed research conditions provide essential information about how the measurements were conducted and in what circumstances, which is crucial for understanding and interpreting the data collected as a result of the performed experiments.

In the signal analyses performed during these measurements, several main diagnostic parameters were considered. These parameters were crucial for understanding the engine's behavior and performance. Here are the main diagnostic parameters selected along with their sources:

1. **Engine Speed:**
   - Source: Data was directly obtained from the BOSCH EDC 16 engine control unit.
   - Engine speed is a fundamental parameter that indicates how fast the engine's crankshaft is rotating, typically measured in revolutions per minute (RPM).
2. **Mass of Injected Fuel:**
   - Source: Data was directly obtained from the BOSCH EDC 16 engine control unit.
   - The mass of injected fuel represents the amount of fuel being delivered to the engine's combustion chamber. It is a key parameter for understanding the engine's fuel consumption and performance.
3. **Coolant Temperature:**
   - Source: Data was directly obtained from the BOSCH EDC 16 engine control unit.
   - Coolant temperature is crucial for monitoring the engine's thermal management system and ensuring it operates within a safe temperature range.
4. **Oil Temperature:**
   - Source: Data was directly obtained from the BOSCH EDC 16 engine control unit.
   - Monitoring oil temperature is important for assessing the engine's lubrication system and ensuring that oil is at the appropriate temperature for optimal performance.
5. **Air Temperature:**
   - Source: Data was directly obtained from the BOSCH EDC 16 engine control unit.
   - Air temperature is significant for understanding how the engine's intake air properties might affect the combustion process and efficiency.
6. **Mass Airflow:**
   - Source: Data was directly obtained from the BOSCH EDC 16 engine control unit.
   - Mass airflow measures the quantity of air entering the engine, which is crucial for fuel injection and combustion control.
7. **Fuel Injection Pressure:**
   - Source: Data was directly obtained from the BOSCH EDC 16 engine control unit.
   - Fuel injection pressure is an important parameter for regulating the atomization and delivery of fuel into the combustion chamber.
8. **Engine Torque:**
   - Source: Data was recorded from the KTR DATAFLEX 42/1000, which is a torque-measuring shaft.
   - Engine torque represents the turning force generated by the engine's crankshaft. It is a key indicator of the engine's power output and performance.
9. **Vibration Accelerations:**
   - Source: Data was recorded using the Bruel&Kjær Pulse 3560-C system.
   - Vibration accelerations were measured in three perpendicular geometrical axes, as previously mentioned. These measurements provide insights into the engine's structural vibrations and can be used for diagnostic and reliability analysis.

These diagnostic parameters, collected through an array of sensors and control units, collectively provided a comprehensive insight into the engine's performance and behavior throughout the experiments. This wealth of data allowed for detailed signal analysis and diagnostic revelations.

Specifically, the Bruel&Kjær 4504A vibration acceleration transducer, having a linear pass band of 12 kHz, was strategically positioned in the lower section of the engine block, precisely adjacent to the second cylinder liner and in close proximity to the crankshaft main bearings. This precise placement was selected carefully to optimize the signal-to-noise ratio, a crucial consideration given that the dynamic processes affecting the cylinder liner and crankshaft bearings serve as the primary sources of engine friction.

For subsequent data analysis and processing, advanced software algorithms developed by Kałużny et al. were used. Impressively, the total measurement error remained below 1% of the actual data values. The software excelled at effectively isolating the active signal components from the recorded physical waveform, concurrently revealing vital attributes associated with their origin processes. This approach facilitated the exploration of diagnostic parameters closely tied to the assessed dynamic processes [144-147].

Fundamentally, the central principle guiding the effort to derive unequivocal functional relationships from vibroacoustic machine testing, particularly in the context of internal combustion engines, relies on the meticulous post-processing of complex measured signals [148-151].

Through comprehensive analysis spanning both the time and frequency domains, it became feasible to distill information components primarily linked to the phenomena resulting from the presence of CNTs in the lubricating oil.

3.6 Thesis and Research Methodology

The study of the literature along with author's preliminary experiments led to the following thesis:

Carbon nanotubes introduced to the journal bearing allow for efficient reduction of sliding friction and friction-induced vibrations.

Figure 3.20 reproduces the scientific approach to verify the thesis.

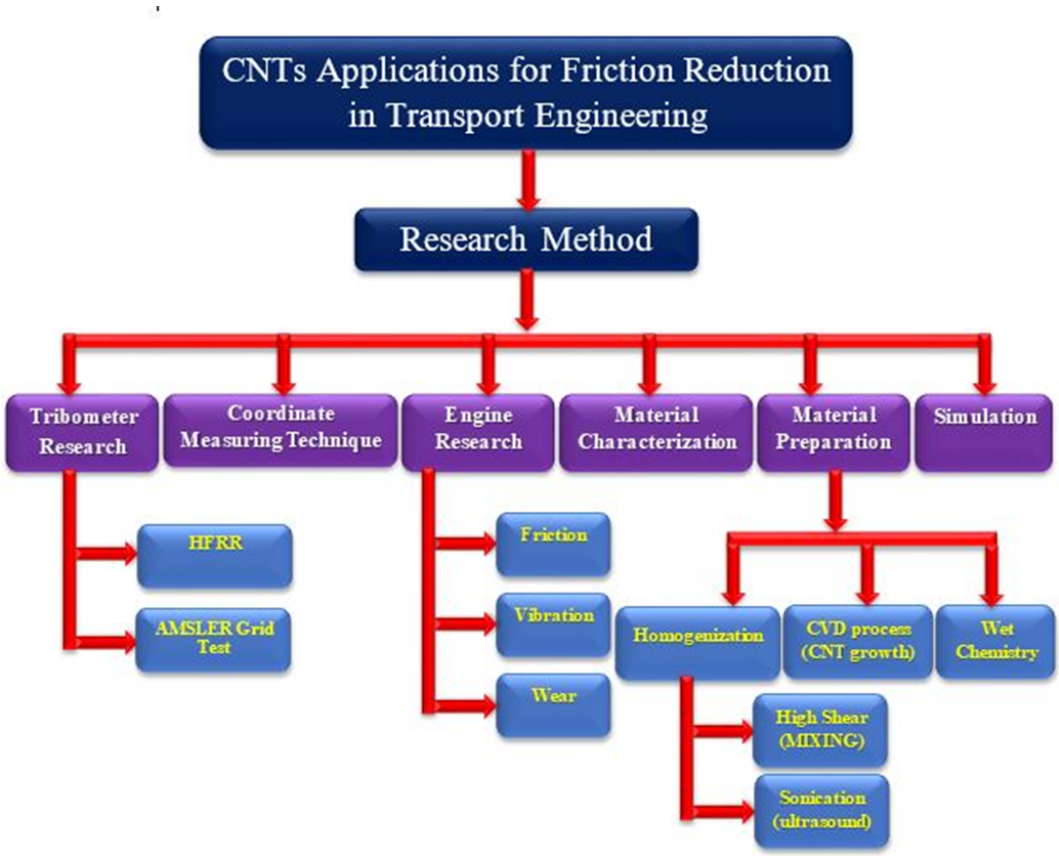

Fig. 3.20 Flow chart of the investigation methodology

4
Molecular Dynamics Simulation

4.1 Molecular Modeling and Simulation

The workability and efficiency of motions in machines could be improved by using a solid lubricant with nanoparticles. This was mentioned by [152-154] where nanoparticle-based lubricants were discussed in three friction mechanisms, at an atomic level. These three mechanisms are sliding, rolling, and exfoliation. The most commonly observed mechanism is sliding which has tribological behavior. The other mechanism, rolling, is important since it is related to the shape of nanoparticles. Finally, the exfoliation mechanism can possibly decrease friction by changing the exfoliated layer to the substrate and then forming a tribofilm [155].

The field of nanoengineering (or nanoscience/technology) is still subject to fundamental studies and more investigation is needed [156]. The ability to understand the properties and phenomena at nano-scales will open more room for manufacturing, synthesizing, or designing devices. Understanding this basic information will reduce the cost of composing the system and performing experiments on it. Thus, computational nanoengineering, more accurately called molecular modeling and simulation, is a very important field of research. Its development will definitely be aided by modern computing [156].

Model building and computation is the way to study molecular functions and structure [157]. Computation of molecular trajectories in multi-body systems can be achieved using an appropriate molecular model of the system [158]. Trajectories output can then be used to analyze and determine the system's properties. Widely used categorizations are as follows [156]:

- Molecular Mechanics

The basic feature of Molecular Mechanics (MM) is atoms in the molecules are assumed to be particles with mass. They interact in a force field. Quantum mechanics calculations are then used to obtain the force field function. On the other hand, the bonds between the atoms simulate the behavior of springs. This includes bending, stretching, and torsion. In order to mimic the non-bonded atoms, van der Waals interactions as well as electrostatic forces are considered. The whole idea is to gain saddle points, using mathematical algorithm, on the potential energy surface [156].

- Quantum Mechanical Methods

As opposed to MM, in quantum mechanical (QM) approach particles are treated as wave functions. The equation related to this is Schrodinger's equation which is applied to many particles. Essentially, the description of spatial probability distributions related to the energy states is involved. Again, the saddle points are the main focus [156].

- Monte Carlo

The Monte Carlo (MC) method is a numerical approach used for computing multidimensional integrals of statistical-mechanical ensemble averages or thermal averages. This technique is utilized for simulating systems with a constant number of particles (N) and volume (V) at an absolute temperature (T). This system has been described in reference [156].

- Molecular Dynamics

MD simulation involves modeling the movement of molecules or atoms within a system to calculate the forces, positions, and velocities of each particle at every time step. MD calculations are akin to computer experiments as they provide complete system information at every step [156].

4.2 Basics of Molecular Dynamics Simulations

4.2.1 The Goal of the Molecular Dynamics Method

The parameters used to compute the end goal in the Molecular Dynamics Method are as follows:

- The starting with a given number of atoms (N) which represents the collection of atoms.
- A simulation shows how these atoms move according to time.
- How will be the displacement of all the atoms change in time.
- What will be the trajectory of all these atoms, and what will be their motion at a given point in time.

The way to do that will be to use the molecular dynamics method. Where the first point is defining where the atoms are located initially, and what is the initial position for this typical relay on the initial vector. Furthermore, it is necessary to know the initial velocity, which depends potentially on the temperature. Where if the temperature is very high then that atoms will be moving very fast. Alternatively, maybe starting with an initial configuration where the atoms are initially mobile so the velocity has not started at zero and want to know how will the velocity change in the future. Therefore its needs to know the initial position and the initial velocity of the atoms as shown in Fig 4.1.

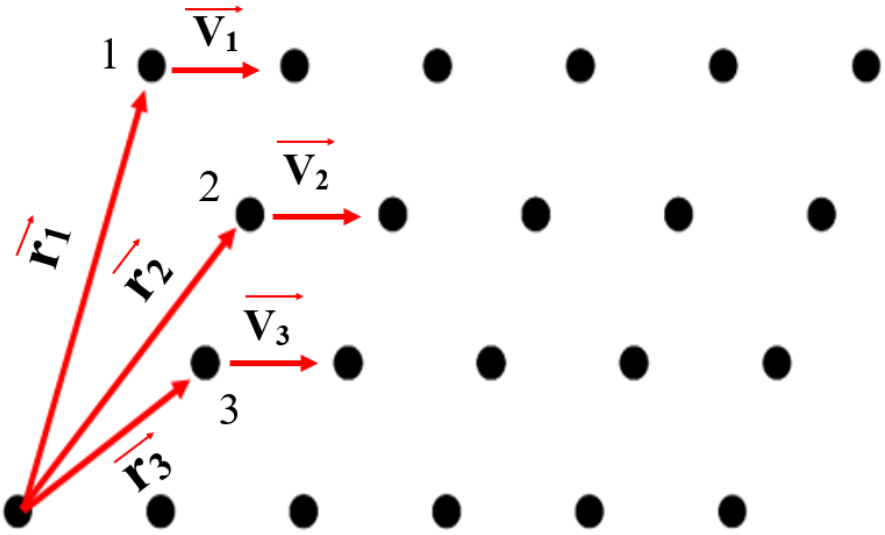

Fig 4.1 The initial atoms coordinates

4.2.2 Interatomic Energy

Interatomic Energy is the energy in between each atom, each pair of atom potentials will have a given energy. In the collection of atoms shown in Fig 4.2, every atom will apply forces on the other atoms. Where force is applied by atom 1 on atom 2 ($F_{1\rightarrow2}$) at the same time there is also a force applied by atom

2 on atom 1 ($F_{2\to1}$) and these two forces are in the same magnitude but in opposite directions due to the principle of action-reaction. However, atom 3 will also apply a force on atom 1 ($F_{3\to1}$) and all other atoms can apply a force on each other.

This integration is very important where there is a need for molecular dynamics to describe the motion of the atoms. With this method one must know what are their forces in order to know the forces its need to know what is the energy between each pair of atoms. That means if there are two atoms 1 and 2 this method needs to know what is going to be the energy (U_{12}) of interaction between atom 1 and atom 2, which will depend on the distance between them (r_{12}).

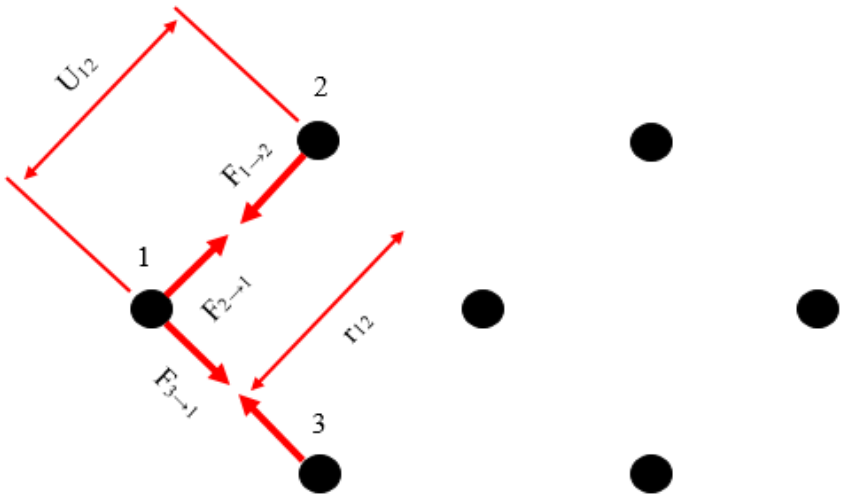

Fig 4.2 Interatomic energy reactions

4.2.3 What is that Interatomic Energy

There are different contributions to interatomic energy. For example in the collection of atoms in Fig 4.2, there are two atoms there may have different contributions of their energy of interaction (Ui_{12}) as below:

1- Coulombic Interaction

$$U_{col} = \frac{1}{4\pi\varepsilon_0}\frac{q_1 q_2}{r r_{12}}$$

Where:

q_1 = The Signed magnitude of the charge for atom one.

q_2 = The Signed magnitude of the charge for atom two.

r = The distance between the charges.

2- Van der Waals Interaction

The forces included in the Van der Waals are basically repulsion and attraction between surfaces, atoms, and molecules. There are also forces in the intermolecular scale. They are caused by the correlations where the nearby particles fluctuate in their polarizations (a consequence of quantum dynamics). The calculation is achieved via the formula:

$$U_{vdw} = -\frac{A}{r^6}$$

3- Electronic Repulsion

In the case of two atoms that come very close to each other, the electrons around each atom will not want to overlap. It cannot have two electrons at the same position at the same time Fig 4.3.

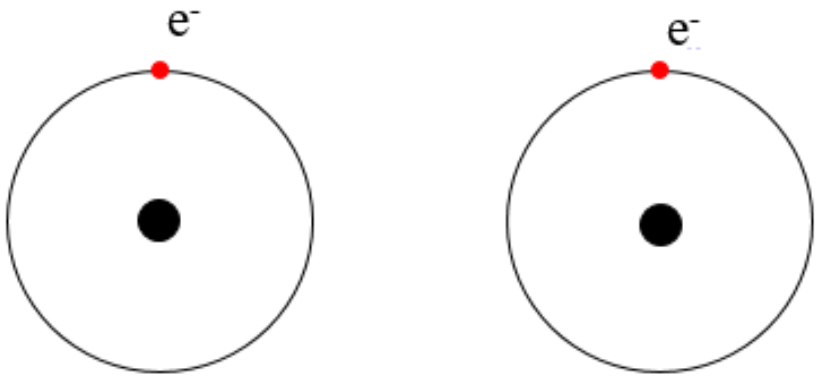

Fig 4.3 The electronic repulsion

4.2.4 Molecular Dynamics Cycle

The goal of the molecular dynamic method is basically, that if the energy in between each pair of atoms as a function of their distance is known, it is possible to use the motion of the atoms to determine their trajectory. This process involves several steps, as described:

- First step: Knowing the initial configurations (the collection of all positions of the atoms at a given time is called a configuration), that means the initial positions and initial velocity of each atom gone from one to N at time zero.

- Second step: Knowing the position of atom 1, the position of atom 2 and all the other atoms then assessing the distance between atom 1 and atom 2 (r_{12}). Moreover, if the distance is known it is possible to calculate the energy (U_{ij}) as a function of the distance (r_{ij}). Which is the energy of the interaction (U_{ij}) between atom i and atom j. In addition, if the energy between each pair of atoms is known, the total energy (U_{tot}) of the whole system will also be known, which will be the sum of all pairs of atoms as in the equation below:

$$U_{tot} = \sum_{i<j} U_{ij}$$

Where:

U_{tot} = The total energy.

U_{ij} = The energy of the interaction between each pair of atoms.

-Third step: Then by knowing the energy it is possible to calculate the force applied by a given atom j on atom i ($\overrightarrow{F_{j\to i}}$) from the equation below:

$$\overrightarrow{F_{j\to i}} = -\overrightarrow{grad}\, U_{ij}$$

Where:

$\overrightarrow{grad}$ = The gradient of the energy (equal to the height of the velocity head, the velocity of a fluid expressed in terms of the static pressure required to produce that velocity).

Then From the calculation of the force of atom j applied on atom i ($\overrightarrow{F_{j\to i}}$) the resultant force applied on atom i can be calculated (what is the sum of all forces that apply on atom i) from the equation below:

$$\overrightarrow{F_i} = \sum_{j \neq i} \overrightarrow{F_{j\to i}}$$

Where:

$\overrightarrow{F_i}$ = The sum of all forces that apply on atom i.

-Fourth step: If the force is known then the newton's law of motion can be used, because if the force and mass of each atom is known, then the acceleration ($\overrightarrow{a_i}$) can also be calculated from the equation below:

$$\overrightarrow{a_i} = \frac{\overrightarrow{F_i}}{m_i}$$

Where:

$\overrightarrow{a_i}$ = The acceleration of each atom.

m_i = The mass of atom.

By the determined initial position of the atoms and their initial velocity, then now knowing their acceleration, it all means that the movement of the atoms after a small increment of time can be calculated.

Furthermore, when the acceleration is known, then how the velocity of the atom changes is also known. Therefore, the new velocity of each atom cam be calculated after a small increment of time $\overrightarrow{v_i}(dt)$. And that leads to calculating what will be the new position of each atom after a small increment of time $\vec{r_i}(dt)$. This is then released to a numerical integration (if the acceleration is known, and then can be integrated to get the position and how the position is changing according to time. And by knowing a new position and the new velocity after a short time (dt), the new energy $U(dt)$ can be calculated at a short time interval later (dt), which leads to calculating the new forces $F(dt)$ at a short time later (dt), so the new acceleration $\overrightarrow{a_i}(dt)$ after a short time (dt) can be calculated.

Once again it is possible to do a new integration to calculate the new velocity at a time $\overrightarrow{v_i}(2dt)$. By doing so, it becomes possible to calculate the new velocity of the atoms according to time. Then by doing this cycle by cycle (as shown in Fig 4.4), it is possible to calculate how the velocity changes in time and how the position is changing in time, so these several things that must be known are the initial position of the atoms and their initial velocity. The second thing that is needed is the interaction between each type of atom considered. What is the general form of the energy between the pair of atoms as a function of their distance.

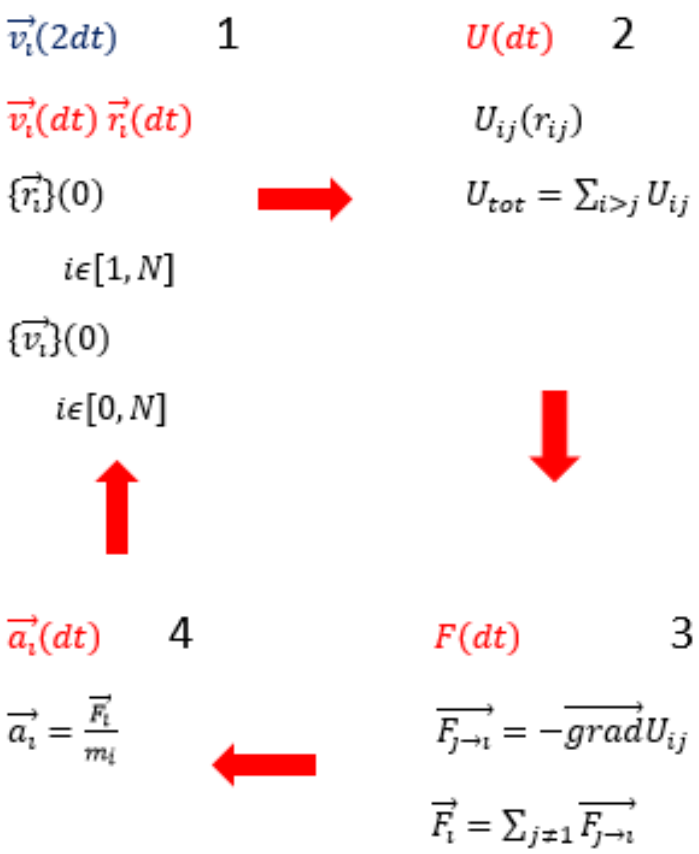

Fig 4.4 The molecular dynamics cycle

4.3 Molecular Dynamics Using LAMMPS

LAMMPS (Large-scale Atomic/Molecular Massively Parallel Simulator) is an open-source code designed to run classical MD simulations on parallel computers or processing units [159]. The ability of LAMMPS includes modeling of liquid, solid, or gaseous states. The level of modeling includes molecular, atomic, polymeric, metallic, biological, granular, and coarse-grained systems. It employs a broad range of boundary conditions as well as force fields. Starting from FORTRAN then rewritten in C++, LAMMPS was designed to be easily modified by the operator to include new functions such as new boundary conditions, atom types, force fields, or diagnostics [156].

LAMMPS is able to run on a single processor as well as parallel computing units. It can employ the same input script that contains various processing abilities [159]. Among other abilities of LAMMPS are commands to create and define the geometry and thermodynamic information as well as customizable text files of required data stated as an output at the end of the simulations. Continuation of the post-processing can also be performed using other software. Thus, it was selected as the MD code of choice for the work presented [156].

4.4 Molecular Dynamics Simulations Examples

4.4.1 Example 1: Copper Model

Another is a copper (Cu) system with a 3D unit cell constructed in C++ programming. The metal, copper, has a face-centered cubic crystal structure (FCC) with a Bravais lattice constant of 3.615 Å, so there are 4 Atoms as shown in Fig 4.5. The FCC structure can be generated from a FCC lattice with a four-atom basis as below:

First atom: N_1 = (0.0, 0.0, 0.0)
Second atom: N_2 = (0.5, 0.5, 0)
Third atom: N_3 = (0.5, 0, 0.5)
Fourth atom: N_4 = (0.0, 0.5, 0.5)

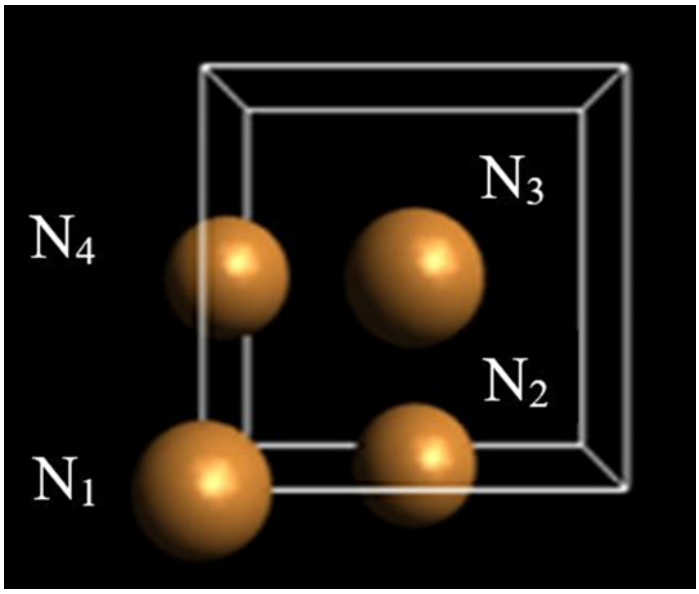

Fig 4.5 Example 1 copper model four basis atoms

Then the system repeated the trend on the x, y, and z-axis and shifted in the z-axis. Visualization of the results by OVITO Fig 4.6.

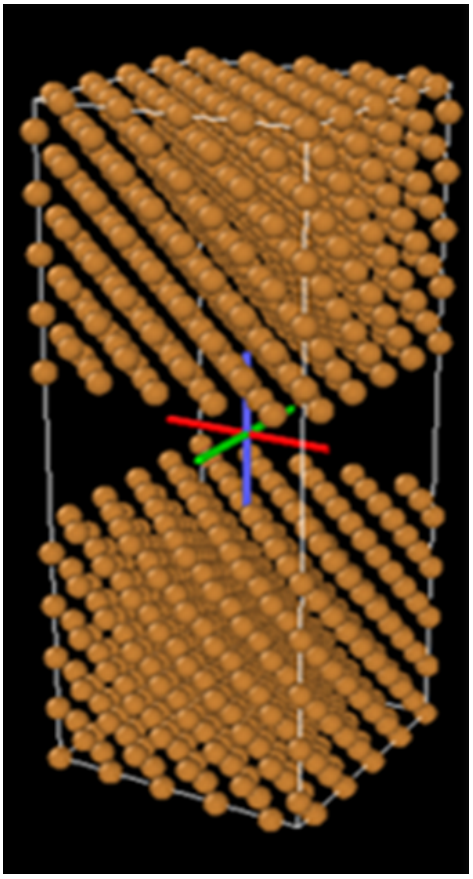

Fig 4.6 Example 1 copper model four basis atom repeated and shifted in the z direction

4.4.2 Example 2: Graphene and Carbon Nanotubes Model

Graphene is a single layer (monolayer) of carbon atoms, strongly bound in a hexagonal honeycomb lattice. It is an allotrope of carbon in the form of a plane of sp2-bonded atoms with a molecular bond length of 0.14 nm as shown (Fig 4.7). Layers of graphene stacked on top of each other form graphite.

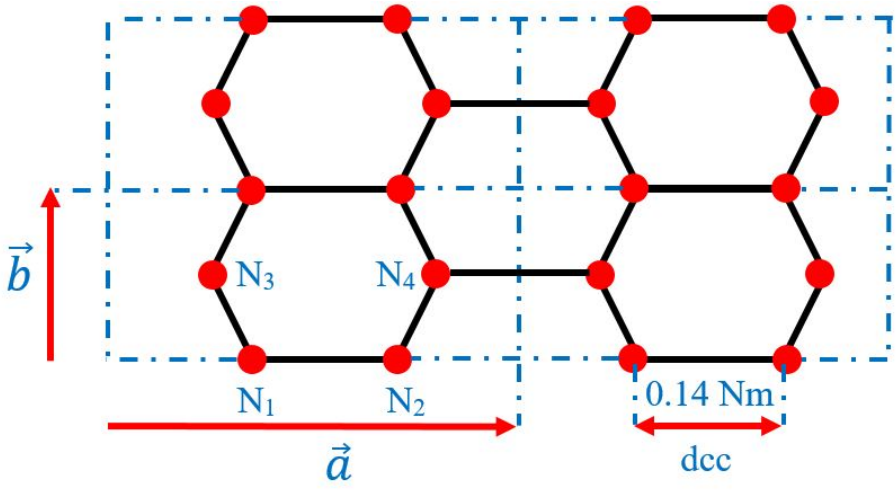

Fig 4.7 Schematic of the structure of a graphene sheet.

A four atoms unit cell fragment of graphene structure ($N_1,\ N_2,\ N_3\ and\ N_4$) was generated by C++ programming Fig 4.7, then atomic coordinates were derived as below:

$\vec{a} = [3\ dcc, 0]$

$\vec{b} = \left[0, \sqrt{3}\ dcc\right]$

$N_1 = [dcc, 0]$

$N_2 = [2dcc, 0]$

$N_3 = \left[\frac{1}{2}dcc, \frac{\sqrt{3}}{2}dcc\right]$

$N_4 = \left[\frac{5}{2}dcc, \frac{\sqrt{3}}{2}dcc\right]$

Replicating the four atoms in a unit cell in x and y directions to become a graphene sheet, which was then rotated around the x-axis to become a carbon nanotube Fig 4.8.

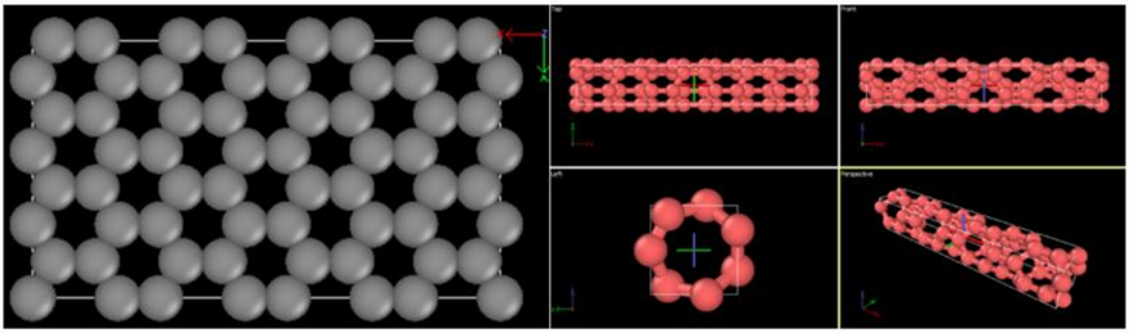

Fig 4.8 Example 2 graphene and CNT model

4.4.3 Example 3: Copper and Graphene Model

The third example was generated using a Large-scale Atomic/Molecular Massively Parallel Simulator (LAMMPS), which was a molecular dynamics program from Sandia National Laboratories. The system, which comprised of two copper (Cu) surfaces with a graphene sheet between them, was set up and visualized (Fig 4.9).

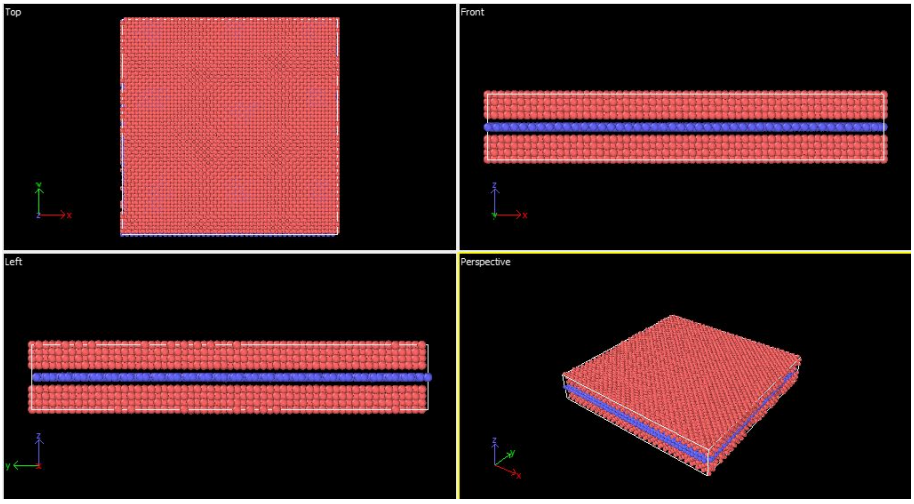

Fig 4.9 Example 3 of copper surfaces with a graphene sheet between them model

4.5 Simulation Method

In this dissertation, a molecular dynamics simulation for tribological behaviors of CNTs, graphene, and copper nanoparticle (Cu) was performed via LAMMPS. In order to investigate the responses of friction coefficients (μ) under different normal forces in the following, detailed method to perform a molecular dynamics simulation, where the simulation is used to study the friction coefficient (μ).

The friction coefficient is defined as the ratio of the tangential force (F_T) to the normal force (F_N). So in the simulation in addition to enforcing slip, the relative motion of two surfaces, a constant normal force (F_N) needs to be applied that acts in the direction that should be normal to the surface, acting on the upper surface layer, towards the bottom layer, moving the upper surface towards the bottom one. Moreover, the resulting tangential force (F_T) needs to be calculated. This is achievable with fixes that are available in LAMMPS. There is a command (fix addforce), which allows adding an external force (by adding constant force to a group of atoms – those belonging to the upper surface), in order to simulate loading.

There is also a command (compute reduce) which allows to reduce (sum) forces (acting on individual atoms), to find the resultant force acting on a group of atoms (those belonging to the upper surface). This reduced operation can be used to find the tangential force (F_T) and to monitor the normal force (F_N) by examining different components of this resultant force. It is important in this case to perform time averaging, as both forces will fluctuate in the simulation. Then by (fix ave/time) command will find the real values that are needed to perform time-averaging.

Therefore, the idea was as follows:

1) Setting up the system, which is comprised of two surfaces.
2) Equilibrating the system to start with (for the chosen temperature).
3) Applying an external interaction enforcing the relative motion of two surfaces, assigning constant velocity to the upper surface from left to right in the direction (x) and fixing the bottom one and at the same time applying normal force (F_N) to the upper surface from top to bottom in (-z) direction (Figure 4.10).
4) From such a simulation two values were obtained: Normal force (F_N) and Tangential force (F_T).
5) During the sliding simulation, the way these two forces, normal (F_N) and tangential (F_T) fluctuate should be noted and used to compute their time averages as previously described.
6) Repeating the above procedure (simulation) for several different values of the normal force. Thus the way the tangential force (F_T) depends on the normal force (F_N) could be determined. This dependence should be (in theory) linear, the slope of it allows to compute the value of the friction coefficient (μ).

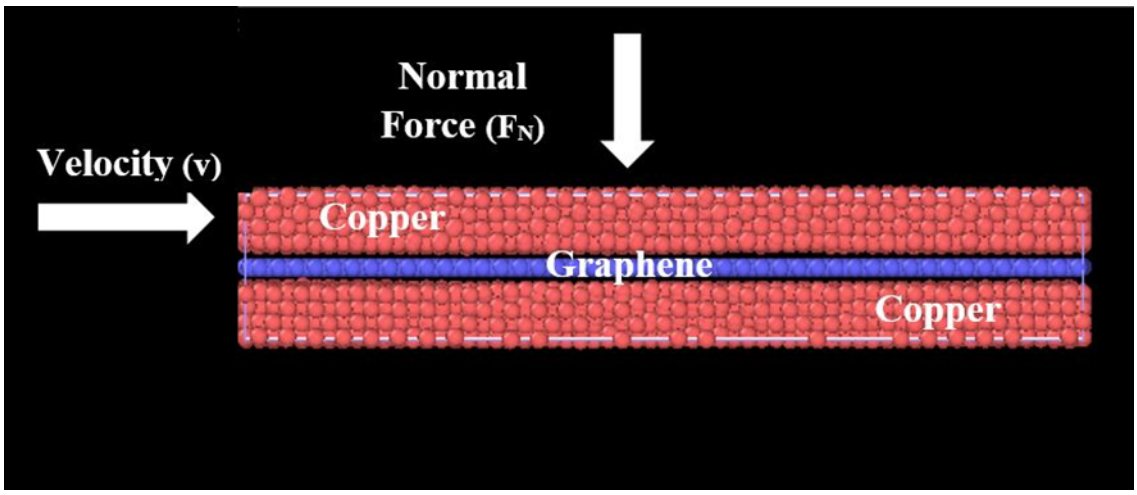

Fig 4.10 An illustration of system setup

So the model was designed using the (LAMMPS) program, which was composed of two FCC copper lattice structures with a graphene sheet between them (Figure 4.9). The length (Lx), width (Ly), and thickness (Lz) of the upper and lower copper surfaces were 108 Å, 108 Å, and 20 Å, respectively (Figure 4.11). At the same time, the graphene sheet has the exact dimensions of length and width as the copper surfaces, but the thickness of only one atom. Therefore, graphene is considered two-dimensional. The system was controlled under a hybrid of a microcanonical NVT. Molecular dynamics simulation was performed with a 1 femtosecond time step and the system temperature was controlled by velocity scaling to remain at 300 K and 423.15 K with different applied forces values as below:

F_N1 = 6.2415e-6 eV/Å F_N2 = 2.4966e-5 eV/Å F_N3 = 6.2415e-5 eV/Å

The above values of the forces controlled the normal forces applied on the upper copper layer. The friction simulations were performed by sliding the upper copper layer laterally (in -x direction) with a sliding rate of 10 m/s. The force field described the covalent bond potential of the (CCu) system coupled with the Bond Order Potential (bop) potential for long-range van der Waals interaction and was implemented in LAMMPS and used in this work.

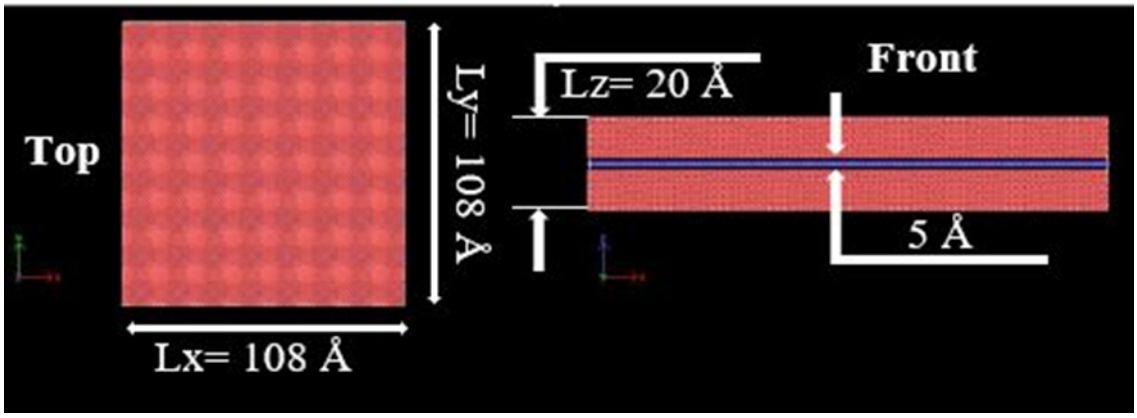

Fig 4.11 Visualization of system dimension arrangement

The acting normal forces (F_N) applied tangential forces (F_T) which lead to the average coefficients of friction (μ), which were obtained by Linear Regression Using Least Squares Method - Line of Best Fit Equation as below.

$$m = \frac{n\sum xy - \sum x \sum y}{n\sum x^2 - (\sum x)^2}$$

Where:

m = The line slope

n = The number of values

x = The coordinate value in the x-direction

y = The coordinate value in the y-direction

4.6 Results and Discussion

The friction coefficients (μ) were determined by calculating the ratio of tangential forces(F_T) to normal forces(F_N) acting on individual atoms of CCu nanoparticles, as shown in Table 4.1.

Table 4.1. The average normal and tangential forces for individual atoms

	300 Kelvin		423.15 Kelvin	
	F_N (eV/Å)	F_T (eV/Å)	F_N (eV/Å)	F_T (eV/Å)
F_N1	0.066270567	0.051898095	0.037733906	0.052596196
F_N2	0.071248345	0.078530236	0.063139716	0.10269945
F_N3	0.076678667	0.210594993	0.075518446	0.216788071

The friction coefficients (μ) were presented in Figures 4.11 and 4.12. The values were obtained by calculating the ensemble average of the normal force to tangential force ratio acting on the CCu nanoparticle. The mean values at 300K and 423.15K were subjected to least square fitting to obtain the average μ, which was found to be 0.209226583 and 0.057723591, respectively.

In this dissertation, the tribological behaviors and the atomistic origins of friction of copper and graphene nanoparticles were analyzed using molecular dynamics simulations, the interaction slip between two FCC copper surfaces with hexagonal graphene flakes between them was simulated using molecular dynamics. The developed LAMMPS code was utilized to set up the friction model and run the simulations.

The effects of the interference between the two copper surfaces with hexagonal graphene flakes between them, sliding velocity and temperature were considered. Furthermore, tangential and normal forces acting on individual atoms, which control friction mechanisms, were studied. The friction coefficients (μ) were determined by calculating the ensemble average of the ratio between the normal force and the tangential force on the upper copper surface nanoparticle.

In the absence of a graphene layer, the atoms will form bonds and act as one single structure. This will occur at high forces during collisions between surfaces. This bonding or cohesion (or adhesion) will define the sliding process in forming an increased value of the effective coefficient of friction. Thus, for current geometry, the friction values at the macro-scale level are not greatly different from those at the nano-scale level, when a graphene layer is present between the sliding surfaces. This is true for overall average values.

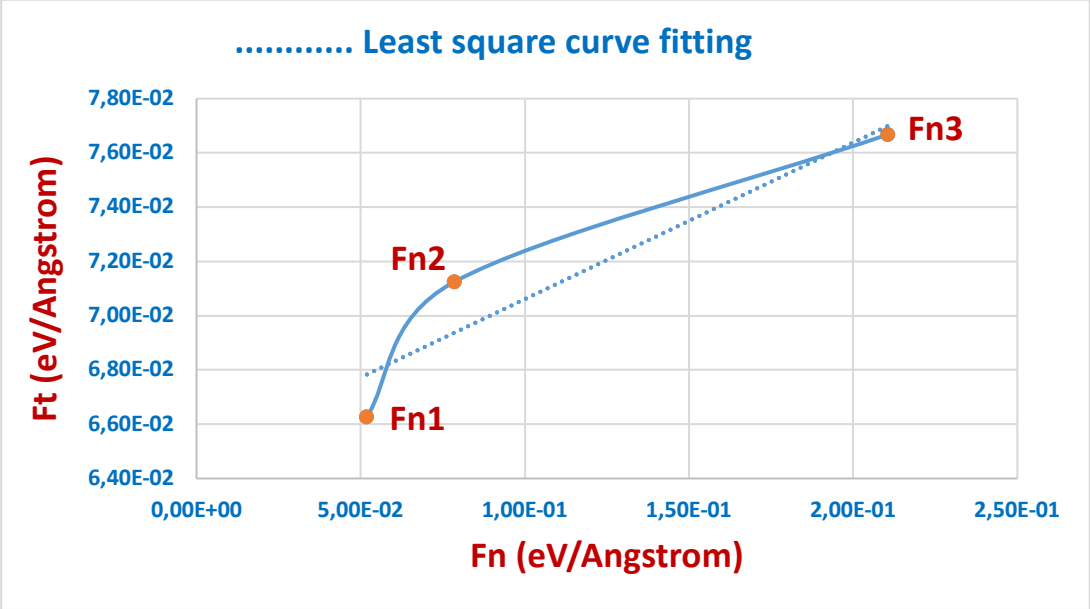

Fig 4.12 Tangential force to the normal force ratio at 300 K and 10 m/s

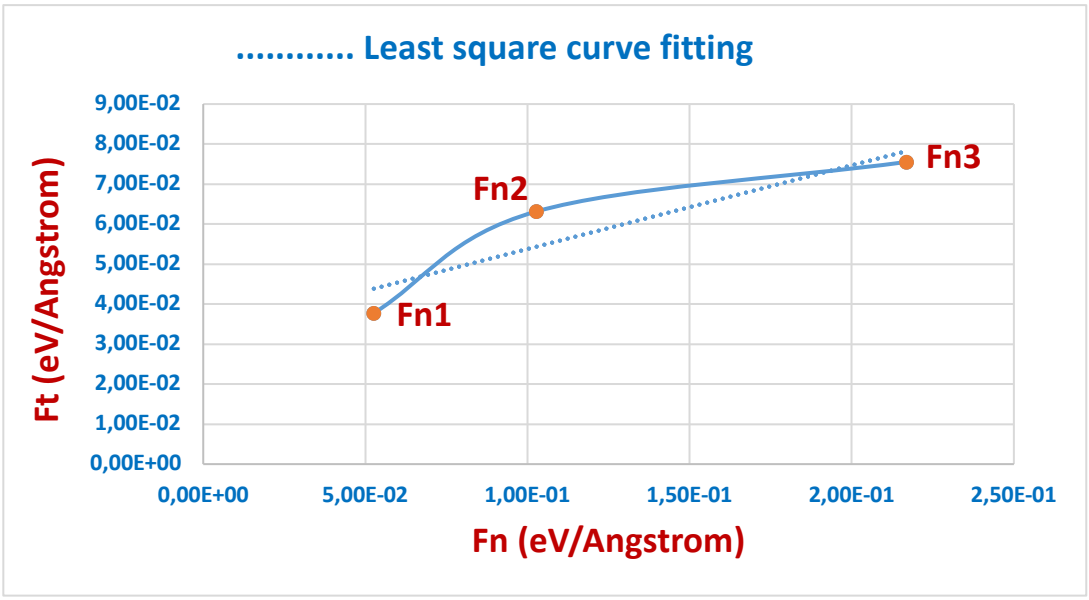

Fig 4.13 Tangential force to the normal force ratio at 423.15 K and 10 m/s

For the current velocity applied in this study, it was shown that a lower range of velocities would provide more contact time thus increasing the adhesion effect.

The nature of the surface or structures at the nano-scale is discretized and not smooth. By controlling the discretization of the surfaces in contact, it is possible to match the lattice orientations, which would directly affect the frictional mechanisms. In the end, the ability to control the lattice orientation would enable the customization of friction characteristics in the process of nanostructures fabrication.

5
Results and Discussion

5.1 Overview

This chapter outlines the experimental tests conducted, the conclusions drawn, and the hypotheses proposed, all aimed at understanding the tribological mechanisms associated with incorporating carbon nanotubes (CNTs) into lubricants. By gaining insight into these mechanisms, we aim to develop more effective lubricants that can reduce friction and vibration, potentially leading to a new generation of lubricant technology.

The experiments included two engine tests, an Amsler tribometer test, and a roller bearing test.

The first engine test involved an experimental piston made of standard aluminum alloy, which was coated with a layer of CNTs applied through an aqueous solution spray with a binder. The objective was to evaluate the potential of CNTs in reducing frictional losses in engines. The second engine test focused on improving the lubrication properties of engine oils by adding trace amounts of CNTs, aiming to address issues related to CNT re-agglomeration.

In the third experiment, we investigated a high-viscosity lubricant using the Amsler tribometer, comparing it to high-quality commercially available lithium grease. The results showed nearly a 50% reduction in wear when the lithium grease was replaced with a CNT-based lubricant. This suggests that CNTs have a potential anti-wear mechanism, although further investigation is needed to fully understand this effect.

Drawing insights from the experimental outcomes, several hypotheses could be postulated:

1) CNTs possess the capability to conduct heat and electrons along their length, thereby influencing tribological mechanisms.
2) The structure of CNTs may undergo modifications during the friction process, potentially resulting in the in-situ creation of carbon-based AW films.
3) Even when introduced in trace amounts, CNTs were able to effectively alter the arrangement of oil molecules, aligning with the shear-induced ordering transition theory.

5.2 The Effect of Carbon Nanotubes Coating on Piston to Engine Performance

5.2.1 Friction Evaluation

A preliminary assessment was conducted on both the test and final versions of the pistons, and only one set of pistons (labeled as A2 and A3) successfully passed the initial engine test, making them eligible for use in the fundamental friction tests. However, the assessment for the test version was halted due to unstable behavior in friction losses.

For the final version of the pistons (pistons A2 and A3), the testing process was successfully completed. Since a consistent measurement method was applied for both the preliminary and final tests, the results were deemed reliable in terms of measurement reproducibility.

5.2.2 Engine Motoring Torque

It's important to note that the recorded engine motoring torque values were influenced by the following primary components:

a) Friction losses taking place between the piston skirt and the cylinder, which constitute the primary focus of this study.

b) Friction losses occurring between the piston rings and the cylinder.

c) Friction losses taking place in the crankshaft bearings.

d) The release of a portion of the compressed mixture from the cylinder into the crankcase (known as blow-by), along with thermodynamic losses associated with the heating of the cylinder walls.

Items (b) to (d) were considered not to be affected by the addition of a CNT layer on the piston skirt surface. Hence, engine motoring torque recorded for an engine with CNT-coated pistons with similar operating conditions as of the engine with standard pistons should be valid for the assessment of the effect of CNT coating on friction losses.

Motoring torques were compared between engines with the experimental CNT coated piston and an engine with standard piston over a range of engine speed with oil temperatures of 50ºC, 80ºC, and 110ºC. The comparison was shown in Figure 5.1 as the mean value of the engine motoring torque over a period of two seconds. Next, Figure 5.2 shows the comparison of instantaneous motoring torque for standard aluminum and CNT-coated pistons at the speed of 500 RPM and oil temperature of 50ºC. Three series of tests were performed with varied values of air supply pressure and oil temperature. Air supply pressure is translated into the amount of force exerted by the piston on the cylinder wall.

The application of CNT on piston skirts reduced the friction losses significantly. This was represented by the decrease in engine motoring torque by up to 16%, as shown in Figure 5.1. The specified reduction, however, was on the overall friction losses that also included the losses at piston rings and crankshaft bearings. The results of this study are comparable to those found in similar literature [160, 161]. The reduction in friction losses in the engine with a CNT-coated experimental piston, with changes only on the skirt surface material, was significant.

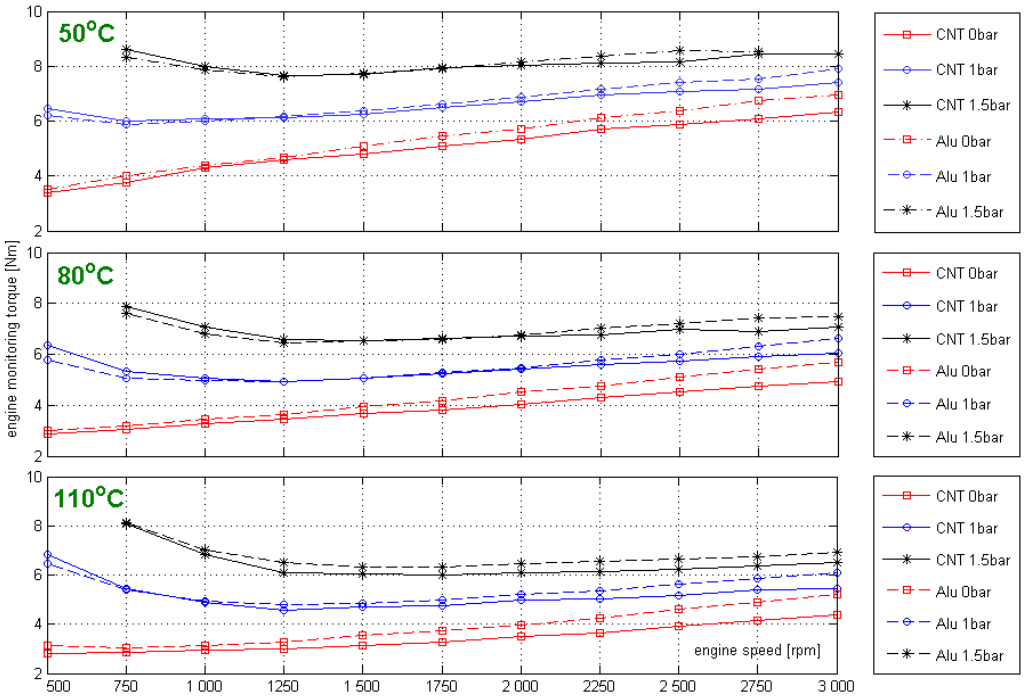

Fig. 5.1 Engine friction losses for CNT-coated experimental pistons and standard pistons with respect to engine speed, with measurement at different cylinder supply pressure and engine oil temperature

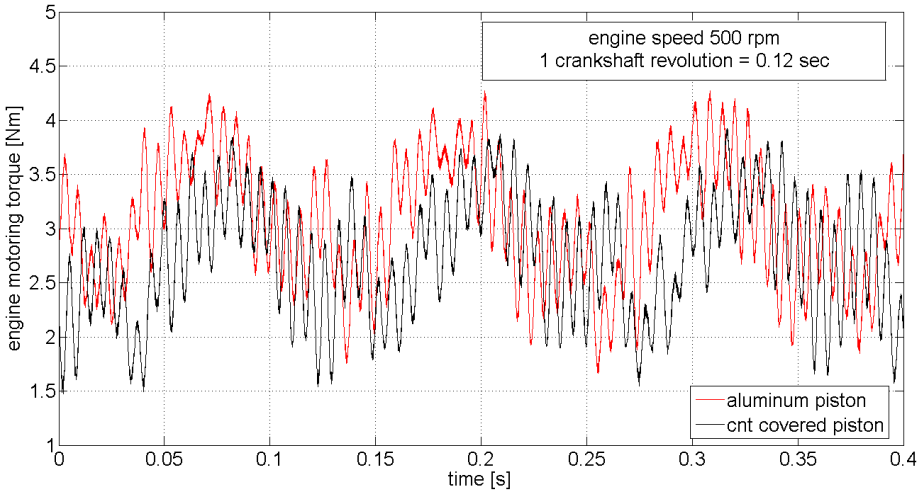

Fig. 5.2 Engine motoring torque signal comparison for CNT-coated experimental pistons and standard pistons

The substantial reduction in friction losses observed in the engine with the CNT-coated experimental piston was likely not solely attributable to changes in the frictional properties of the piston skirt. This study revealed that the applied CNT coating underwent rapid wear during testing. After several hours of operation, the thickness of the CNT coating had diminished by approximately 20 µm, as depicted in Figure 5.3 and Figure 5.5. It is plausible that the worn off CNT material dispersed into the engine oil and could have circulated with it, reaching surfaces experiencing friction along with the lubricating oil. It is possible, that this factor was likely to contribute to the substantial reduction in friction losses that was observed in the research.

Graphite or molybdenum disulfide-containing resins are widely used as piston coating for the benefit of friction reduction [161-164]. However, the benefits those provide seem to be limited compared to the materials used in this study. In normal operating conditions, frictional losses mostly occur at the hydrodynamic friction region. At both low and high engine speeds, frictional losses become more pronounced in the mixed friction region. The presence of CNT in lubricating oil appears to have reduced frictional losses in both regions [64].

The relationship between the reduction of frictional losses as a result of the application of nanotubes with engine speed and load was demonstrated in this study. At high engine speed with low load, the benefit of the nanotubes addition was most significant. This finding may suggest that CNT content in oil had contributed to frictional losses mainly at the hydrodynamics friction region. However, the reduction in frictional losses in relation to the engine speed could include a more complex mechanism as suggested in the literature [64]. It is possible that the high engine speed had contributed to better dispersion of nanotubes in the lubricant.

5.2.3 Carbon Nanotubes Coating Effect on Piston and Cylinder Wall Surface

Post-test observations on the experimental CNT coated piston found that the CNT adhesion on the aluminum surface was sufficiently strong. There was no sign of CNT layer peeling observed on the aluminum surface. The abrasion sign of CNTs on the cylinder wall was visible and had been smoothed. However, there was no exposed aluminum surface observed on the coated piston as a result of the

abrasion.

Figure 5.3 illustrates the extent of abrasion observed on the CNT-coated piston. This abrasion intensity was determined by comparing the profile of the experimental piston skirt's shape before and after the engine tests. Furthermore, the abrasion occurring on the CNT surface layer played a role in decreasing the surface roughness of the experimental piston skirt during engine operation. Figure 5.4 provides an overview of the key features of the piston's surface profile, while Table 5.1 presents the parameters used to describe the surface roughness of the experimental piston.

The CNT coating was initially applied at an estimated thickness of 40 microns as shown in Figure 5.3. The radius of the CNT-coated piston skirt was taken on the piston thrust side at horizontal levels L1, L2, and L3. These measurements were conducted using coordinate measuring techniques both before the engine test (solid lines L1B, L2B, L3B) and after the engine test (dashed lines L1A, L2A, L3A). The exact thickness was difficult to measure due to the surface roughness of both aluminum and CNTs, this was similar in the case of standard graphite and molybdenum coating.

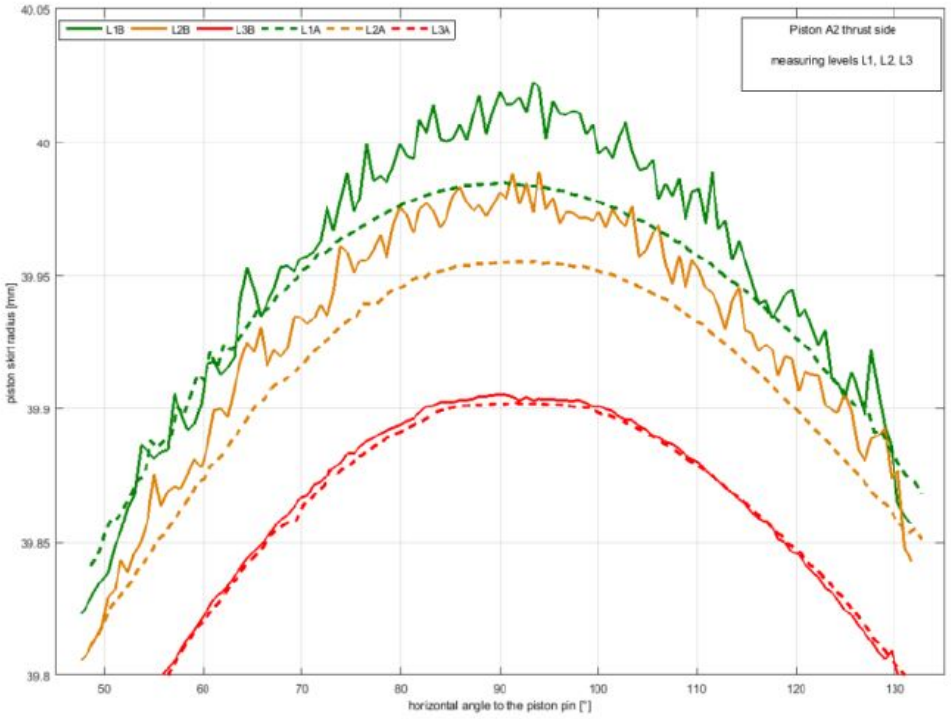

Fig. 5.3 CNT-coated piston skirt radius, taken on the piston thrust side at horizontal levels L1, L2, and L3

Table 5.1. Parameters used to characterize the surface roughness of the pistons

Piston		Reference	A2 and A3 Experimental (average values)				
Research phase		after engine tests	before applying CNTs	before engine tests	after engine tests		
Measurement method		mean	mean	mean	major thrust side	minor thrust side	mean after tests
Parameter	Ra	3.99	3.39	4.72	3.33	4.18	3.75
	Rq	4.57	3.95	5.78	3.80	4.85	4.33

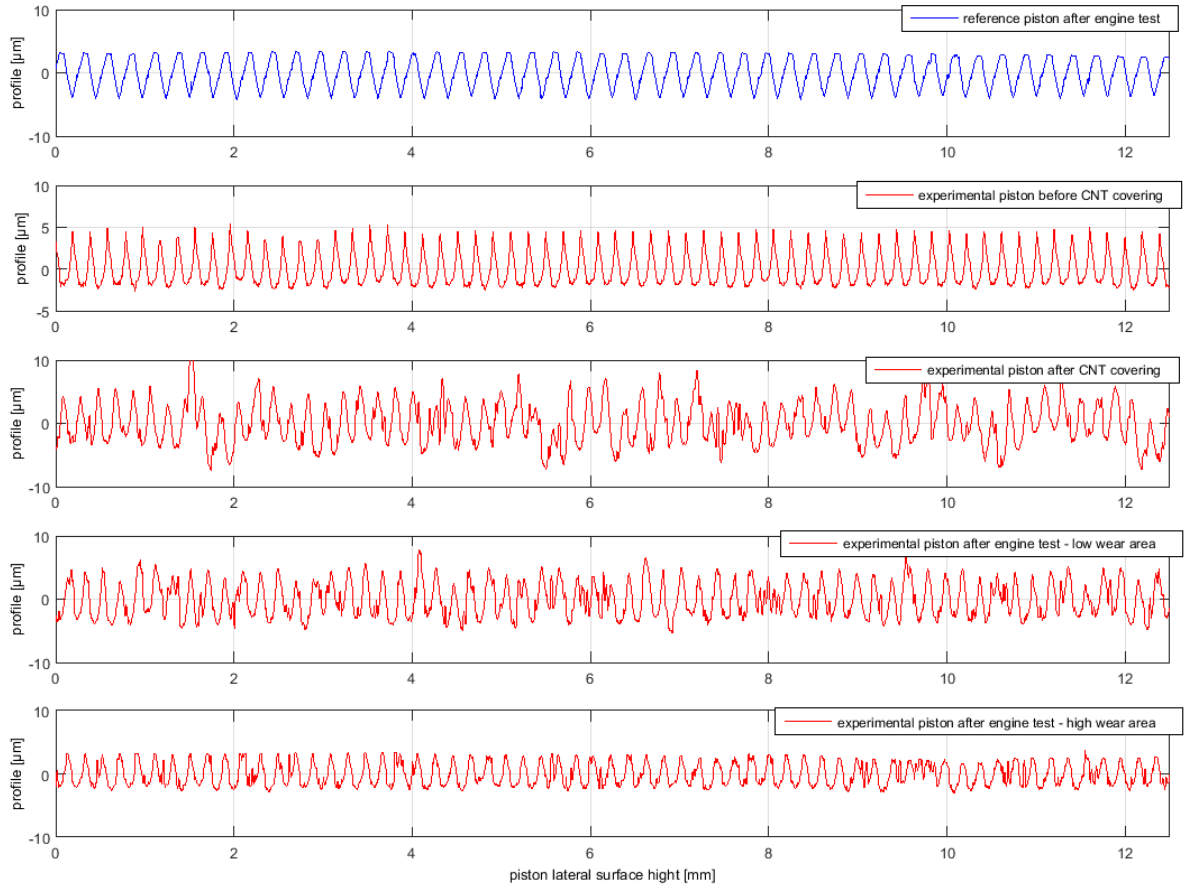

	Rt	15.57	16.91	38.41	17.42	24.21	20.82
	Rsk	-0.06	0.79	0.4	0.26	0.23	0.24

Fig. 5.4 Profile of the piston's lateral surface, which was utilized for the friction measurements

Fig. 5.5 Illustrates the piston wear resulting from the engine tests. It showcases the bearing surface on the major thrust side on the left and the minor thrust side on the right. The top section presents the shape of the bearing surface of the piston coated with nanotubes, while the bottom section displays the surface topography. Figure 5.5 (a) and (b) show the bearing surface contour for the CNT-coated piston. While Figure 5.5 (c) and (d) show the topographic profile of the same bearing surface. Figure 5.5 (a) and (c) correspond to the major thrust side of the piston, and Figure 5.5 (b) and (d) correspond to the minor thrust side of the piston. The results in Figure 5.5 are related to piston A3 at the end of the engine test. As for other experimental pistons, the relative values were similar to those found for piston A3. The piston was measured at 52 sections for its cylindrical diameter before and after the engine tests. Surface wear was found to be insignificant with an average wear of 0.8 µm observed.

The pistons' shape was measured with the coordinate measurement method before and after the engine test for both standard and CNT-coated experimental pistons. Piston diameters after the engine test were 79.998 mm and 79.990 mm for the standard piston and CNT-coated experimental piston respectively. The recorded piston diameters were close and the thickness difference of 8 microns was assumed to have no direct effect on the friction losses.

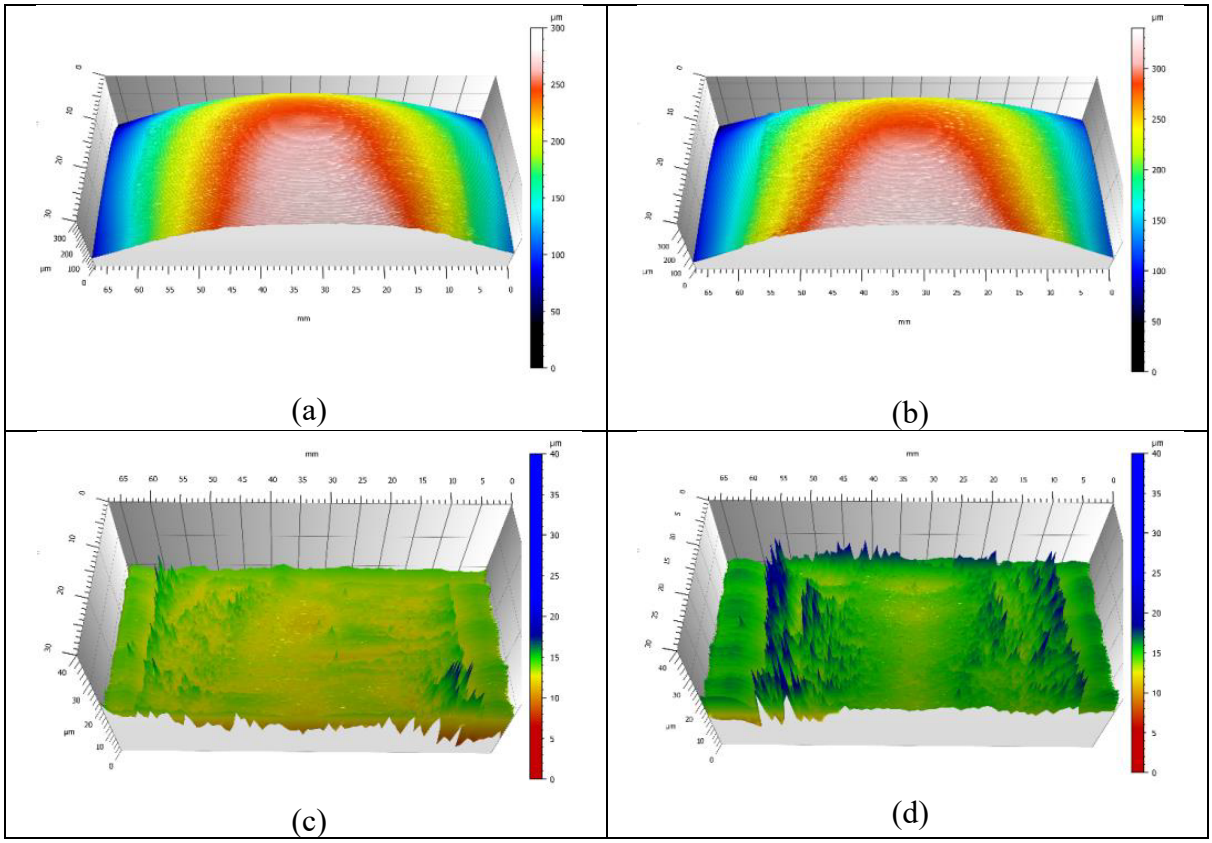

Fig. 5.5 Piston wear resulting from the engine tests

Surface roughness (Ra) values of 3.99 microns and 3.75 microns were measured for the standard piston and CNT-coated experimental piston respectively. The values were found to be close to each other, which indicates that the frictional losses were comparable.

Towards the conclusion of the test, the regions coated with nanotubes displayed distinct wear patterns, primarily concentrated near the coordinates of 5 mm and 60 mm where they intersect with the horizontal axis, as depicted in Figure 5.5. The wear characteristics of the CNT layer were depicted through surface topography, revealing a noticeable reduction in CNT layer roughness at the piston's center. As anticipated, more substantial wear was observed on the major piston thrust side.

The CNT layer experiences wear during engine operation due to the cohesion weakness of the spray-coated layer. However, further examination under SEM at the end of the test showed that the occurring wear phenomena did not lead to the destruction of the CNT layer.

Cylinder measurements conducted at both the start and the end of the piston test did not exhibit any notable wear on the cylinder liner. However, it's imperative to acknowledge that real durability tests cannot be supplanted by brief evaluations. Subsequent to the test involving the CNT-coated experimental piston, engine disassembly was conducted, revealing no indications of accelerated wear on any friction-related components, particularly the crankshaft bearings and piston assembly.

The SEM images in Figure 5.6 and the EDS analysis in Figure 5.7 revealed CNTs' capability to attract and retain foreign particles on their surfaces. While these particles may appear as contaminants in the technical evaluation of CNT images during engine operation, they could potentially play a beneficial

role from a tribological perspective. This behavior of CNTs opens up the possibility of functionalizing CNTs by decorating them with other nanoparticles known to possess desirable tribological properties.

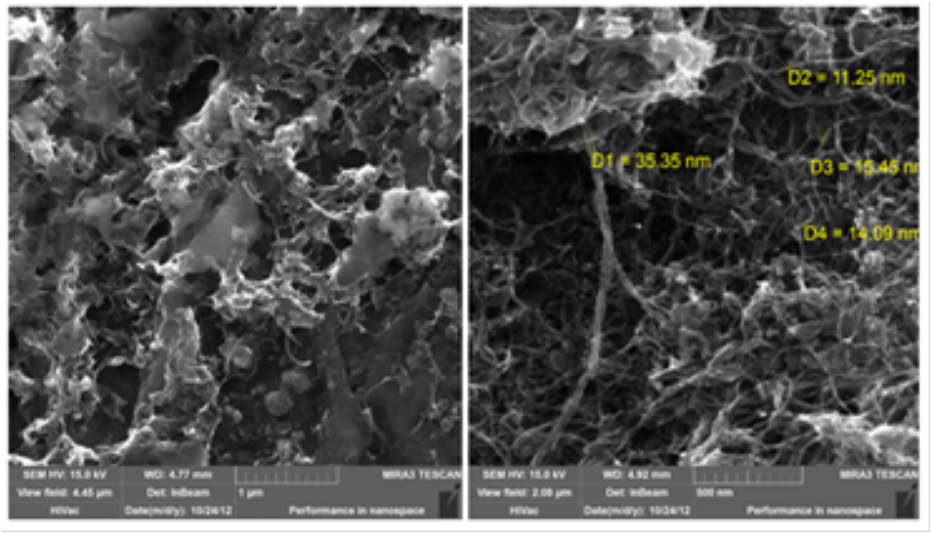

Fig. 5.6. Surface of the piston coated with CNTs. This image was captured after the engine tests from a sample that had undergone a washing process using acetone

SEM imaging of the CNT coating layer structure on the experimental CNT-coated piston was shown in Figure 5.6. The image was recorded at the end of the engine test. Through EDS analysis, it was found that apart from carbon, the material composition of the surface also consisted of aluminum and iron. These were the abrasion products of the piston surface that was subject to friction. Additionally, silicon, which was a component of the aluminum alloy, was also found. The elements oxygen and potassium were present due to the substance used to apply the CNT coating onto the piston surface. Figure 5.7 shows the details of the spectroscopy findings.

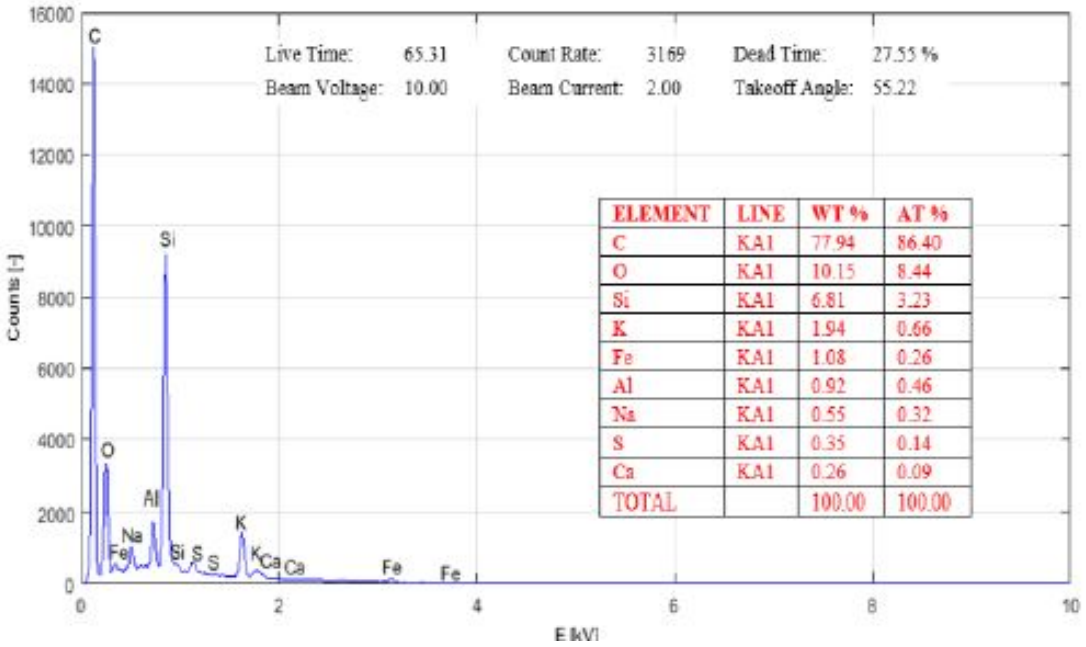

ELEMENT	LINE	WT %	AT %
C	KA1	77.94	86.40
O	KA1	10.15	8.44
Si	KA1	6.81	3.23
K	KA1	1.94	0.66
Fe	KA1	1.08	0.26
Al	KA1	0.92	0.46
Na	KA1	0.55	0.32
S	KA1	0.35	0.14
Ca	KA1	0.26	0.09
TOTAL		100.00	100.00

Fig. 5.7 EDS spectroscopy results for the surface of the CNT layer on the piston dismounted after the engine tests were completed

Subsequently, a computer X-ray tomography (CT) scan was conducted on the CNT-coated experimental piston. The CT scan revealed a strong adhesion of the CNT layer to the piston wall, with no presence of air bubbles along the layer's border.

5.2.4 Advanced Carbon Nanotubes Coating Technology

The CNT application technique on the piston skirt selected for this study was the spraying method. However, previous studies suggested that application of CNTs by the use of polymer resins would also give advantageous tribological properties [73, 165-171]. IG type CNT with ferromagnetic catalyst nanoparticles ends has specific benefit in this application. The use of that type of CNTs would enable them to interact with the electromagnetic field, hence allowing for the possibility to produce an ordered spatial structure.

The possibility of using a method based on electrolytic MWCNT deposition from aqueous solution was also evaluated in this study. A layer of high adhesion and good properties can be obtained through performing the CNT deposition by periodic reversing current, provided suitable piston preparation. Figure 5.8 shows the relatively ordered spatial structure that characterized the obtained layer. The layer characteristics were different from the layer structure of sprayed CNTs. CNT layer application by electrodeposition has its advantage on the anisotropic properties that could contribute to friction reduction.

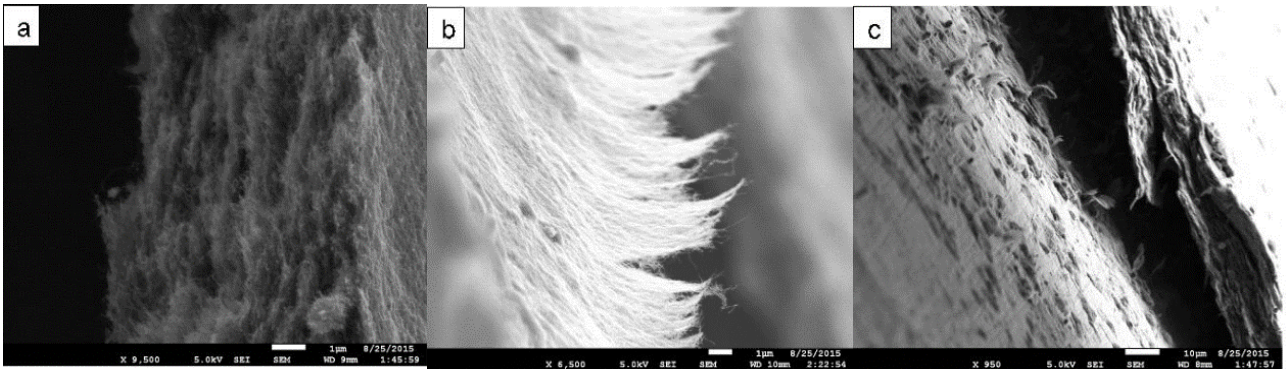

Fig. 5.8 CNT layers acquired through the process of electrolytic deposition: a) structured arrangement of CNTs within the layers, as seen in a cross-section. b) ordered CNT structure on the layer's surface after bending and rupture. c) The oxide layer, created chemically on the metal surface

It is possible that a multi-layered application of CNT onto the piston skirt could be done, where each layer would perform a specialized function. This, however, was seen as a long-term effort in this field of CNTs application. The layer closest to the cylinder wall, that was in contact with the cylinder wall, should protect the engine from seizing. Moving inwards towards the piston surface, the next layer should have advantageous tribological properties, which would also act as a damping layer. The layer nearest to the piston surface should provide a strong adhesion. The use of nanoparticles with known advantageous tribological properties such as Co, Mo, and W could also improve the multi-layer CNT properties.

5.3 The Effect of Carbon Nanotubes Dispersion on Engine Performance

During the experiment, a concentration of 0.03% MWCNT was discovered to be effective in enhancing the viscosity of lubrication oil. Other carbon allotropes did not exhibit this improvement, which is

attributed to the high aspect ratio of CNTs. Thus, the change in oil viscosity can serve as a dependable indicator for evaluating the quality of CNT dispersion. It's worth noting that the tests were conducted using OIL 1, as detailed in Chapter 3, and that changes in viscosity didn't significantly affect friction. The viscosity of the oil was more affected by temperature changes during engine warm-up. It's intriguing to observe that lubricating oil containing well-dispersed CNT functions like a non-Newtonian fluid, making it ideal for use in a complex tribological system with various entrainment speeds and contact points.

5.3.1 Analysis of Engine Oil Tested During Engine Warm Up

During the engine warm-up test, a very low concentration of CNT additive in the lubricating oil contributed to a friction reduction of 6% in the engine. Additionally, acceleration vibration reduction was also observed during the initial 5 minutes of the experiment. The findings are represented in Figure 5.9.

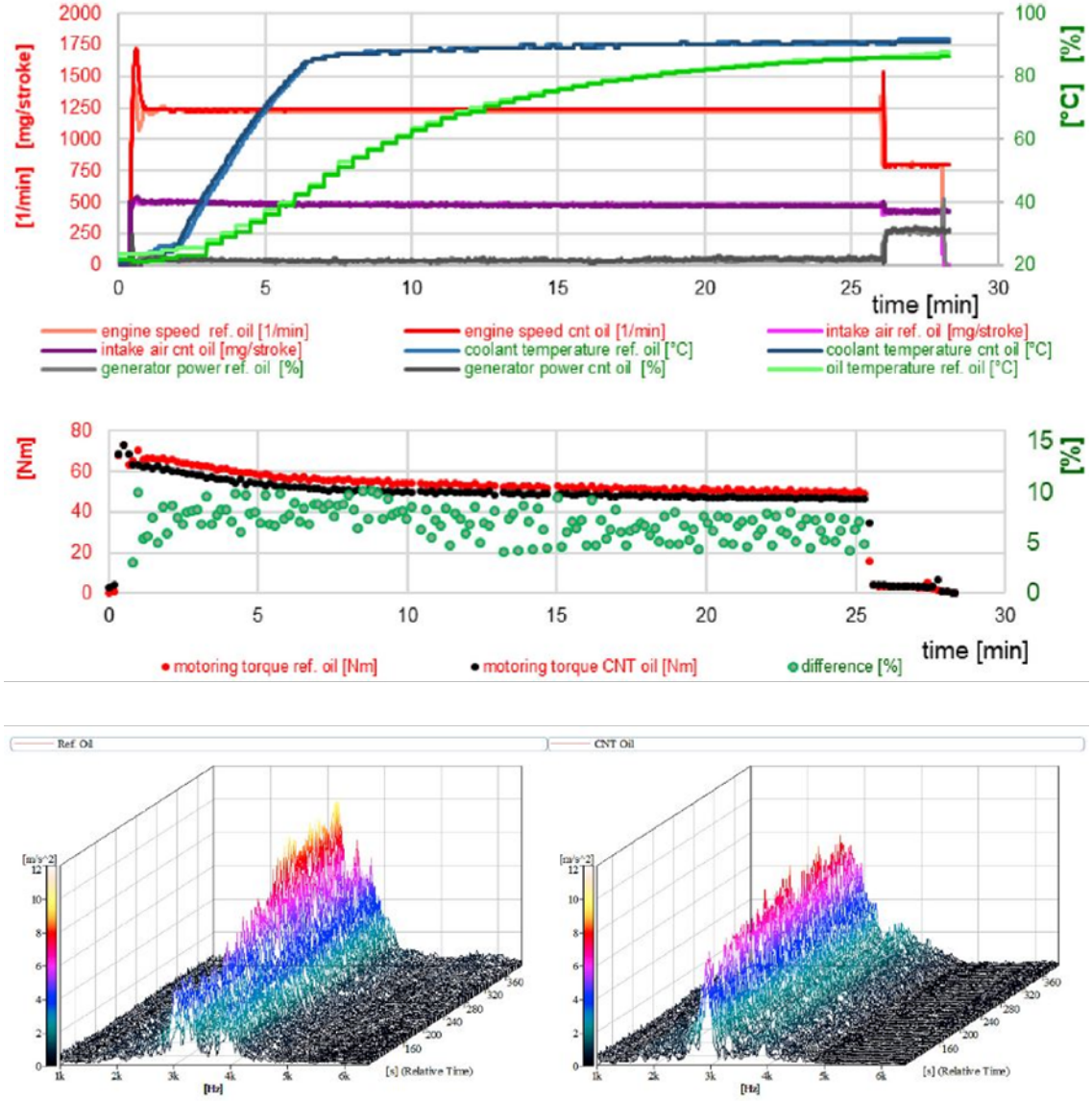

Fig. 5.9 Engine parameters measured from experiment 1 (top), motoring torque comparison between reference oil and CNT-enriched oil (middle), and vibrations at the axis of the secondary motion of the piston (bottom).

The lubricating oil was later re-examined under an optical microscope after the engine tests.

Significant changes were observed in the lubrication oil as shown in Figure 5.10. CNT dispersion had improved with the engine operating condition. The CNT dispersion was visible under the microscope as large and agglomerate fragments after the engine tests. It can also be observed that the dispersion of CNTs was at a greater surface area and appeared with less contrast and darkness, indicating that CNT formed very thin to nearly two-dimensional structures that allowed more light transmission.

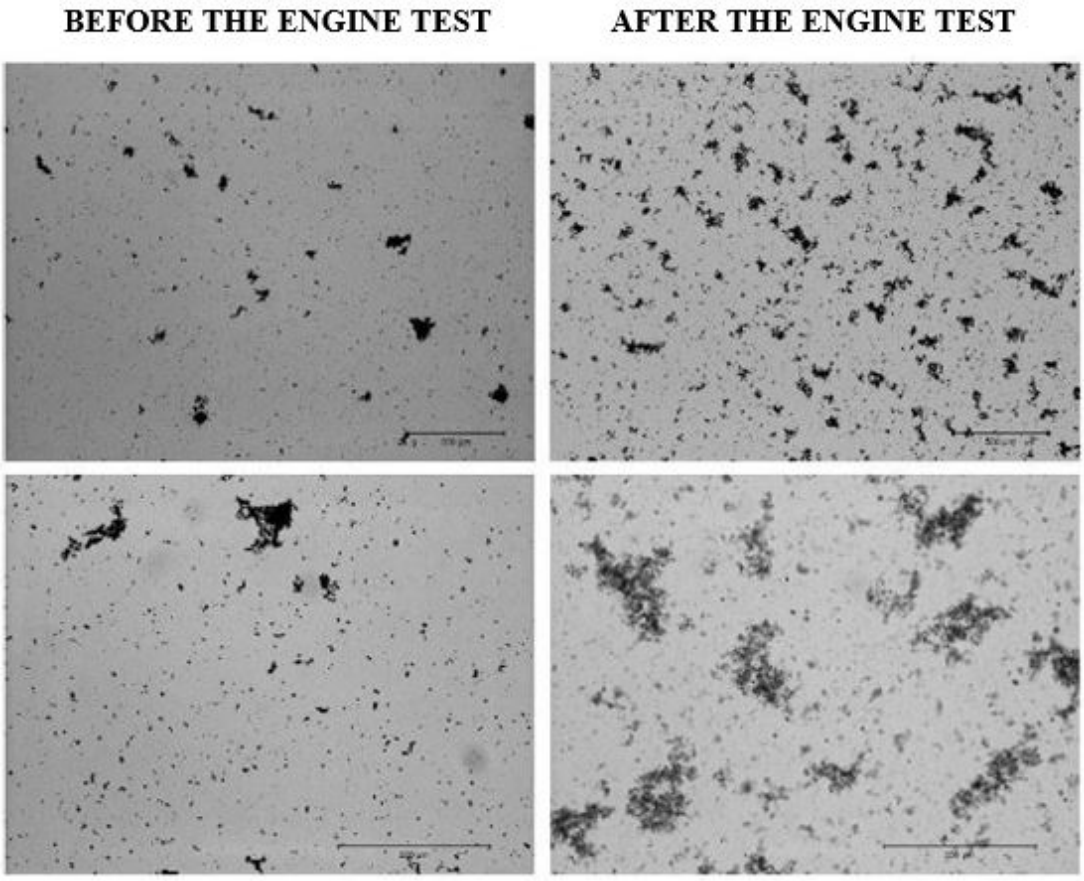

Fig. 5.10 Comparison of the CNT dispersion image acquired immediately after sonication (left) and after the engine test (right) using CNTs containing an oil drop in the optical microscope

Figure 5.11 shows the images of MWCNTs in the engine oil observed under a SEM after the engine test. Subtle changes in the CNT morphology were observed as compared to the bulk material. Due to the friction in the engine operation, the CNTs were seen to be shortened and torn. This is supported by the literature on CNT exfoliation [86].

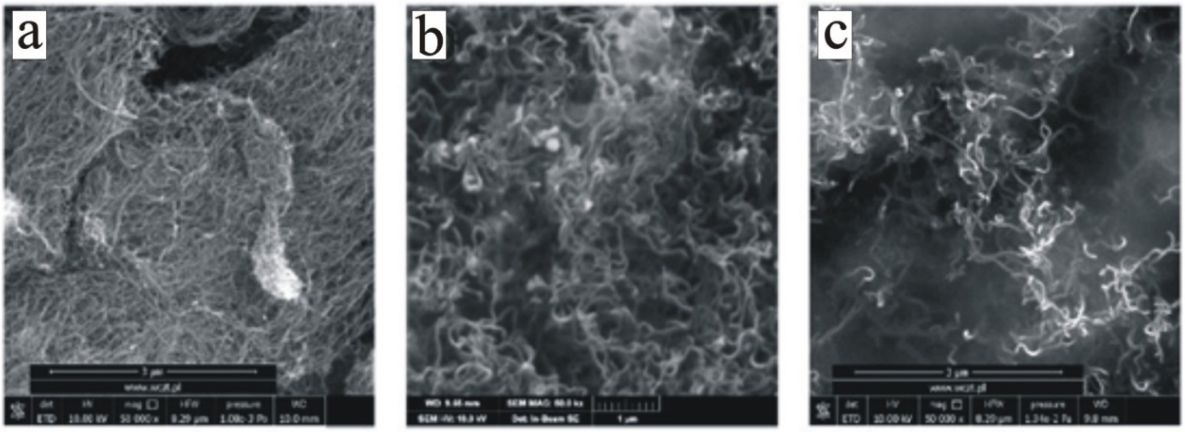

Fig. 5.11 Images taken with a scanning electron microscope (SEM) showing CNTs as bulk material (a), CNTs dispersed in oil using ultrasonic (b), and CNTs discovered in the oil during engine tests (c).

5.3.2 Analysis of Engine Vibration during Engine Warm Up

The test parameters evaluated were presented in Figure 5.9. The engine test ensured the reproducibility of engine operating conditions for all lubricating oil types. Compatibility regarding the coolant and oil temperature profile was successfully maintained without any issues.

Figures 12–14 and Tables 2–10 provide the results of the frequency analysis of vibrations recorded during the initial minute of the engine warm-up test. These diagrams illustrate the analysis of vibration accelerations across three directions, accompanied by tabular data. The tables include the following information:

1) Effective value of accelerations across the entire frequency range (a_{RMS}).
2) Effective value of accelerations within the specific range corresponding to the ($a_{RMS\ passband}$) maximum.
3) Maximum value of accelerations (a_{MAX}) and their respective frequencies f (a_{max}), at which these maximum values occurred.

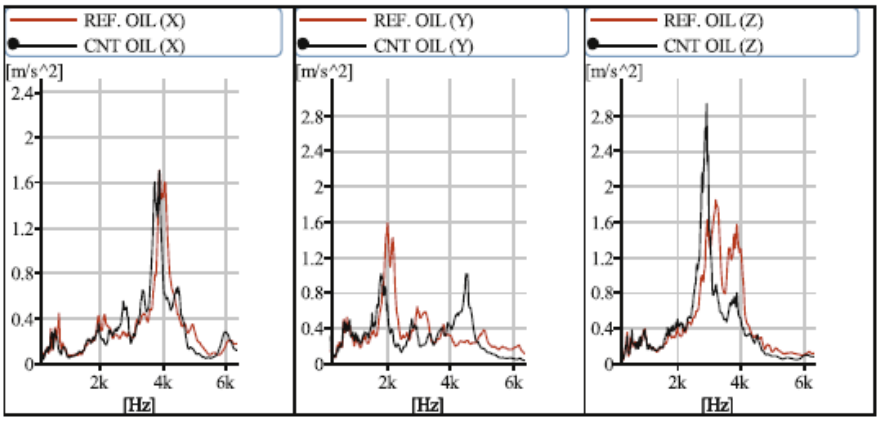

Fig. 5.12 FFT spectrum of the acceleration signal for the first minute of engine operation (according to Fig. 5.9, 1:30 – 2:30 min of the whole test)

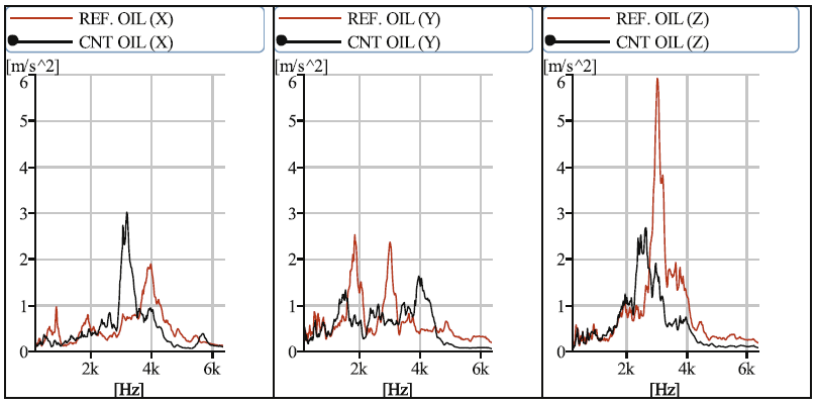

Fig. 5.13 FFT spectrum of the acceleration signal for the 15th minute of the engine operation (according to Fig. 5.9, 15 – 16 min of the whole test)

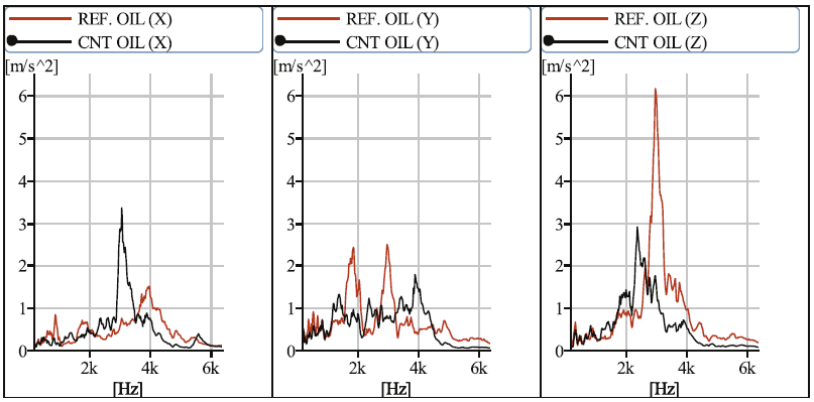

Fig. 5.14 FFT spectrum of the acceleration signal for the final minute of the engine operation (according to Fig. 5.9, 24:30 – 25:30 min of the whole test)

Table 5.2. The vibration signals' X-direction parameters determined through frequency analysis

Oil type and direction of the vibration measurement	$a_{RMS\ overall}$ [m/s^2]	$a_{RMS\ 3–5.5}$ kHz [m/s^2]	a_{MAX} [m/s^2]/f (a_{max}) [kHz]
REF. OIL (X)	7.40	6.80	1.7/3.90
CNT OIL (X)	7.20	6.50	1.7/3.90

Table 5.3. The vibration signals in the Y direction parameters characterized based on their frequency analysis

Oil type and direction of the vibration measurement	$a_{RMS\ overall}$ [m/s^2]	$a_{RMS\ 1–5.5}$ kHz[m/s^2]	a_{MAX} [m/s^2]/f (a max) [kHz]
REF. OIL (Y)	7.20	6.80	1.6/2.0
CNT OIL (Y)	6.20	5.90	1.0;1.0/1.8;4.5

Table 5.4. The vibration signals' Z-direction parameters determined through frequency analysis

Oil type and direction of the vibration measurement	$a_{RMS\ overall}$ [m/s^2]	$a_{RMS\ 2–5}$ kHz [m/s^2]	a_{MAX} [m/s^2]/f (a_{max}) [kHz]
REF. OIL (Z)	11.00	10.50	1.9/3.20
CNT OIL (Z)	10.60	10.00	2.9/2.90

Table 5.5. The vibration signals in the X direction parameters characterized based on their frequency analysis

Oil type and direction of the vibration measurement	$a_{RMS\ overall}$ [m/s^2]	$a_{RMS\ 2.5–4.5\ kHz}$ [m/s^2]	a_{MAX}[m/s^2]/f (a_{max}) [kHz]
REF. OIL (X)	11.90	8.70	1.9/3.20
CNT OIL (X)	10.00	11.30	3.0/4.00

Table 5.6. The vibration signals in the Y direction characterized based on their frequency analysis

Oil type and direction of the vibration measurement	$a_{RMS\ overall}$ [m/s^2]	$a_{RMS\ 1–5.5\ kHz}$ [m/s^2]	a_{MAX}[m/s^2]/f (a max) [kHz]
REF. OIL (Y)	12.90	12.40	2.4/1.90
CNT OIL (Y)	10.80	10.50	1.6/4.00

Table 5.7. The Z-direction vibration signal parameters determined through frequency analysis

Oil type and direction of the vibration measurement	$a_{RMS\ overall}$ [m/s^2]	$a_{RMS\ 2.2–4.2\ kHz}$ [m/s^2]	a_{MAX} [m/s^2]/f (a_{max}) [kHz]
REF. OIL (Z)	22.20	21.20	5.9/3.10
CNT OIL (Z)	13.90	12.40	2.7/2.60

Table 5.8. The vibration signals' X-direction parameters determined through frequency analysis

Oil type and direction of the vibration measurement	$a_{RMS\ overall}$ [m/s^2]	$a_{RMS\ 2.5–4.5\ kHz}$ [m/s^2]	a_{MAX} [m/s^2]/f (a_{max}) [kHz]
REF. OIL (X)	9.00	7.70	1.5/4.0
CNT OIL (X)	12.00	11.30	3.4/3.1

Table 5.9. The vibration signals in the Y direction parameters characterized based on their frequency analysis

Oil type and direction of the vibration measurement	$a_{RMS\ overall}$ [m/s^2]	$a_{RMS\ 1–5.5\ kHz}$ [m/s^2]	a_{MAX} [m/s^2]/f (a_{max}) [kHz]
REF. OIL (X)	13.60	13.10	2.5/3.00
CNT OIL (X)	11.50	11.30	1.8/4.00

Table 5.10. The vibration signals' Z-direction parameters determined through frequency analysis

Oil type and direction of the vibration measurement	$a_{RMS\ overall}$ [m/s^2]	$a_{RMS\ 1–5.5\ kHz}$ [m/s^2]	a_{MAX} [m/s^2]/f (a_{max}) [kHz]
REF. OIL (X)	22.80	21.80	6.3/3.0
CNT OIL (X)	13.80	11.70	2.9/2.4

The data in Tables 5.2 to 5.4 suggested that the CNT additive had contributed to the reduction of vibration acceleration on an overall basis and in all directions. Additionally, the effective vibration acceleration for the characteristic frequency bands was also reduced. As for the vibration signal spectra, there were reductions in the X and Y directions, while increasing in the Z direction. At maximum vibration acceleration, simultaneous frequency reduction was observed.

Tables 5.5 to 5.7 correspond to Figure 5.13, which depicts the vibration frequencies recorded during the engine warm-up process with the coolant temperature stabilized at 90°C, and the oil temperature rising above 75°C. These measurements were taken at the 15th minute of the engine test, still during the warm-up phase. The data indicated that the inclusion of CNTs in the lubricant led to an overall reduction in effective vibration acceleration levels in all directions. However, it's noteworthy that during this period, the vibration signal spectra increased in the X direction while decreasing in the Y and Z directions. This pattern was also observed in the vibration acceleration signals within specific frequency bands.

The increase in RMS amplitude reached a maximum of 2.6 m/s² in the X direction, while a decrease of 2.1 m/s² was observed in the Y direction, and a significant decrease of 8.3 m/s² was noted in the Z direction. At the beginning of the warm-up test, it was initially suggested that the addition of CNTs to the lubricating oil led to a reduction in vibration acceleration. However, this effect was only confirmed in the X and Z directions, and not in the Y direction. Despite the lower maximum vibration acceleration in the Y direction and a flatter curve, the effect observed in the X and Z directions did not extend uniformly. Figure 5.14 presents the vibration data recorded during the final minute of the engine warm-up test, along with its progression, supported by additional data in Tables 5.8 to 5.10.

Therefore, based on the data presented in Tables 5.8 to 5.10, the introduction of CNT into the lubricating oil led to an enhancement in vibration parameters in the Y and Z directions, but it resulted in an increase in the X direction. Specifically, the RMS amplitude exhibited a 3.6 m/s² increase in the X direction, while showing decreases of 2.1 m/s² in the Y direction and 10.1 m/s² in the Z direction. The frequency changes at the point of maximum vibration acceleration exhibited similar patterns to those observed during the 15th minute of the warm-up test.

5.3.3 Analysis of Engine Vibration during Engine Run at High Speed

As the engine speed was elevated to a consistent 2500 rpm, the FFT spectrum of the vibration acceleration signal exhibited a behavior similar to that observed during the final minute of the engine warm-up test. Figure 5.15 is a visual representation of the FFT spectrum during the engine test at 2500 rpm, and Tables 5.11 to 5.13 provide detailed data on these observations. These results collectively suggest that the increase in engine speed led to a corresponding increase in vibration amplitude.

The data presented in Tables 5.11 to 5.13 indicates that the introduction of CNTs into the lubricating oil had a notable impact on the vibration parameters. Specifically, it led to an increase in all vibration parameters in the X direction, while causing a reduction in the Y and Z directions. The RMS vibration amplitude saw an increase of up to 3.3 m/s^2 in the X direction. In contrast, the Y direction experienced a decrease of 3.6 m/s^2, and the Z direction saw a substantial reduction of 17.5 m/s^2. Notably, the increase in vibration amplitude in the X direction was significantly less pronounced compared to the reduction observed in the Y and Z directions.

Furthermore, it was observed that doubling the speed of the crankshaft resulted in reduced changes in vibration acceleration in the X direction with the addition of CNTs to the lubrication oil, while it increased by 1.7 times in the Y and Z directions. During the final 3 minutes of the engine test, the average motoring torque was measured at 51.49 Nm for standard lubricating oil and 48.25 Nm for lubricating oil with the CNT additive. This reduction in motoring torque amounted to 6.3%.

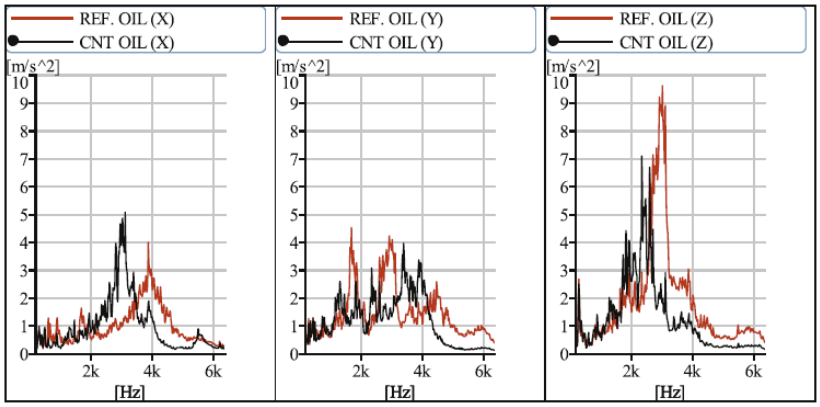

Fig. 5.15 The FFT spectrum obtained for the acceleration signal during the final minute of the test, specifically from 6.30 – 7.30, while the engine was operating at 2500 rpm

Table 5.11. The vibration signals' X-direction parameters determined through frequency analysis

Oil type and direction of the vibration measurement	a RMS overall [m/s^2]	a RMS 2–5 kHz [m/s^2]	a MAX [m/s^2]/f (a_{max}) [kHz]
REF. OIL (X)	19.00	17.30	4.0/3.90
CNT OIL (X)	21.80	20.60	5.1/3.10

Table 5.12. The Z-direction vibration signal parameters determined through frequency analysis

Oil type and direction of the vibration measurement	a RMS overall [m/s^2]	a RMS 1–5.5 kHz [m/s^2]	a MAX [m/s^2]/f (a_{max}) [kHz]
REF. OIL (Y)	26.70	25.80	4.5/1.70
CNT OIL (Y)	23.10	22.60	3.9/3.40

Table 5.13. The vibration signals in the Z direction are characterized by their frequency analysis parameters

Oil type and direction of the vibration measurement	a RMS overall [m/s^2]	a RMS 2.2–4.2 kHz [m/s^2]	a MAX [m/s^2]/f (a_{max}) [kHz]
REF. OIL (Z)	42.50	40.0	9.6/3.10
CNT OIL (Z)	28.30	22.5	7.0/2.40

5.3.4 Analysis of Engine Vibration during Engine Run at Low Speed and Low Torque

The subsequent engine test aimed to assess the vehicle's performance in urban traffic conditions, characterized by low engine speeds of 1200 rpm and fuel supply at 11 mg/cycle, representing a low-speed, low-torque engine condition with torque measuring at approximately 50 Nm. The vibration frequency analysis was depicted in Figure 5.16 and complemented by Tables 5.14 to 5.16. The data presented in Tables 5.14 to 5.16 indicated that the inclusion of the CNT additive in the lubricating oil led to a reduction in all vibration parameters in all directions, including frequencies corresponding to maximum vibration acceleration.

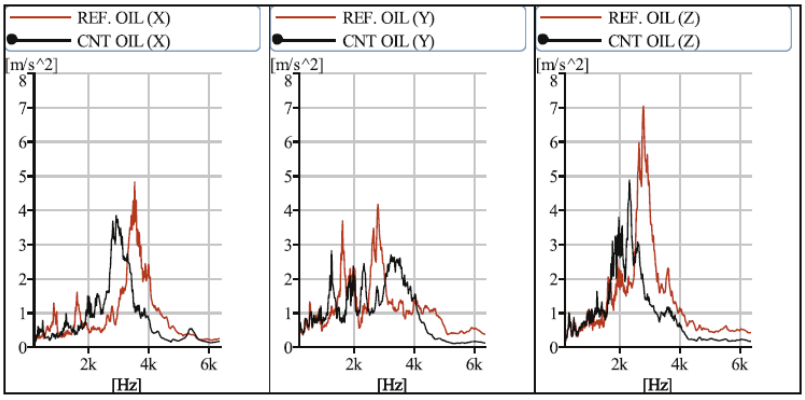

Fig. 5.16 The FFT spectrum obtained for the acceleration signal over the last minute, with an engine speed of 1200 rpm and a fuel dose of 11mg per cycle

Table 5.14. Frequency analysis determined vibration signal parameters in the X direction

Oil type and direction of the vibration measurement	$a_{RMS\ overall}$ [m/s^2]	$a_{RMS\ 2.2–4.2\ kHz}$ [m/s^2]	a_{MAX} [m/s^2]/f (a_{max}) [kHz]
REF. OIL (X)	20.40	19.0	4.8/3.60
CNT OIL (X)	19.50	18.5	3.8/2.90

Table 5.15. The Y-direction vibration signal parameters determined through frequency analysis

Oil type and direction of the vibration measurement	$a_{RMS\ overall}$ [m/s^2]	$a_{RMS\ 1–5.5\ kHz}$ [m/s^2]	a_{MAX} [m/s^2]/f (a_{max}) [kHz]
REF. OIL (Y)	21.50	20.80	4.2/2.80
CNT OIL (Y)	19.90	19.40	2.8/1.30

Table 5.16. The vibration signals in the Z direction are characterized by their frequency analysis parameters

Oil type and direction of the vibration measurement	$a_{RMS\ overall}$ [m/s^2]	$a_{RMS\ 2.2–4.2\ kHz}$ [m/s^2]	a_{MAX} [m/s^2]/f (a_{max}) [kHz]
REF. OIL (X)	30.80	28.10	7.0/2.80
CNT OIL (X)	23.00	17.10	4.9/2.30

5.3.5 Analysis of Engine Vibration during Engine Run at High Speed and High Torque

Figure 5.17, along with Tables 5.17 to 5.19, illustrates the vibration behavior of the engine operating at high speed and high torque conditions. The test was conducted at 2500 rpm engine speed, 25 mg/cycle of fuel feed, and generated approximately 160 Nm of torque. Interestingly, the addition of CNTs to the lubricating oil produced results that were consistent with the previous engine tests. Vibration acceleration was reduced in all directions for all parameters, even in this specific case with increased speed and torque. This reduction in vibration acceleration coincided with a decrease in frequency at maximum vibration acceleration. It's worth noting that the results of engine tests conducted in low-speed, low-torque, and high-speed, high-torque conditions may have been influenced by vibrations stemming from engine kinematics and combustion dynamics.

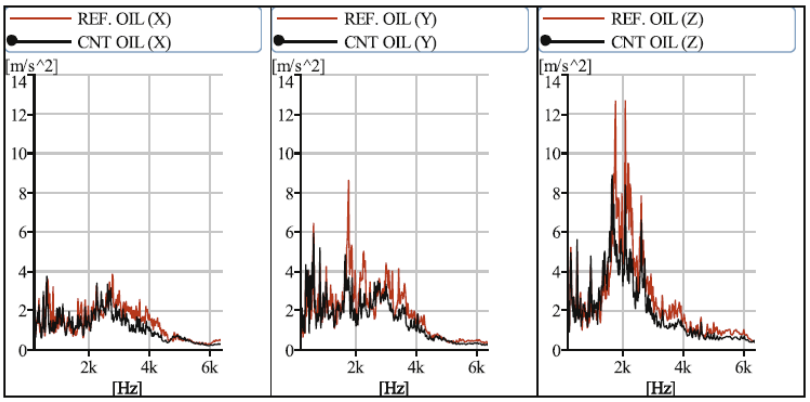

Fig. 5.17 The FFT spectrum obtained for the acceleration signal over the last minute, with an engine speed of 2500 rpm and a fuel dose of 25 mg per cycle

Table 5.17. The vibration signals' X-direction parameters determined through frequency analysis

Oil type and direction of the vibration measurement	$a_{RMS\ overall}$ [m/s^2]	$a_{RMS\ 1.5–5.0\ kHz}$ [m/s^2]	a_{MAX} [m/s^2]/f (a_{max}) [kHz]
REF. OIL (X)	25.30	21.30	3.8/2.80
CNT OIL (X)	21.50	17.40	3.7/0.60

Table 5.18. The vibration signals in the Y direction are characterized by their frequency analysis parameters.

Oil type and direction of the vibration measurement	$a_{RMS\ overall}$ [m/s^2]	$a_{RMS\ 1.5–5.0\ kHz}$ [m/s^2]	a_{MAX} [m/s^2]/f (a_{max}) [kHz]
REF. OIL (Y)	37.30	32.60	8.6/1.80
CNT OIL (Y)	30.30	24.60	5.9/0.60

Table 5.19. The vibration signals' Z-direction parameters determined through frequency analysis

Oil type and direction of the vibration measurement	$a_{RMS\ overall}$ [m/s^2]	$a_{RMS\ 1–5.5\ kHz}$ [m/s^2]	a_{MAX} [m/s^2]/f (a_{max}) [kHz]
REF. OIL (Z)	53.70	49.10	12.6/2.10
CNT OIL (Z)	42.00	37.40	8.9/1.70

5.3.6 The Effect of Carbon Nanotubes Additive in Lubrication Oil on Engine Vibration

At the beginning of the engine test (the warm up stage) the temperature increase had contributed to engine vibration for engines with standard lubricating oil as well as for lubricating oil with CNT additive. The CNT additive had significantly reduced the vibration of the engine block in general. At about 2.9 kHz of frequency as indicated in Figure 5.12, the vibration amplitude was recorded at a relatively high value for engine with CNTs added to lubricating oil. However, the amplitude was then decreased as the engine heated up. This was illustrated in Figures 5.13 and 5.14.

A thin layer of oil on the cylinder walls at the beginning of the engine operation might have contributed to the large vibration amplitudes due to the intensity of piston movement during that period of time. The cylinder walls of the engine in this study were lubricated with the lubrication oil supplied from the crank bearings. The increase in engine vibration in the Z direction in the 1st minute could possibly be due to minimum oil flow through the bearings because of CNTs agglomeration.

Vibrations along the Y direction, which align with the crankshaft axis, were anticipated to be relatively minor, in line with the force directions within the piston-cylinder mechanism. As a result, the impact of the CNT additive on engine vibrations in this direction could not be conclusively determined.

The engine speed does affect the engine vibrations changes between engines with standard lubricating oil and one with a CNT additive, but gave lesser impact compared to engine temperature. On the other hand, the engine load increase due to the combustion process of an increased supplied fuel dose led to an increase in Z direction's vibration significantly. This is the direction normal to the pressing force between the cylinder and piston which induced secondary piston movements.

Therefore, the highest amplitudes of vibration was in the Z direction, that is in the direction normal to the pressing force between the cylinder and piston. Additionally, a large amplitude of vibration was also recorded in the X direction, so in the direction of the reciprocating motion inertial forces. Theoretically, these situations were expected based on their directional nature.

The introduction of CNTs into the lubricating oil was found to shift the peak of vibration acceleration from higher frequencies to lower frequencies. This effect was particularly pronounced in the X and Z directions, where it significantly reduced vibrations within the frequency range of 3.5 to 4 kHz and even higher.

Maximum vibration acceleration shift to lower frequencies with reduction of the magnitude itself could suggest that there was a reduction in the oil film stiffness, probably due to its thickness having been increased. This idea is well in line with the issues observed in the effort of reducing engine frictional losses globally.

The evaluations in this study were conducted in real engine operating conditions, which provided a more comprehensive and realistic understanding compared to isolated studies conducted in a tribometer. The engine used for testing had the advantage of operating at high cylinder pressures. Furthermore, the engine was constructed using modern materials and technologies, including plasma-coated cylinder liners, and it incorporated various frictional components made from a combination of metals and plastics. Examining the effects of entrainment velocity and contact pressures on the engine's frictional components within the engine itself, as opposed to studying them independently, yielded valuable insights and highlighted potential differences in the results.

5.3.7 Contributing Factors on CNT Role as Lubricating Oil Additive

The trace amount of CNT additive in the lubricating oil, in as low as 0.03% by mass fraction, did not significantly modify the viscosity of the lubrication oil. Hence, the effect of CNT additive to engine friction and vibration in this study did not relate strongly with the oil rheology itself. On the other hand, the findings pointed out that the tribological process complexity was suggested to happen in the engine with CNTs added to lubricating oil. This section was used to discuss the aspects that affect the role of CNTs as a lubricating oil additive.

1- Quality of CNT Dispersion

The hypothesis that the increase in nanotubes concentration would be counterproductive in the effort of reducing friction losses had been confirmed in this study through comparison with previous works [72]. This is due to the CNTs tendency to form agglomerates, which is made easier as the nanotubes concentration with sizes of several micrometers increased. Effective reduction of friction losses can be achieved with a lower concentration of CNTs but with their much better dispersion in lubricating oil. CNTs can be supplied through a continuous feed with controlled abrasion of the CNT layer. Replacement of oil with different types of lubrication liquid is a promising way to overcome the problem of natural agglomeration of CNTs. In the recent development, ionic liquids reveal their outstanding tribological properties functioning on their own [87, 172], or being miscible with oil [173-175], or through interaction with CNTs to produce an entirely new class of lubricants [86, 88, 176, 177].

2- Heat and Energy Conduction along the CNT Length

Despite being classified as nanomaterials due to their nanoscale diameter, CNTs can have lengths measuring up to tens of micrometers, which is comparable to or even greater than the thickness of the typical oil film found on the friction surfaces of machinery. Consequently, the introduction of CNTs can alter the temperature distribution within the oil film, thereby influencing friction and vibrations.

3- Interaction of CNTs with Anti-Wear Additives and Other Chemical Compounds in the Oil

CNTs exhibit exceptional chemical stability under typical experimental conditions encountered during friction processes. In tribocatalytic processes, CNTs can assume a significant role in facilitating energy transfer. Carbon, renowned for its catalytic properties in zinc reactions, could potentially influence the anti-wear capabilities of zinc dithiophosphates when employed as an additive in oil.

4- Carbon-Based Anti-Wear Film Formation

Deposition of a carbon layer onto the surface of metals as a result of friction processes has been documented, especially when carbon nanostructures were introduced as additives into lubricating oils [62, 65, 77]. Conversely, earlier literature contradicted the notion of long-lasting carbon deposits on the friction surface [63]. This phenomenon was understood as the dynamic formation of a carbon-based anti-wear layer. Because of its weak adhesion to the metal surface, this layer was periodically removed and regenerated during the course of friction. Tribometer tests failed to reveal any such layer on the friction track, leading to the assumption that it had been washed away during sample preparation.

5- Preventing the Arrangement of Oil Molecules in the Lubrication Gap Volume

The theory of shear-induced ordering transitions suggests that the incorporation of CNTs into lubricating oil may contribute to reducing friction-induced vibrations by disrupting the symmetric arrangement of oil molecules [81, 82, 178, 179]. A similar concept can be applied to the creation of a CNT-induced anti-wear layer, introducing a form of asymmetry on the frictional surface.

The implications of this study are believed to extend to various types of machinery, including power transmission systems. However, practical application hinges on addressing several challenges, primarily the long-term stability of nanotube dispersion in lubricating oil. One potential solution involves incorporating a friction surface composed of CNT composites that deliberately releases CNTs into the oil through continuous wear processes.

Another pressing concern pertains to the lifecycle of oil containing nanomaterials and the potential health impact of CNTs. It's important to note that CNTs are highly carcinogenic when inhaled, posing a significant risk to human respiratory health. However, the threat of oil itself to human health is generally considered to be low.

5.4 CNTs in High Viscosity Lubricants

Even though the literature presented promising preliminary laboratory test results, the early commercialization attempts for CNTs were discouraging. There are two main aspects to be addressed prior to the application attempt of CNTs in large-scale industrial settings for lubrication purposes. These are; the CNT dispersion stability, and understanding of the CNT tribological effect mechanism. The engine test in the earlier part of this study concluded that CNTs could contribute to significant friction reduction only if they were well dispersed. The same total engine friction reduction was measured for CNT concentration in oil of 0.5% and with over ten times lower concentration. Both gave the results of about 5%. Ultrasonic homogenization was used for the first case, but major improvement was achieved for low CNT concentration in terms of CNT dispersion with simple but effective chemical methods [7].

Initial efforts to harness the friction-reducing capabilities of carbon nanotubes (CNTs) by elevating their concentration in lubricating oil faced challenges, particularly when concentrations reached as high as 1%. Concentration this high led to a greasy consistency of oil that posed difficulties in

effectively pumping the lubricant. Fortunately, the unsuccessful engine test provided an opportunity to explore alternative testing scenarios outside of the engine, allowing for a comparison with high-quality grease.

Pertinent tribometer test outcomes were presented to gain a comprehensive understanding of the influence of CNTs in lubricants and the associated physical phenomena. The tests were conducted using an Amsler tribometer, where a rotating steel ring exerted pressure on various material samples employed as friction surfaces. These friction surfaces were lubricated with CNT-enhanced lubricants of different formulations, along with a high-quality commercial grease for comparison purposes.

Polymer materials were extensively utilized as samples for friction components due to their cost-effectiveness, low friction coefficients, favorable mechanical properties, and ease of manufacturing. A detailed discussion on this can be found in Chapter 3, as previously mentioned.

5.4.1 Preliminary Test Results

The following set of labels, as already mentioned in the methodology section, was recapped for the discussion purpose in this section:

S0 – grease produced from the experiments of the engine
S1 – PAO synthetic oil (lithium soap used as thickener with CNTs)
S2 – PAO synthetic oil (lithium soap used as thickener)
S4, S5, S6 – obtained from ultrasound disintegrator

For initial assessments, a high-viscosity lubricant was extracted from the engine oil reservoir (referred to as S0). The objective was to assess its lubricating characteristics with respect to commonly employed friction materials. Polymer, aluminum, brass, and cast iron were selected as test samples and evaluated using the Amsler tribometer. Each sample was subjected to a one-minute testing duration during the preliminary evaluation. The applied load was set at 110 kg, and the rotational speed was maintained at 200 rpm.

Figure 5.18. is the comparison of lubrication performance between S0 grease and S1 grease. S0 grease with CNT additive was unable to achieve high-quality commercially available equivalent lubrication performance when tested with most samples. Due to the low S0 grease adhesion to the surface of the metal, high wear was observed on metal samples. However, the test on a polymer gave better results, which is desired as a polymer is one of the common materials for friction components in various applications. Hence, the subsequent tests of this study were focused on polymers.

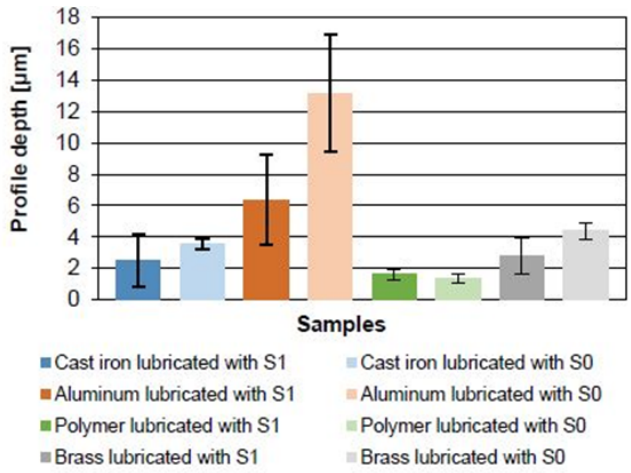

Fig. 5.18 Comparison of the effectiveness of lubricants S0 and S1 in reducing wear on the surfaces of samples made from various materials. Wear was measured after one-minute friction tests, and mean values and confidence intervals were determined at a significance level of 0.1

5.4.2 15-Minutes Test Conducted On a Polymer Surface

Each of the lubricants (S1 to S6) was tested with three samples and rings. The initial lubricant thickness to cover the sample's friction surface was set to at least 2mm at the beginning of the test. While the test was in progress, at the 6th minute and 10th minute, additional lubricant was added to cover the friction surfaces on the ringside only. A thermocouple was placed at a depth of about 3 mm under the sample surface to measure temperature and motion resistance.
The tests were performed with the following conditions as shown in Table 5.20:

Table 5.20. The test conditions

Total test duration	15 minutes
Measurement intervals	50s, 2 minutes, 5 minutes, 7 minutes, 10 minutes 13 minutes and 15 minutes
Ring speed	228 rpm
Load	120 kg

Figure 5.19 shows the results of surface roughness measurement, Ra for polymer samples lubricated with S1 to S6 lubricants. S1 lubricant contributed to surface roughness reduction on the sample with Ra of 0.11 ± 0.03 µm. On the other hand, the S5 lubricant had increased the sample surface roughness with the highest Ra as compared to all other lubricants. At the end of the 15-minute test, the highest surface roughness, Ra, recorded by the sample with S5 lubricant applied was at 0.33 ± 0.05 µm.

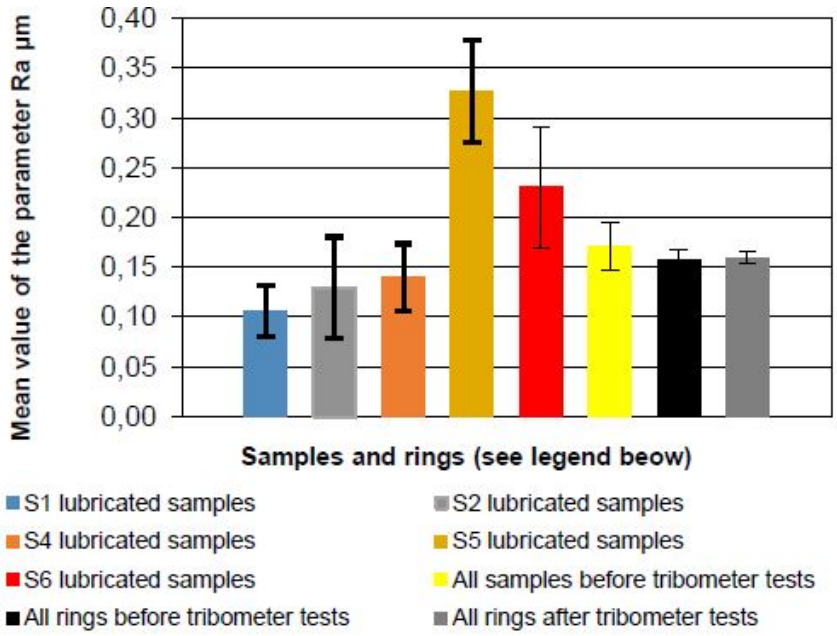

Fig. 5.19 The Ra parameter of samples and rings was measured by the Amsler tribometer before and after testing. Mean values and confidence intervals for the mean values calculated at a significance level of 0.1

Next, with regards to the surface roughness of the rings, there was no significant difference in Ra values before and after the friction test. This could suggest that all of the lubricants have less or no impact on the steel spigot wear in plain bearing coupled with the polymer sample in the friction test.

Lubricants S2, S4, and S6 had no major impact on surface roughness increase or reduction by the end of the friction test. Since there were no surface roughness (Ra) differences between the sample friction surface and the rings at the beginning of the friction test, minimum preparation was required, which was beneficial to the results.

There was no difference in surface roughness between samples that used S5 lubricant and samples using S6 lubricant as suggested by the average Ra parameter in Figure 5.19. The sign of abrasive wear was found with the presence of scratches in parallel behavior at the end of the friction test. Figure 5.20 shows the visible scratches on the sample with S6 lubricant applied during the test.

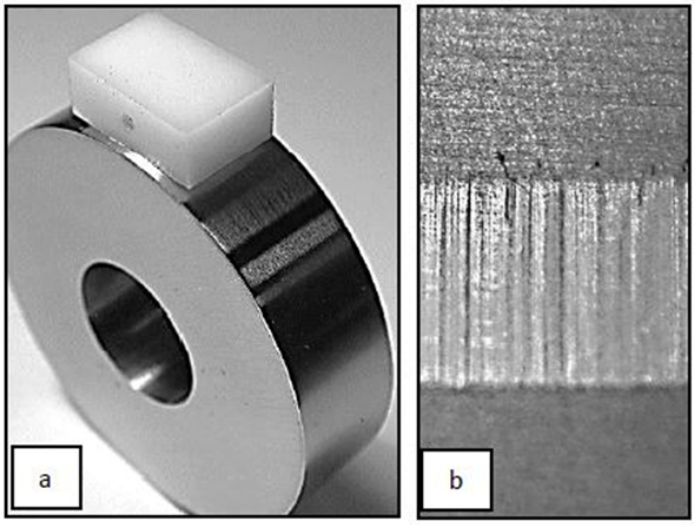

Fig. 5.20 The Amsler tribometer used to measure friction components (a) and scratches on a polymer sample following a lubricant test with S6 (b)

Figure 5.21 shows the measured groove depth of the surface roughness profile to represent the wear on the friction surface after the friction test. Measurements of average groove depth found that applying S2, S4, and S6 lubricants did not cause a difference in their wear level as compared between the samples. However, the average wear on friction surfaces by applying these three lubricants was higher than the wear on the friction surfaces with the S1 lubricant being applied.

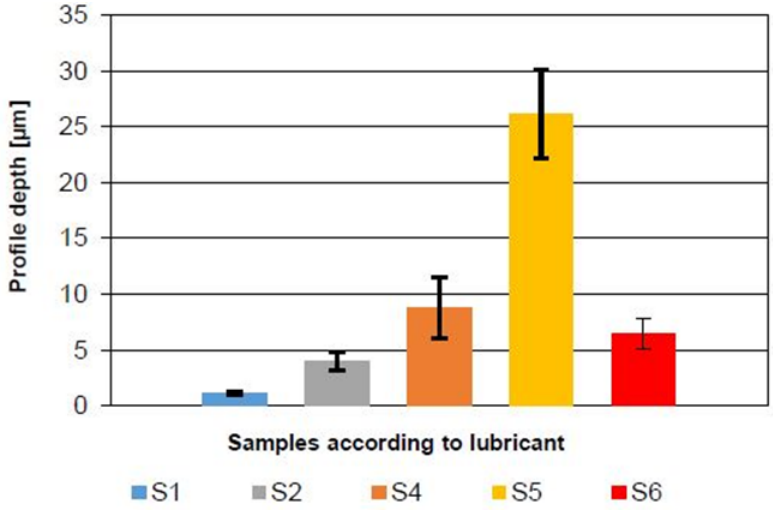

Fig. 5.21 Measured wear on polymer samples subjected to various lubricants. The depth of the friction track profile was also measured, and mean values with confidence intervals were calculated at a significance level of 0.1

Additionally, the results in Figure 5.21 also show that the S1 lubricant contributed to the least wear to the friction surface in the simulated sliding friction test. On the other hand, the use of S5 lubricant contributed to the greatest friction surface wear to the sample among all lubricants used in the friction test. This was supported by the observed increase in temperature along the test duration, which for S5 lubricant reached temperatures above those of other lubricants, as shown in Figure 5.22.

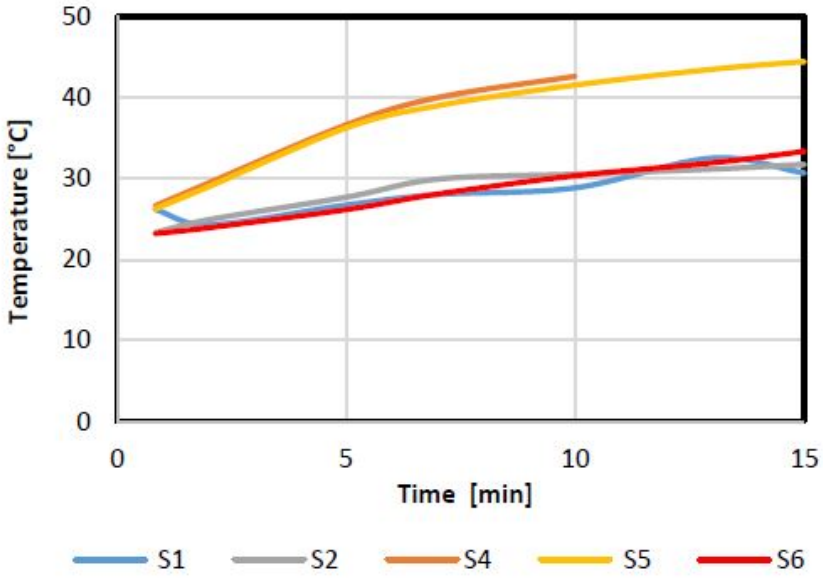

Fig. 5.22 Temperature values of the sample material during friction testing in a tribometer for various lubricants

5.4.3 30-Minutes Test Conducted on a Polymer Surface

Friction tests were extended to observe the impact of prolonged exposure on polymer samples, allowing for a comparison between the standard lubricant (S1) and the CNT-enhanced lubricant (S4) on the friction surfaces. The test parameters mirrored those of the 15-minute test on polymer surfaces, with the exception that the total testing time per sample was extended to 30 minutes, and the load applied in the Amsler tribometer was set at F = 1200 N.

Figure 5.23 illustrates the depth of the measured grooves appearing by the end of the 30-minute friction test for samples lubricated with S1 and S4 lubricants. Interestingly, while the S1 lubricant had initially shown promise in the 15-minute friction test, it failed to minimize wear in this extended test. Samples using S1 lubricant exhibited groove depths exceeding 64 µm, indicative of pronounced wear characteristics. Conversely, samples utilizing S4 lubricant displayed a groove depth of 38 µm, outperforming S1 lubricant in the extended friction testing periods.

It was observed that the poor performance of the S1 lubricant was due to the rapid acceleration of wear that took place after a certain time. In the case of S4 lubricant with the addition of CNTs, however, prolonged friction time did not promote that rapid surface wear acceleration as it did with the S1 lubricant. Hence, it was anticipated that there exists a CNT related mechanism in promoting anti-wear effects on the surface which requires further explanation.

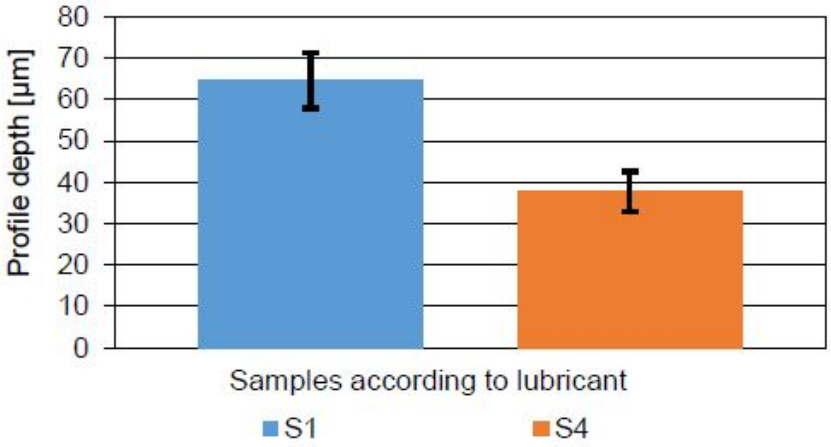

Fig. 5.23 Mean wear values, measured as groove profile depth, of polymer samples lubricated with S1 and S4 lubricants. Mean values and confidence intervals reported at a significance level of 0.1

5.4.4 Raman Spectroscopy of the Polymer Surface Following the Friction Test

Raman spectroscopy was conducted on the polymer sample (as depicted in Figure 5.24) following an extended 30-minute friction test, enabling a deeper understanding of the wear-protective role of CNTs [7]. The CNTs introduced via the S4 lubricant likely became integrated into the polymer surface, if not forming a resilient protective layer on the polymer's surface, thereby reducing wear. Interestingly, there was an absence of any CNT signals in the vicinity of the friction track, even though this area came into contact with the grease during the friction test. This observation ruled out the possibility of misinterpreting the presence of simple contaminants, as CNTs only produced a Raman signal in the regions where the polymer sample interacted with the rotating ring.

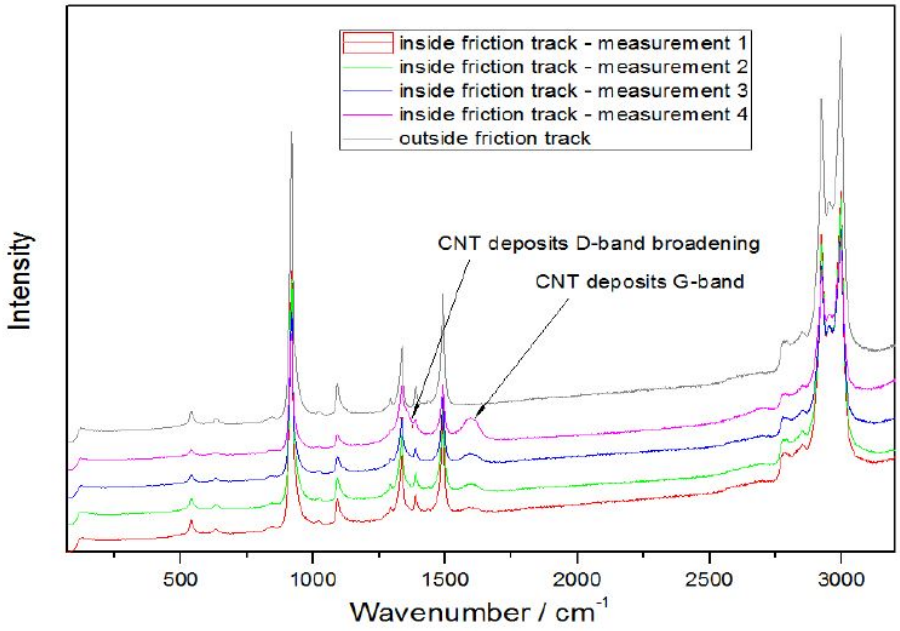

Fig. 5.24 CNTs interaction with polyoxymethylene (POM) surface;
durable CNT deposits revealed in friction track in Raman spectroscopy

5.4.5 Grease Structure Microscopy

Primarily, the microstructure of the CNTs-based lubricants showed exciting similarity to a standard lithium soap grease, whereby the CNTs were slightly thinner than the soap fibers (Figure 5.25). Thinner fibers in a standard grease are usually believed to improve the tribological properties, moreover it is believed they should intentionally vary in diameter in a certain range. If this observation also applies to grease with CNTs it should be possible to control the diameter distribution easily. The grease can be effectively produced by using thin MWCNTs, preferably NC7000 from Nanocyl, they have a diameter of about 10 nm. At the same 1% concentration in oil, thick MWCNTs (50nm) were absolutely not able to act as a thickener, apparently, they have even not changed the oil viscosity. On the other hand, it was possible to add these thick MWCNTs to a grease based on the standard used in the research, where the most-suitable were the NC 7000 CNTs.

When trying to adopt the knowledge from standard grease microscopy to CNTs-based grease formulation it's interesting, that avoiding aligned fibers orientation was believed to improve grease adhesion, Fig. 5.25.

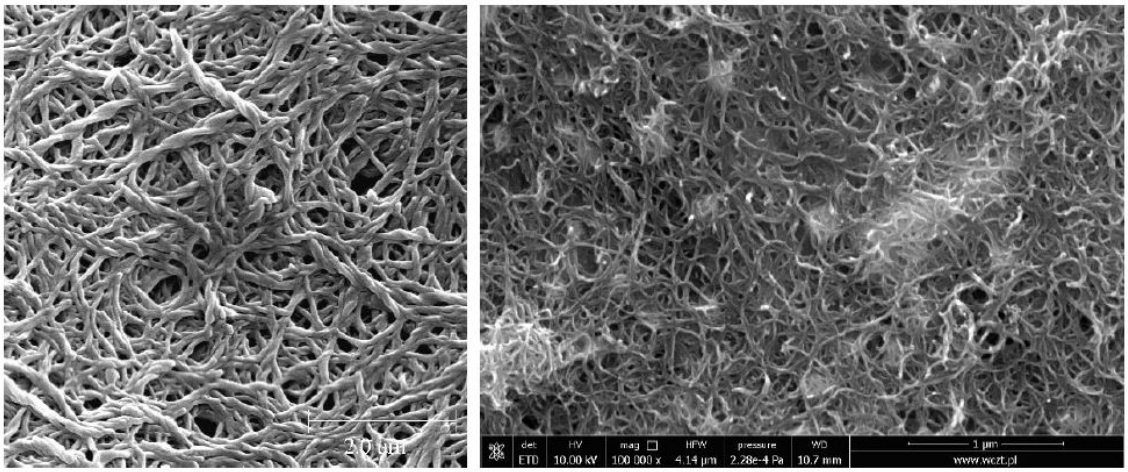

Fig. 5.25 Micrography comparison of a top-quality lithium grease (left) and CNTs-based grease (right)

The tribological function of the fibers acting as a thickener in a standard grease is still not fully understood, conclusions made by various researchers are to some extent clearly inconsistent. The rather outdated theory states that the one and only function of the thickener is to increase lubricant viscosity allowing them to stay inside the tribological contact, e.g. ball bearing. It's believed that the fiber structure soaked with oil as a sponge reveals it under high local contact pressure e.g. between the ball and the race in the bearing, and solely the small amount of squeezed oil plays the tribological function. Nowadays it's believed that this mechanism of action occurs in reality, but only at high speeds and relatively low contact pressure. On the contrary, on the lubricated surface operated at a low speed and a high contact pressure remnants of broken soap fibers were reported.

Thus, the theory states, that the tribological function of the thickener used for the grease formulation is limited to high-load/low-speed operating conditions. That’s in line with the results of this study, where an impressive wear reduction in ball bearing was observed at low speed when the CNTs were added to the regular lithium grease, Fig. 5.26-5.28.

For the CNTs-based grease, clear changes in the morphology of CNTs before and after bearings tests was observed (Fig. 5.29). No HRTEM pictures of grease remnants from the bearing race could be

taken, however, SEM pictures revealed that the CNTs became shorter and the number of bends increased. This aspect will be followed up on in further studies.

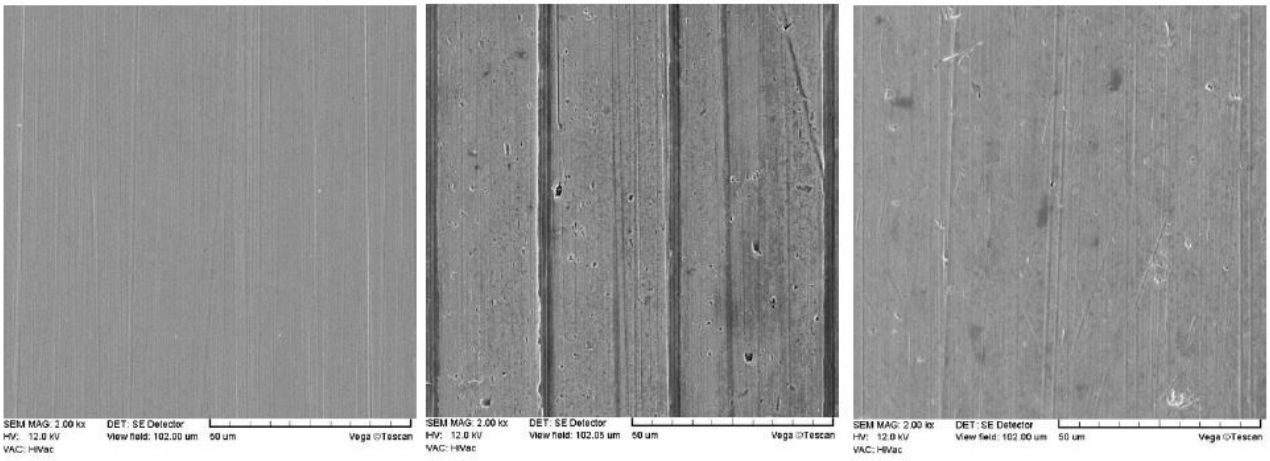

Fig. 5.26 SEM pictures of the outer ball bearing. From the left to the right: 1: new bearing, 2:bearing lubricated with reference lithium grease, 3:bearing lubricated with reference grease enriched with CNTs.

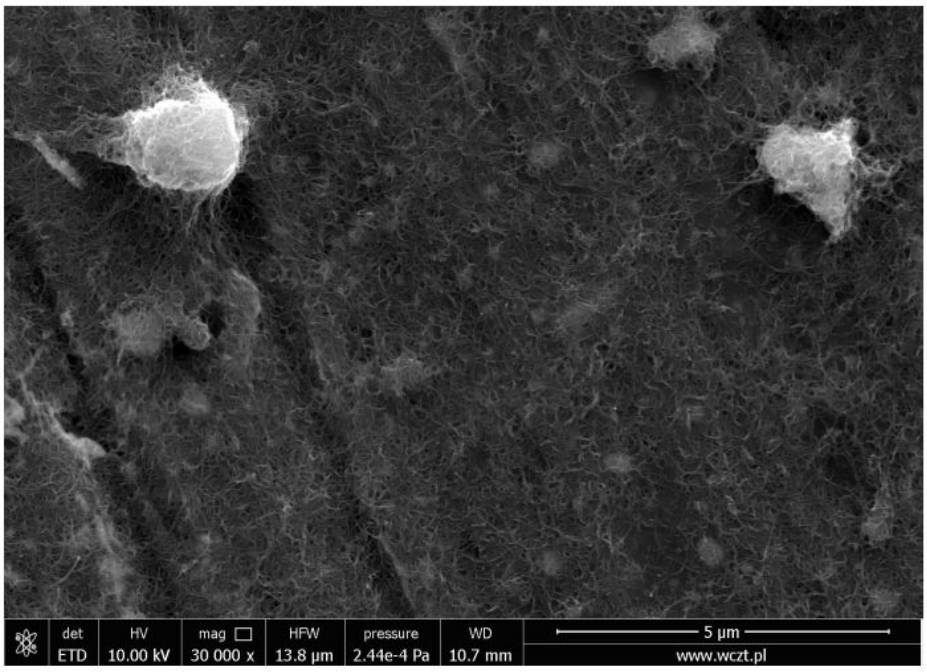

Fig. 5.27 S4 grease, as produced (corresponds to the tribometer research described above), SEM picture, large view

The effect of high-shear on the CNTs morphology occurring in tribological contacts was clearly observed in the engine tests performed with CNTs enriched oil. The CNTs diameter increased, this may indicate that the friction in machines forces CNTs to exfoliate and possibly to produce graphene ribbons. This in-situ produced graphene in excellent dispersed form may be the dominant tribologically active compound.

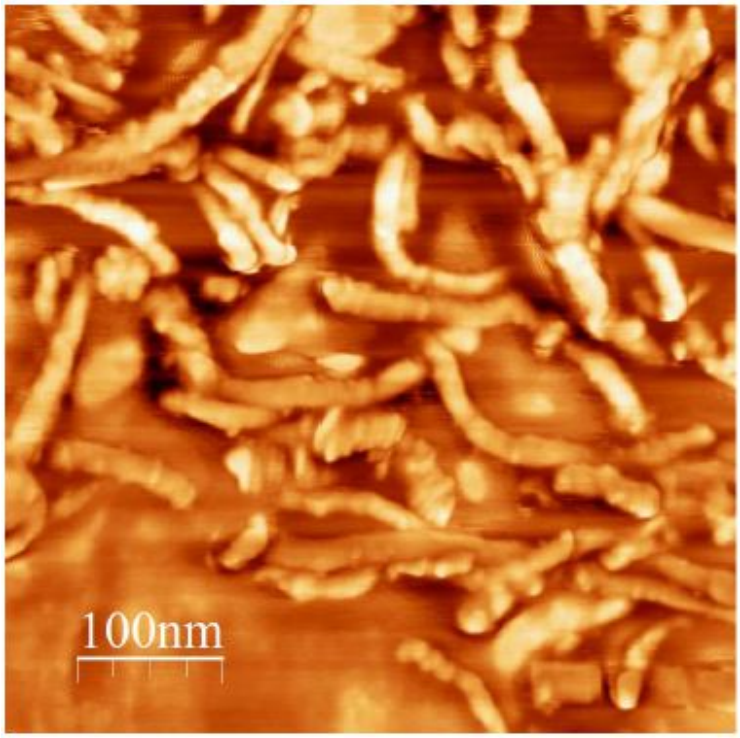

Fig. 5.28 S4 grease, first approach to the AFM microscopy for CNTs diameter and length assessment

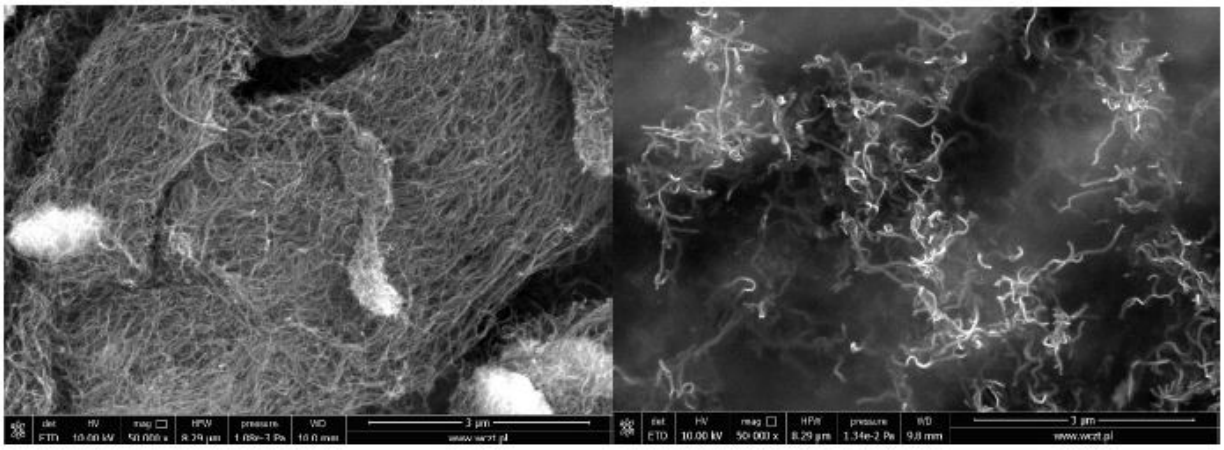

Fig. 5.29 SEM images of CNTs as bulk material and after engine tests in oil

5.4.6 Dispersion of Carbon CNTs in Regular Lithium Grease

MWCNTs (Nanocyl NC7000) dispersed quite well in the commercially available lithium grease, even if they were only roughly mixed using mortar and pestle (Fig. 5.30). In normal bearing operation, the dispersion quality was improved significantly, especially during the first few hours, Fig. 5.31 and 5.32. Thereby remarkable differences were observed for the ball and roller bearings of the same dimensions, working in the same conditions. The outer bearing diameter was about 80 mm, and the speed was 375 rpm.

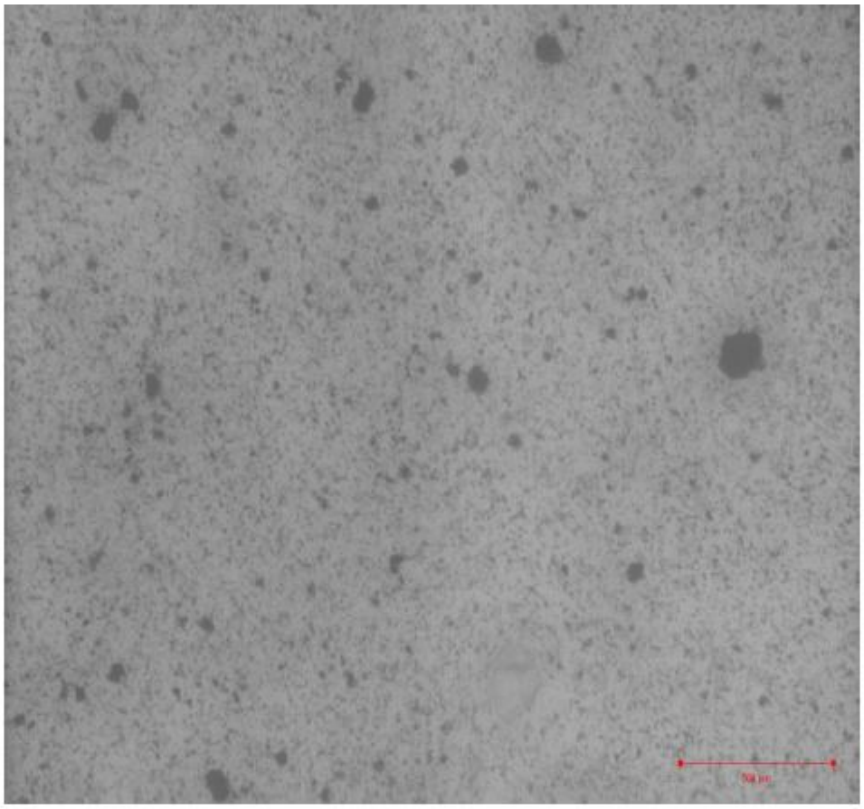

Fig 5.30 Hand-made grease dispersion, CNTs concentration limited to 0,1% wt.

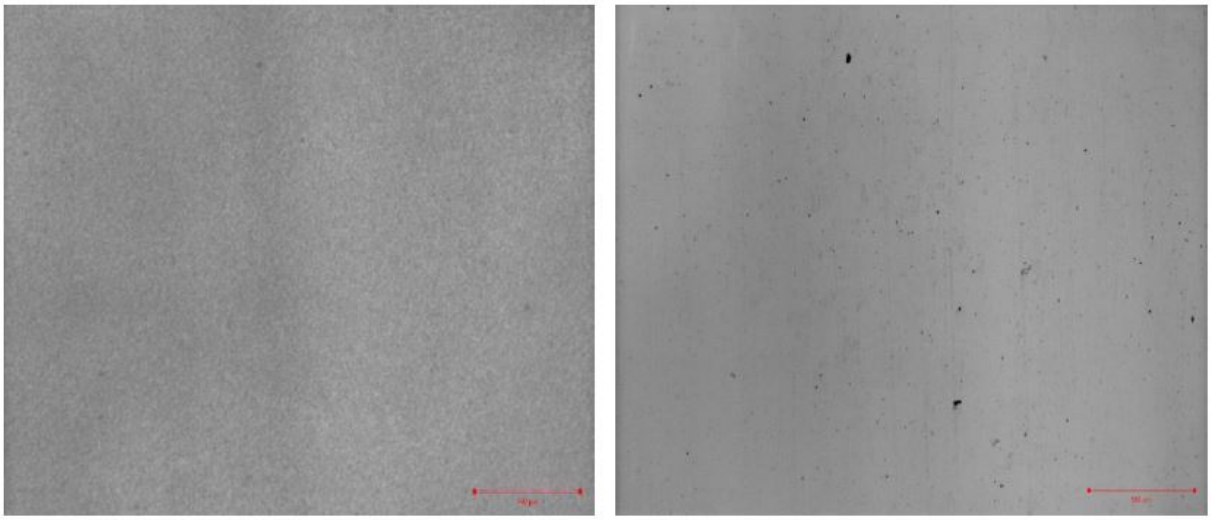

Fig. 5.31 CNTs in grease, dispersion obtained during 1-hour operation in a ball bearing (left) and roller bearing (right), CNTs concentration 0.5% wt.

The progress in 0.5 wt% CNTs dispersion in regular lithium grease could be clearly observed in the next pictures where the grease samples were taken after 1 hour, 22 hours, 190 hours, and 720 hours of ball bearing run, Fig. 5.33. As opposed to the oil, CNTs can be easily dispersed in regular, commercially available lithium grease. The dispersion is time-stable.

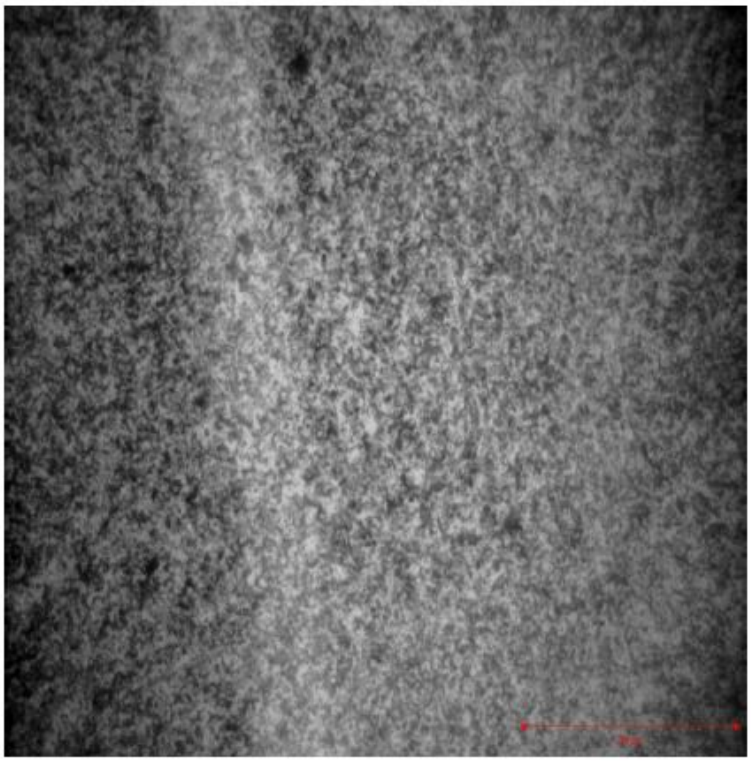

Fig 5.32 CNTs in grease, dispersion obtained after 1-hour operation in a ball bearing, CNTs concentration 0.5% wt, closer view

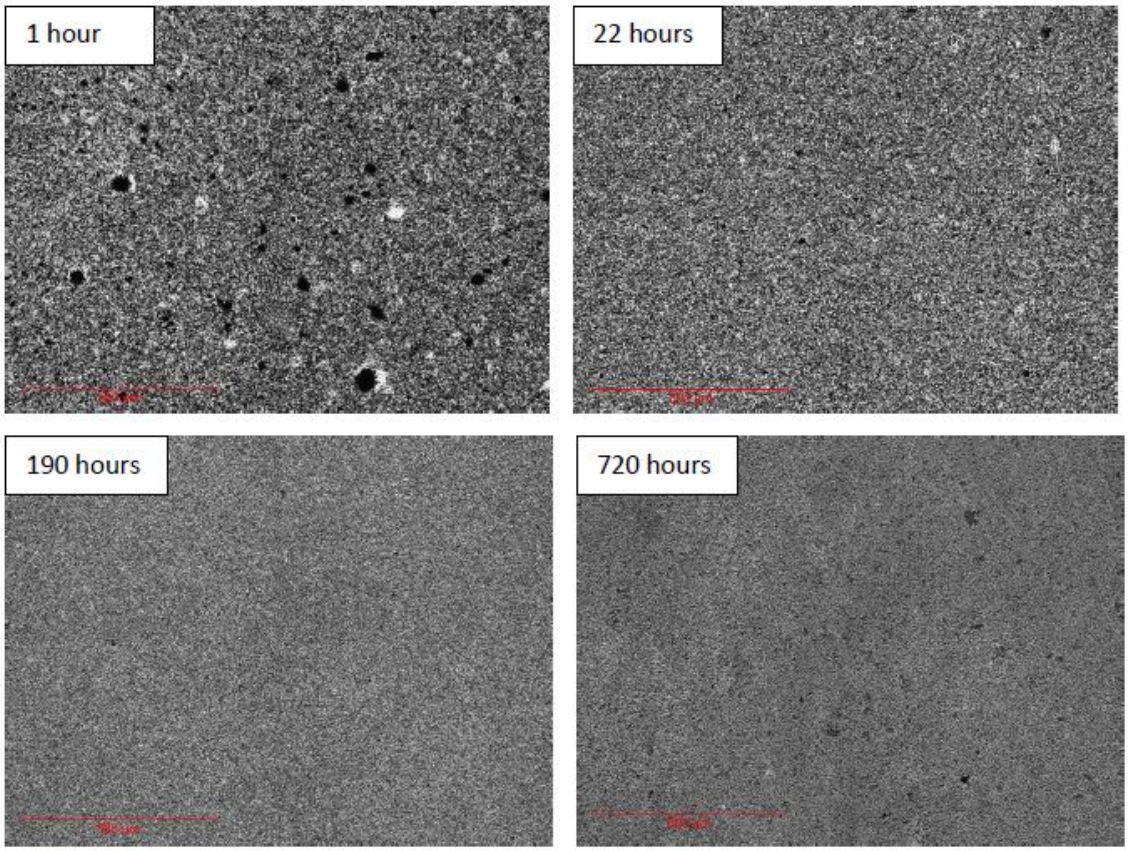

Fig 5.33 0.5 wt% CNTs in lithium grease, improvement of the dispersion during normal bearing run

5.5 Chapter Summary

5.5.1 Piston with CNT Coating

A prototype featuring a CNT-coated skirt piston was successfully developed and tested within an engine. The layer application technique employed in this study enabled the creation of a piston coated with CNTs. However, further enhancements were needed to bolster the durability of the CNT layer. As a result, the developed prototype is not yet ready for industrial implementation. Only after successful modifications will this technology be suitable for real world applications.

Examination of the piston's surface under SEM confirmed the resilience of the CNT layer, showcasing its ability to withstand mechanical stresses and chemical exposure within the piston skirts. Remarkably, the CNT-coated experimental piston, measured at the end of the engine test, exhibited no significant differences in diameter or surface roughness compared to the standard piston. This met the criteria for comparability in terms of friction losses.

Applying a CNT coating on the experimental piston resulted in a substantial reduction in friction losses. Engines equipped with CNT-coated experimental pistons recorded lower motoring torque, with reductions of up to 16% compared to engines using standard pistons. The measurement of piston surface roughness before and after testing revealed that a significant abrasion of the CNT layer took place. However, this issue was attributed to the type of binder used and was deemed not to be an inherent property of CNTs. Therefore, it could be readily addressed in the future.

The notable reduction in engine motoring torque for engines equipped with CNT-coated experimental pistons may not be solely attributed to modifications in the contact conditions between the piston and the cylinder. Continuous abrasion of CNTs from the piston's surface led to their dispersion in the lubricating oil, ultimately reaching the engine's other friction components. If these effects were indeed observed during engine operation, a mechanism for controlling the release of CNTs into the oil could be employed, offering a potential solution to the issue of instability of CNT-enriched oil. Additionally, the study's results indicated that CNTs do not significantly impact the wear process of the cylinder liner.

Lastly, an alternative method involving electrodeposition for applying CNT layers onto the piston surface has been investigated. The results have been evaluated, leading to the proposal of a specialized hierarchical CNT multilayer coating with specific functionalities.

5.5.2 CNT in Lubricating Oil

The test outcomes in this study have validated the hypothesis that even a small mass concentration of 0.03% of CNTs added to the lubricating oil in dispersed form can enhance engine friction performance.

The inclusion of CNTs in the lubricating oil led to a reduction of up to 6% in engine motoring torque across a broad range of tested engine speeds and oil temperatures. Additionally, there was a significant reduction in engine block vibrations, particularly in the direction of the lateral force exerted by the piston, with the introduction of trace amounts of CNTs into the lubricating oil. The ($a_{RMS\ overall}$) parameters were reduced up to 39% in motored tests and up to 25% in fired engine tests.

6

Conclusions and Recommendations

6.1 CNTs Coated Pistons

This study has successfully concluded and validated several crucial findings regarding the incorporation of CNTs into various lubricants. Numerous tests were conducted under a range of diverse conditions to replicate real-world industrial scenarios involving these mixtures.

The core objective of this study was to underscore the capacity of CNTs, when introduced into lubricants, to mitigate friction phenomena in machinery while gaining insights into the tribological contributions made by CNTs in friction reduction.

In the first engine test the aim was to determine the feasibility of a CNT-coated piston to reduce friction. Several types of solutions were applied onto the tested surface as layers and finally compared. The results showed that lubricants with CNTs added to them were proven to be successful in reducing surface friction. However, the durability of the layer was in question before it could be reliably used in long running devices.

The subsequent phase involved refining the CNT layer to enhance its strength and durability. Numerous tests were conducted, yielding highly favorable results. Surface scans of the pistons were carried out and compared in detail. The outcomes unequivocally validated the durability of the CNTs and their ability to withstand both the chemical environment and mechanical stresses encountered on the piston skirts. In-depth examinations of the pistons further indicated that there was no substantial variance in mass loss when considering piston diameter measurements. Additionally, the piston surfaces exhibited low surface roughness, providing further affirmation that the CNT layer had performed its role successfully. Moreover, a comparison of motoring torque revealed that engines equipped with pistons coated with CNTs exhibited a reduction in motoring torque of up to 16%.

On the other hand, based on the pistons surface roughness measurements, performed before and after the engine tests, a significant abrasion was observed on the CNT layer. Further investigation has shown that the abrasion problem was a result of a problem with the binder used in the tests, not due to the properties of the CNTs themselves. It was also possible that the reduction in engine motoring torque was not solely due to the presence of the CNT layer.

6.2 CNTs Added to the Oil for Reduction of the Vibrations

The abrasion of the CNT layer during operation had the consequence of dispersing CNTs in the oil, necessitating a comprehensive investigation into the impact of their presence in the oil concerning the resulting friction reduction. It was imperative to ascertain the threshold of CNT presence.

Subsequent analyses have revealed that CNTs did not exert adverse effects on the wear process of the cylinder liner. Additionally, the research results pertaining to alternative methods of applying CNT

layers to piston surfaces via electro-deposition have been presented, proposing a specialized hierarchical CNT multilayer coating.

Notably, findings from tests conducted on a second engine underscored the positive impact of even a minuscule share of CNTs in the oil, determined to be 0.03%. Further engine tests demonstrated improvements in motoring torque of up to 6%, encompassing a broad spectrum of motor speeds and operating temperatures.

Additionally, these tests yielded a particularly intriguing observation. It became apparent that engine block vibrations were significantly reduced, especially in the critical direction affected by the lateral force exerted by the piston. The ($a_{RMS\ overall}$) reduction parameters reached 39% in motored tests and 25% in fired engine tests. To comprehensively understand the physical phenomena responsible for these advantageous effects, it is essential to consider the multidimensional mechanisms of CNTs' tribological actions.

Among the numerous known mechanisms, this study placed emphasis on the significance of the CNTs dispersion quality, which facilitates macro-scale benefits stemming from the exceptional properties of nanomaterials. Furthermore, it was postulated that the presence of CNTs in the oil mass can modify the temperature distribution within the lubrication gap due to the inherent structure of CNTs. This phenomenon could also enhance tribochemical action through energy transfer, akin to the behavior of conventional anti-wear additives. A suppression of shear-induced vibrations was also observed.

6.3 High Viscosity Lubricants

The initial tests involving a high-viscosity lubricant, formulated using commercially available engine lubricating oil with the addition of CNTs, have uncovered a remarkable and robust interaction between nanotubes and the polymer surfaces.

In extended-duration friction tests, the wear observed on polymer sample surfaces lubricated with CNT-based grease was nearly 50% lower than that observed with the reference high-quality lithium complex grease. However, friction tests conducted with the CNT-based lubricant on metal samples were unsuccessful, primarily due to poor adhesion of the lubricant to metal surfaces.

Across all tested surfaces, the influence of the CNT-based lubricant formulation on wear outcomes was pronounced, underscoring the need for further experiments aimed at understanding the role of nanocarbon morphology in friction processes.

7

Summary

This literature studies followed by experiments presented in this thesis led to the final conclusions listed below.

1) Pistons with CNT layers deposited on their skirts allowed for significant reduction of the measured overall engine friction. Significant reduction of the wear of the CNTs layers and improvement of their adhesion is necessary to enable the commercial applications of the CNT coated pistons.
2) CNTs, when added in a small amounts to the lubricating oil, have the capacity to reduce the engine vibrations, as well as reducing the friction and engine motoring torque.
3) The current formulation of the CNT-based high-viscosity lubricant has proven to be unsuitable for general application due to its poor adhesion to metal surfaces. In contrast, initial tests involving polymer samples commonly used in industry as friction components revealed a robust interaction between CNTs and the polymer surface.

Regarding the findings mentioned above the final conclusion was drawn that the CNTs introduced to the journal bearings suppress friction-induced vibrations and allow for efficient reduction of sliding friction. Thereby the thesis was confirmed.

Bibliography

[1] Huang, J., Tan, J., Fang, H., Gong, F., and Wang, J., **(2019)**. *"Tribological and wear performances of graphene-oil nanofluid under industrial high-speed rotation".* Tribology International. **135**, p. 112-120. https://doi.org/10.1016/j.triboint.2019.02.041

[2] Kałużny, J., Iskra, A., Giersig, M., and Kempa, K., **(2015)**. *"The application of carbon nanotubes for reducing the friction losses of internal combustion engine".* Combustion Engines. **162**(3), p. 64-77. https://doi.org/10.19206/CE-116866

[3] Kałużny, J., Waligórski, M., Szymański, G.M., Merkisz, J., Różański, J., Nowicki, M., Al Karawi, M., and Kempa, K., **(2020)**. *"Reducing friction and engine vibrations with trace amounts of carbon nanotubes in the lubricating oil".* Tribology International. **151**, p. 106484. https://doi.org/10.1016/j.triboint.2020.106484

[4] Joly-Pottuz, L., Dassenoy, F., Vacher, B., Martin, J.M., and Mieno, T., **(2004)**. *"Ultralow friction and wear behaviour of Ni/Y-based single wall carbon nanotubes (SWNTs)".* Tribology International. **37**(11-12), p. 1013-1018. https://doi.org/10.1016/j.triboint.2004.07.019

[5] Buongiorno Nardelli, M., Fattebert, J.L., Orlikowski, D., Roland, C., Zhao, Q., and Bernholc, J., **(2000)**. *"Mechanical properties, defects and electronic behavior of carbon nanotubes".* Carbon. **38**(11), p. 1703-1711. https://doi.org/10.1016/S0008-6223(99)00291-2

[6] Kałużny, J., Merkisz, J., Kempa, K., Gapiński, B., Wróblewski, E., Stepanenko, A., and Al-Karawi, M., **(2018)**. *"Friction reducing performance of carbon nanotubes covered pistons in internal combustion engines–engine test results".* Combustion Engines. **172**(1), p. 14-24. https://doi.org/10.19206/CE-2018-102

[7] Kałużny, J., Kinal, G., Stepanenko, A., and Merkisz, J., **(2019)**. *"Experimental study of carbon nanotubes in high viscosity lubricants".* Combustion Engines. **179**(4), p. 216-219. https://doi.org/10.19206/CE-2019-436

[8] Kałużny, J., Merkisz-Guranowska, A., Giersig, M., and Kempa, K., **(2017)**. *"Lubricating performance of carbon nanotubes in internal combustion engines – engine test results for CNT enriched oil".* International Journal of Automotive Technology. **18**(6), p. 1047-1059. https://doi.org/10.1007/s12239-017-0102-9

[9] Knauder, C., Allmaier, H., Sander, D.E., and Sams, T., **(2019)**. *"Investigations of the friction losses of different engine concepts. Part 1: A combined approach for applying subassembly-resolved friction loss analysis on a modern passenger-car diesel engine".* Lubricants. **7**(5), p. 39. https://doi.org/10.3390/lubricants7050039

[10] Jia, B., Mikalsen, R., Smallbone, A., and Roskilly, A.P., **(2018)**. *"A study and comparison of frictional losses in free-piston engine and crankshaft engines".* Applied Thermal Engineering. **140**, p. 217-224. https://doi.org/10.1016/j.applthermaleng.2018.05.018

[11] Chen, C.S., Chen, X.H., Xu, L.S., Yang, Z., and Li, W.H., **(2005)**. *"Modification of multi-walled carbon nanotubes with fatty acid and their tribological properties as lubricant additive".* Carbon. **43**(8), p. 1660-1666. https://doi.org/10.1016/j.carbon.2005.01.044

[12] Shahnazar, S., Bagheri, S., and Abd Hamid, S.B., **(2016)**. *"Enhancing lubricant properties by nanoparticle additives".* International Journal of Hydrogen Energy. **41**(4), p. 3153-3170. https://doi.org/10.1016/j.ijhydene.2015.12.040

[13] Buldum, A. and Lu, J.P., **(1999)**. *"Atomic Scale Sliding and Rolling of Carbon Nanotubes".* Physical Review Letters. **83**(24), p. 5050-5053. https://doi.org/10.1103/PhysRevLett.83.5050

[14] Ni, B. and Sinnott, S.B., **(2001)**. *"Tribological properties of carbon nanotube bundles predicted from atomistic simulations".* Surface Science. **487**(1), p. 87-96. https://doi.org/10.1016/S0039-6028(01)01073-1

[15] Hwang, Y., Lee, C., Choi, Y., Cheong, S., Kim, D., Lee, K., Lee, J., and Kim, S.H., **(2011)**. *"Effect of the size and morphology of particles dispersed in nano-oil on friction performance between rotating discs".* Journal of Mechanical Science and Technology. **25**(11), p. 2853-2857. https://doi.org/10.1007/s12206-011-0724-1

[16] Alagarasi, A., **(2013)**. *"Chapter-introduction to nanomaterials".* Indian Institute of Technology Madras, p. 1-24. https://cdnx.uobabylon.edu.iq/lectures/v6xohTeNakpC2b8PTHB2w.pdf

[17] Deutsche Forschungsgemeinschaft (DFG) Senatskommission zur Prüfung Gesundheitsschädlicher Arbeitsstoffe (German Research Foundation) Commission for the Investigation of Health Hazards of Chemical Compounds in the Work Area, **(2013)**. *"Nanomaterials: Report"*. John Wiley & Sons. 94 pages. https://books.google.iq/books?id=fwUeCgAAQBAJ

[18] Oberdörster, G., Oberdörster, E., and Oberdörster, J., **(2005)**. *"Nanotoxicology: an emerging discipline evolving from studies of ultrafine particles".* Environmental health perspectives. **113**(7), p. 823-839. https://doi.org/10.1289/ehp.7339

[19] Kreyling, W.G., Semmler-Behnke, M., and Chaudhry, Q., **(2010)**. *"A complementary definition of nanomaterial".* Nano Today. **5**(3), p. 165-168. https://doi.org/10.1016/j.nantod.2010.03.004

[20] Lövestam, G., Rauscher, H., Roebben, G., Klüttgen, B.S., Gibson, N., Putaud, J.-P., and Stamm, H., **(2010)**. *"Considerations on a definition of nanomaterial for regulatory purposes"*. Joint Research Centre (JRC) Reference Reports. **80**, p. 00-41.
https://doi.org/10.2788/98686

[21] Rahmandoust, M. and Ayatollahi, M.R., **(2016)**. *"Carbon nanotubes*", in: Characterization of Carbon Nanotube Based Composites under Consideration of Defects. Advanced Structured Materials, Editors: Rahmandoust, M. and Ayatollahi, M.R., 39, Chapter (2), Springer International Publishing, Cham. p. 5-63.
https://doi.org/10.1007/978-3-319-00251-4_2

[22] Madkour, L.H., **(2019)**. *"Introduction to nanotechnology (NT) and nanomaterials (NMs)*", in: Nanoelectronic Materials: Fundamentals and Applications, Advanced Structured Materials, Editor: Madkour, L.H., 116, Springer International Publishing, Cham. p. 1-47.
https://doi.org/10.1007/978-3-030-21621-4_1

[23] Tinkle, S., Teague, C., Earles, T., and Holdridge, G., **(2009)**. *"The National Nanotechnology Initative: Research and Development Leading to a Revolution in Technology and Industry, Supplement to the President's FY 2010 Budget"*. p. 1-36.
https://apps.dtic.mil/sti/citations/ADA503929

[24] Hulla, J.E., Sahu, S.C., and Hayes, A.W., **(2015)**. *"Nanotechnology: History and future"*. Human & Experimental Toxicology. **34**(12), p. 1318-1321.
https://doi.org/10.1177/0960327115603588

[25] Pandey, P. and Dahiya, M., **(2016)**. *"Carbon nanotubes: types, methods of preparation and applications"*. International Journal of Pharmaceutical Science and Research. **1**(4), p. 15-21.
https://www.researchgate.net/publication/303994564

[26] Iijima, S. and Ichihashi, T., **(1993)**. *"Single-shell carbon nanotubes of 1-nm diameter"*. Nature. **363**(6430), p. 603-605.
https://doi.org/10.1038/363603a0

[27] Eatemadi, A., Daraee, H., Karimkhanloo, H., Kouhi, M., Zarghami, N., Akbarzadeh, A., Abasi, M., Hanifehpour, Y., and Joo, S.W., **(2014)**. *"Carbon nanotubes: properties, synthesis, purification, and medical applications"*. Nanoscale Research Letters. **9**(1), p. 393.
https://doi.org/10.1186/1556-276X-9-393

[28] Kim, H., Lee, J., Kahng, S.J., Son, Y.W., Lee, S.B., Lee, C.K., Ihm, J., and Kuk, Y., **(2003)**. *"Direct observation of localized defect states in semiconductor nanotube junctions"*. Physical Review Letters. **90**(21), p. 216107.
https://link.aps.org/doi/10.1103/PhysRevLett.90.216107

[29] Chico, L., Crespi, V.H., Benedict, L.X., Louie, S.G., and Cohen, M.L., **(1996)**. *"Pure carbon nanoscale devices: Nanotube heterojunctions"*. Physical Review Letters. **76**(6), p. 971-974.
https://doi.org/10.1103/PhysRevLett.76.971

[30] Popov, V.N., **(2004)**. *"Carbon nanotubes: properties and application"*. Materials Science and Engineering: R: Reports. **43**(3), p. 61-102.
https://doi.org/10.1016/j.mser.2003.10.001

[31] We're Going to Put a Carbon Nanotube Computer in Your Hand. Impact Lab, (accessed **April 15, 2023**). Copyright 2020 Impact Lab LLC: Available from:
http://www.impactlab.net/2016/07/13/were-going-to-put-a-carbon-nanotube-computer-in-your-hand/

[32] Harris, P.J., **(2001)**. *Carbon nanotubes and related structures: new materials for the twenty-first century*. Cambridge: Cambridge University Press.
https://personal.ems.psu.edu/~radovic/HarrisBook_Ch1.pdf

[33] Ghaffoori, A.J. and Abdul-Adheem, W.R., **(2019)**. *"A review on carbon nanotubes structural types and techniques"*. Journal of Al-Ma'moon College, (34), p. 346-378.
https://www.iasj.net/iasj/article/173701

[34] Musso, S., Tulliani, J.-M., Ferro, G., and Tagliaferro, A., **(2009)**. *"Influence of carbon nanotubes structure on the mechanical behavior of cement composites"*. Composites Science and Technology. **69**(11-12), p. 1985-1990.
https://doi.org/10.1016/j.compscitech.2009.05.002

[35] Ribeiro, B., Botelho, E.C., Costa, M.L., and Bandeira, C.F., **(2017)**. *"Carbon nanotube buckypaper reinforced polymer composites: a review"*. Polímeros. **27**(3), p. 247-255.
http://dx.doi.org/10.1590/0104-1428.03916

[36] Monthioux, M., Serp, P., Flahaut, E., Razafinimanana, M., Laurent, C., Peigney, A., Bacsa, W., and Broto, J.-M., **(2010)**. *"Introduction to carbon nanotubes*", in: Springer Handbook of Nanotechnology, Editor: Bhushan, B., Springer Berlin Heidelberg: Berlin, Heidelberg. p. 47-118.
https://doi.org/10.1007/978-3-642-02525-9_3

[37] Golnabi, H., **(2012)**. *"Carbon nanotube research developments in terms of published papers and patents, synthesis and production"*. Scientia Iranica. **19**(6), p. 2012-2022.

https://doi.org/10.1016/j.scient.2012.10.036

[38] Stramel, A.A., Gupta, M.C., Lee, H.R., Yu, J., and Edwards, W.C., **(2010)**. *"Pulsed laser deposition of carbon nanotube and polystyrene–carbon nanotube composite thin films".* Optics and Lasers in Engineering. **48**(12), p. 1291-1295. *https://doi.org/10.1016/j.optlaseng.2010.06.002*

[39] Varshney, K., **(2014)**. *"Carbon nanotubes: a review on synthesis, properties and applications".* International Journal of Engineering Research and General Science. **2**(4), p. 660-677. *http://www.ijergs.org/*

[40] García-Gutiérrez, M.C., Nogales, A., Rueda, D.R., Domingo, C., García-Ramos, J.V., Broza, G., Roslaniec, Z., Schulte, K., Davies, R.J., and Ezquerra, T.A., **(2006)**. *"Templating of crystallization and shear-induced self-assembly of single-wall carbon nanotubes in a polymer-nanocomposite".* Polymer. **47**(1), p. 341-345. *https://doi.org/10.1016/j.polymer.2005.11.018*

[41] Siochi, E.J., Working, D.C., Park, C., Lillehei, P.T., Rouse, J.H., Topping, C.C., Bhattacharyya, A.R., and Kumar, S., **(2004)**. *"Melt processing of SWCNT-polyimide nanocomposite fibers".* Composites Part B: Engineering. **35**(5), p. 439-446. *https://doi.org/10.1016/j.compositesb.2003.09.007*

[42] Bhattacharyya, A.R., Pötschke, P., Abdel-Goad, M., and Fischer, D., **(2004)**. *"Effect of encapsulated SWNT on the mechanical properties of melt mixed PA12/SWNT composites".* Chemical Physics Letters. **392**(1-3), p. 28-33. *https://doi.org/10.1016/j.cplett.2004.05.045*

[43] Saeed, K. and Park, S.-Y., **(2007)**. *"Preparation of multiwalled carbon nanotube/nylon-6 nanocomposites by in situ polymerization".* Journal of Applied Polymer Science. **106**(6), p. 3729-3735. *https://doi.org/10.1002/app.26942*

[44] Prashantha, K., Soulestin, J., Lacrampe, M.-F., Claes, M., Dupin, G., and Krawczak, P., **(2008)**. *"Multi-walled carbon nanotube filled polypropylene nanocomposites based on masterbatch route: Improvement of dispersion and mechanical properties through PP-g-MA addition".* Express Polymer Letters. **2**(10), p. 735-745. *https://doi.org/10.3144/expresspolymlett.2008.87*

[45] Zhang, X.-x., Meng, Q.-j., Wang, X.-c., and Bai, S.-h., **(2011)**. *"Poly(adipic acid-hexamethylene diamine)-functionalized multi-walled carbon nanotube nanocomposites".* Journal of Materials Science. **46**(4), p. 923-930. *https://doi.org/10.1007/s10853-010-4836-2*

[46] Ibrahim, K.S., **(2013)**. *"Carbon nanotubes-properties and applications: a review".* Carbon letters. **14**(3), p. 131-144. *https://doi.org/10.5714/CL.2013.14.3.131.*

[47] Frackowiak, E. and Béguin, F., **(2002)**. *"Electrochemical storage of energy in carbon nanotubes and nanostructured carbons".* Carbon. **40**(10), p. 1775-1787. *https://doi.org/10.1016/S0008-6223(02)00045-3*

[48] Wong, S.S., Joselevich, E., Woolley, A.T., Cheung, C.L., and Lieber, C.M., **(1998)**. *"Covalently functionalized nanotubes as nanometre- sized probes in chemistry and biology".* Nature. **394**(6688), p. 52-55. *https://doi.org/10.1038/27873*

[49] Collins, P.G., Bradley, K., Ishigami, M., and Zettl, A., **(2000)**. *"Extreme Oxygen Sensitivity of Electronic Properties of Carbon Nanotubes".* Science. **287**(5459), p. 1801-1804. *https://doi.org/10.1126/science.287.5459.1801*

[50] Chopra, S., Pham, A., Gaillard, J., Parker, A., and Rao, A.M., **(2002)**. *"Carbon-nanotube-based resonant-circuit sensor for ammonia".* Applied Physics Letters. **80**(24), p. 4632-4634. *https://doi.org/10.1063/1.1486481*

[51] Wood, J.R. and Wagner, H.D., **(2000)**. *"Single-wall carbon nanotubes as molecular pressure sensors".* Applied Physics Letters. **76**(20), p. 2883-2885. *https://doi.org/10.1063/1.126505*

[52] Park, S.-J. and Lee, S.-Y., **(2009)**. *"Hydrogen storage behaviors of carbon nanotubes/metal-organic frameworks-5 hybrid composites".* Carbon letters. **10**(1), p. 19-22. *https://doi.org/10.5714/cl.2009.10.1.019.*

[53] Liu, C., Fan, Y.Y., Liu, M., Cong, H.T., Cheng, H.M., and Dresselhaus, M.S., **(1999)**. *"Hydrogen storage in single-walled carbon nanotubes at room temperature".* Science. **286**(5442), p. 1127-1129. *https://doi.org/10.1126/science.286.5442.1127*

[54] Gadd, G.E., Blackford, M., Moricca, S., Webb, N., Evans, P.J., Smith, A.M., Jacobsen, G., Leung, S., Day, A., and Hua, Q., **(1997)**. *"The world's smallest gas cylinders?"*. Science. **277**(5328), p. 933-936.
https://doi.org/10.1126/science.277.5328.933

[55] Hirscher, M., Becher, M., Haluska, M., Quintel, A., Skakalova, V., Choi, Y.M., Dettlaff-Weglikowska, U., Roth, S., Stepanek, I., Bernier, P., Leonhardt, A., and Fink, J., **(2002)**. *"Hydrogen storage in carbon nanostructures"*. Journal of Alloys and Compounds. **330-332**, p. 654-658.
https://doi.org/10.1016/S0925-8388(01)01643-7

[56] Tans, S.J., Verschueren, A.R.M., and Dekker, C., **(1998)**. *"Room-temperature transistor based on a single carbon nanotube"*. Nature. **393**(6680), p. 49-52.
https://doi.org/10.1038/29954

[57] Durairaj, A. and Basak, S., **(2010)**. *"Carbon nanotubes (cnts) production, characterisation and its applications"*. International Journal of Advances in Pharmaceutical Sciences. **1**(3), p. 187-195.
doi: 10.5138/ijaps.2010.0976.1055.01024

[58] Al-Bender, F., **(2005)** *"On the Definition and Laws of Friction"*. in: Proceedings of the World Tribology Congress III, Washington, D.C., USA, Vol. 1, p. 871-872.
https://doi.org/10.1115/WTC2005-63518

[59] Byju's. (accessed **March 23, 2023**), *"Kinetic Friction - Definition, Types, Examples, Questions*". Indian multinational educational technology company: Available from:
https://byjus.com/physics/kinetic-friction/

[60] Toppr. (accessed **March 20, 2023**), *"Kinetic Friction Formula: Definition, Concepts and Examples"* Available from:
https://www.toppr.com/guides/physics-formulas/kinetic-friction-formula/

[61] Randall, N.X., **(2013)**. *"Experimental methods in tribology*", in: Tribology for Scientists and Engineers: From Basics to Advanced Concepts, Editors: Menezes, P.L., Nosonovsky, M., Ingole, S.P., Kailas, S.V., and Lovell, M.R., Springer New York: New York, NY. p. 141-175.
https://doi.org/10.1007/978-1-4614-1945-7_4

[62] Song, W., Yan, J., and Ji, H., **(2018)**. *"Tribological study of the SOCNTs@MoS_2 composite as a lubricant additive: synergistic effect"*. Industrial & Engineering Chemistry Research. **57**(20), p. 6878-6887.
https://doi.org/10.1021/acs.iecr.8b00740

[63] Chauveau, V., Mazuyer, D., Dassenoy, F., and Cayer-Barrioz, J., **(2012)**. *"In situ film-forming and friction-reduction mechanisms for carbon-nanotube dispersions in lubrication"*. Tribology Letters. **47**(3), p. 467-480.
https://doi.org/10.1007/s11249-012-0006-9

[64] Chauveau, V., **(2010)**. *"Le pouvoir lubrifiant des nanotubes de carbonne"*. Ph.D. Thesis. Sciences de l'ingénieur [physics], Ecully, L'Ecole Centrale de Lyon, Lyon, France.
https://theses.fr/2010ECDL0041

[65] Meng, Y., Su, F., and Chen, Y., **(2016)**. *"Supercritical Fluid Synthesis and Tribological Applications of Silver Nanoparticle-decorated Graphene in Engine Oil Nanofluid"*. Scientific Reports. **6**(1), p. 31246.
https://doi.org/10.1038/srep31246

[66] Eswaraiah, V., Sankaranarayanan, V., and Ramaprabhu, S., **(2011)**. *"Graphene-based engine oil nanofluids for tribological applications"*. ACS Applied Materials & Interfaces. **3**(11), p. 4221-4227.
https://doi.org/10.1021/am200851z

[67] Cursaru, D.-L., Andronescu, C., Pirvu, C., and Ripeanu, R., **(2012)**. *"The efficiency of Co-based single-wall carbon nanotubes (SWNTs) as an AW/EP additive for mineral base oils"*. Wear. **290-291**, p. 133-139.
https://doi.org/10.1016/j.wear.2012.04.019

[68] Dai, W., Kheireddin, B., Gao, H., and Liang, H., **(2016)**. *"Roles of nanoparticles in oil lubrication"*. Tribology International. **102**, p. 88-98.
https://doi.org/10.1016/j.triboint.2016.05.020

[69] Khalil, W., Mohamed, A., Bayoumi, M., and Osman, T.A., **(2016)**. *"Tribological properties of dispersed carbon nanotubes in lubricant"*. Fullerenes, Nanotubes and Carbon Nanostructures. **24**(7), p. 479-485.
https://doi.org/10.1080/1536383X.2016.1188804

[70] Song, H., Wang, Z., and Yang, J., **(2016)**. *"Tribological properties of graphene oxide and carbon spheres as lubricating additives".* Applied Physics A. **122**(10), p. 933.
https://doi.org/10.1007/s00339-016-0469-x

[71] Zhang, Z., Liu, J., Wu, T., and Xie, Y., **(2017)**. *"Effect of carbon nanotubes on friction and wear of a piston ring and cylinder liner system under dry and lubricated conditions".* Friction. **5**(2), p. 147-154.
https://doi.org/10.1007/s40544-016-0126-6

[72] Kałużny, J., **(2013)**. *"Experimental applications of carbon nanotubes in the construction of internal combustion engines".* Ph.D. Thesis. Poznan University of Technology, Poznań, Poland.
https://scholar.google.com/scholar?cluster=16485576225939190 01&hl=en&as_sdt=2005&sciodt=0,5

[73] Huang, Y.Y. and Terentjev, E.M., **(2012)**. *"Dispersion of carbon nanotubes: Mixing, sonication, stabilization, and composite properties".* Polymers. **4**(1), p. 275-295.
https://doi.org/10.3390/polym4010275

[74] Cornelio, J.A.C., Cuervo, P.A., Hoyos-Palacio, L.M., Lara-Romero, J., and Toro, A., **(2016)**. *"Tribological properties of carbon nanotubes as lubricant additive in oil and water for a wheel–rail system".* Journal of Materials Research and Technology. **5**(1), p. 68-76.
https://doi.org/10.1016/j.jmrt.2015.10.006

[75] Salah, N., Abdel-wahab, M.S., Habib, S.S., and Khan, Z.H., **(2017)**. *"Lubricant additives based on carbon nanotubes produced from carbon-rich fly ash".* Tribology Transactions. **60**(1), p. 166-175.
https://doi.org/10.1080/10402004.2016.1155784

[76] Reinert, L., Suárez, S., and Rosenkranz, A., **(2016)**. *"Tribo-mechanisms of carbon nanotubes: friction and wear behavior of CNT-reinforced nickel matrix composites and CNT-coated bulk nickel".* Lubricants. **4**(2), p. 1-15.
https://doi.org/10.3390/lubricants4020011

[77] Erdemir, A., Ramirez, G., Eryilmaz, O.L., Narayanan, B., Liao, Y., Kamath, G., and Sankaranarayanan, S.K.R.S., **(2016)**. *"Carbon-based tribofilms from lubricating oils".* Nature. **536**(7614), p. 67-71.
https://doi.org/10.1038/nature18948

[78] Kajdas, C., Kulczycki, A., and Ozimina, D., **(2017)**. *"A new concept of the mechanism of tribocatalytic reactions induced by mechanical forces".* Tribology International. **107**, p. 144-151.
https://doi.org/10.1016/j.triboint.2016.08.022

[79] Bhushan, B., Israelachvili, J.N., and Landman, U., **(1995)**. *"Nanotribology: friction, wear and lubrication at the atomic scale".* Nature. **374**(6523), p. 607-616.
https://doi.org/10.1038/374607a0

[80] Heyes, D.M., Smith, E.R., Dini, D., Spikes, H.A., and Zaki, T.A., **(2012)**. *"Pressure dependence of confined liquid behavior subjected to boundary-driven shear".* The Journal of Chemical Physics. **136**(13), p. 134705.
https://doi.org/10.1063/1.3698601

[81] Gattinoni, C., Heyes, D.M., Lorenz, C.D., and Dini, D., **(2013)**. *"Traction and nonequilibrium phase behavior of confined sheared liquids at high pressure".* Physical Review E. **88**(5), p. 052406.
https://doi.org/10.1103/PhysRevE.88.052406

[82] Maćkowiak, S., Heyes, D.M., Dini, D., and Brańka, A.C., **(2016)**. *"Non-equilibrium phase behavior and friction of confined molecular films under shear: A non-equilibrium molecular dynamics study".* The Journal of Chemical Physics. **145**(16), p. 164704.
https://doi.org/10.1063/1.4965829

[83] Uy, D., Simko, S.J., Carter, R.O., Jensen, R.K., and Gangopadhyay, A.K., **(2007)**. *"Characterization of anti-wear films formed from fresh and aged engine oils".* Wear. **263**(7-12), p. 1165-1174.
https://doi.org/10.1016/j.wear.2006.12.026

[84] Gachot, C., Hsu, C., Suárez, S., Grützmacher, P., Rosenkranz, A., Stratmann, A., and Jacobs, G., **(2016)**. *"Microstructural and chemical characterization of the tribolayer formation in highly loaded cylindrical roller thrust bearings".* Lubricants. **4**(2), p. 19.
https://doi.org/10.3390/lubricants4020019

[85] Chen, X. and Li, J., **(2020)**. *"Superlubricity of carbon nanostructures".* Carbon. **158**, p. 1-23.
https://doi.org/10.1016/j.carbon.2019.11.077

[86] Fan, X. and Wang, L., **(2015)**. *"Ionic liquids gels with in situ modified multiwall carbon nanotubes towards high-performance lubricants".* Tribology International. **88**, p. 179-188.
https://doi.org/10.1016/j.triboint.2015.03.026

[87] Avilés, M.-D., Saurín, N., Sanes, J., Carrión, F.-J., and Bermúdez, M.-D., **(2017)**. *"Ionanocarbon lubricants. The combination of ionic liquids and carbon nanophases in tribology".* Lubricants. **5**(2), p. 1-14.
https://doi.org/10.3390/lubricants5020014

[88] Vyavhare, K. and Aswath, P.B., **(2019)**. *"Tribological properties of novel multi-walled carbon nanotubes and phosphorus containing ionic liquid hybrids in grease".* Frontiers in Mechanical Engineering. **5**(15), p. 18.
https://doi.org/10.3389/fmech.2019.00015

[89] Avilés, M.-D., Pamies, R., Sanes, J., and Bermúdez, M.-D., **(2020)**. *"Graphene-ionic liquid thin film nanolubricant".* Nanomaterials. **10**(3), p. 535.
https://doi.org/10.3390/nano10030535

[90] Spikes, H., **(2004)**. *"The history and mechanisms of ZDDP".* Tribology Letters. **17**(3), p. 469-489.
https://doi.org/10.1023/B:TRIL.0000044495.26882.b5

[91] Gosvami, N.N., Bares, J.A., Mangolini, F., Konicek, A.R., Yablon, D.G., and Carpick, R.W., **(2015)**. *"Mechanisms of antiwear tribofilm growth revealed in situ by single-asperity sliding contacts".* Science. **348**(6230), p. 102-106.
https://doi.org/10.1126/science.1258788

[92] Zhang, J. and Spikes, H., **(2016)**. *"On the mechanism of ZDDP antiwear film formation".* Tribology Letters. **63**(2), p. 24.
https://doi.org/10.1007/s11249-016-0706-7

[93] Aldana, P.U., Vacher, B., Le Mogne, T., Belin, M., Thiebaut, B., and Dassenoy, F., **(2014)**. *"Action mechanism of WS_2 nanoparticles with ZDDP additive in boundary lubrication regime".* Tribology Letters. **56**(2), p. 249-258.
https://doi.org/10.1007/s11249-014-0405-1

[94] Xiang, L., Gao, C., Wang, Y., Pan, Z., and Hu, D., **(2014)**. *"Tribological and tribochemical properties of magnetite nanoflakes as additives in oil lubricants".* Particuology. **17**, p. 136-144.
https://doi.org/10.1016/j.partic.2013.09.004

[95] Tomala, A., Vengudusamy, B., Rodríguez Ripoll, M., Naveira Suarez, A., Remškar, M., and Rosentsveig, R., **(2015)**. *"Interaction between selected MoS_2 nanoparticles and ZDDP tribofilms".* Tribology Letters. **59**(26), p. 1-18.
https://doi.org/10.1007/s11249-015-0552-z

[96] Kulczycki, A., Kajdas, C.K., and Liang, H., **(2014)**. *"On the mechanism of catalysis induced by mechano-activation of solid body".* Materials Science-Poland. **32**(4), p. 583-591.
https://doi.org/10.2478/s13536-014-0228-7

[97] Akchurin, A., Bosman, R., Lugt, P.M., and van Drogen, M., **(2016)**. *"Analysis of wear particles formed in boundary-lubricated sliding contacts".* Tribology Letters. **63**(16), p. 1-14.
https://doi.org/10.1007/s11249-016-0701-z

[98] Popov, V.L., **(2018)**. *"Is tribology approaching its golden age? grand challenges in engineering education and tribological research".* Frontiers in Mechanical Engineering. **4**(16), p. 1-16.
https://doi.org/10.3389/fmech.2018.00016

[99] Wikipedia contributors, (accessed **March 23, 2023**), *"Diesel Engine".* Wikipedia, The Free Encyclopedia: Available from:
https://en.wikipedia.org/w/index.php?title=Diesel_engine&oldid=1215855156

[100] ProCarManuals.com, (accessed **June 15, 2023**), *"The 2.5 l R5 TDI engine Design and function: Self-study programme 305".* Volkswagen AG, Wolfsburg: Available from:
https://procarmanuals.com/self-study-program-305-2-5-l-r5-tdi-engine-design-function/

[101] Balahari Krishnan, S., Aezhisai Vallavi, M., Arunkumar, M., and Haripraveen, A., **(2017)**. *"Design and analysis of an IC engine piston using composite material".* European Journal of Advances in Engineering and Technology. **4**(3), p. 209-215.
https://ejaet.com/PDF/4-3/EJAET-4-3-209-215.pdf

[102] Chakravarthy, L.K. and Srikanth, P., **(2015)**. *"Assembly analysis of piston, connecting rod and crankshaft".* International Journal of Science and Research. **4**(6), p. 1803–1807.
https://www.ijsr.net/getabstract.php?paperid=SUB155788

[103] Aljaberi, H.A., Hairuddin, A.A., and Abdul Aziz, N., **(2017)**. *"The use of different types of piston in an HCCI engine: A review"*. International Journal of Automotive and Mechanical Engineering. **14**(2), p. 4348-4268. *https://doi.org/10.15282/ijame.14.2.2017.17.0346*

[104] Gopal, G., Kumar, L.S., Gopinath, D., and Maheshwara, U., **(2016)**. *"Design and analysis of assembly of Piston, connecting rod and crank shaft"*. International Journal of Current Engineering and Technology. **6**(1), p. 235-242.

[105] Sowjanya, V. and Reddy, C.R., **(2016)**. *"Design and analysis of a crank shaft"*. International Journal of Engineering Science and Computing, Research Article. **6**(12), p. 3814-3821.

[106] Baragetti, S., **(2015)**. *"Design criteria for high power engines crankshafts"*. The Open Mechanical Engineering Journal. **9**(1), p. 271-281. *doi: 10.2174/1874155X01509010271*

[107] Berruga García, V., **(2018)**. *"Four-stroke internal combustion engine crankshaft fundamentals"*. Bachelor Thesis. University Degree in Mechanical Engineering. *http://hdl.handle.net/10016/29306*

[108] Mallikarjuna, V., Jashuva, N., Nagaraju, G., and Reddy, B.R.B., **(2014)**. *"Design manufacturing and cost estimation of camshaft used in two wheeler"*. IOSR Journal of Mechanical and Civil Engineering. **11**(1), p. 53-67. *http://www.iosrjournals.org*

[109] Kopeliovich, D., **(2015)**. *"Camshaft bearings"*. Engine Professional, p. 82-86. http://www.engineprofessional.com

[110] Kovacevic, A. (accessed **May 23, 2023**), *"Mechanical Elements-Bearings"* in ME 1110 -engineering practice 1: engineering drawing and design -lecture 14. City University, School of Engineering and Mathematical Sciences, London. Engineering Design@City web Page: Available from: *http://www.staff.city.ac.uk/~ra600/ME1105/Lectures/ME1110-14.pdf*

[111] Ingalls, R.G., **(2011)** *"Introduction to simulation"*. in: Proceedings of the 2011 Winter Simulation Conference (WSC), p. 1374-1388. *https://doi.org/10.1109/WSC.2011.6147858*

[112] Banks, J., **(1999)** *"Introduction to simulation"*. in: Proceedings of the 31st conference on Winter simulation: Simulation-a bridge to the future, Phoenix, Arizona, USA, Vol. 1, p. 7–13. *https://doi.org/10.1145/324138.324142*

[113] McClements, D.J., **(2002)**. *"Lipid-based emulsions and emulsifiers*", in: Food lipids: Chemistry, Nutrition, and Biotechnology, Editors: Akoh, C.C. and Mineditors, D.B., 2nd Edition, Marcel Dekker: New Youk, USA. p. 63–101. *https://www.cabidigitallibrary.org/doi/full/10.5555/20053045481*

[114] Danilatos, G.D., **(1994)**. *"Environmental scanning electron microscopy and microanalysis"*. Microchimica Acta. **114**, p. 143-155. *https://doi.org/10.1007/BF01244538*

[115] Rossi, M.P., Ye, H., Gogotsi, Y., Babu, S., Ndungu, P., and Bradley, J.-C., **(2004)**. *"Environmental Scanning Electron Microscopy Study of Water in Carbon Nanopipes"*. Nano Letters. **4**(5), p. 989-993. *https://doi.org/10.1021/nl049688u*

[116] Wikipedia contributors, (accessed **March 16, 2023**), *"High-Shear Mixer"*. Wikipedia, The Free Encyclopedia: Available from: *https://en.wikipedia.org/w/index.php?title=High-shear_mixer&oldid=1184146361*

[117] Chung, D.D.L., **(2017)**. *Carbon composites, composites with carbon fibers, nanofibers and nanotubes*. 2nd Edition.: Butterworth-Heinemann. 682 Pages. *https://doi.org/10.1016/C2014-0-02567-1*

[118] Brukh, R. and Mitra, S., **(2006)**. *"Mechanism of carbon nanotube growth by CVD"*. Chemical Physics Letters. **424**(1-3), p. 126-132. *https://doi.org/10.1016/j.cplett.2006.04.028*

[119] Wikipedia contributors, (accessed **March 16, 2023**). *"Wet Chemistry"*. Wikipedia, The Free Encyclopedia: Available from: *https://en.wikipedia.org/w/index.php?title=Wet_chemistry&oldid=1200248868*

[120] Das, R., Ali, M.E., Abd-Hamid, S.B., Annuar, M.S.M., and Ramakrishna, S., **(2014)**. *"Common wet chemical agents for purifying multiwalled carbon nanotubes"*. Journal of Nanomaterials. **2014**, p. 945172.

https://doi.org/10.1155/2014/945172

[121] Wikipedia contributors, (accessed **April 16, 2024**). *"Microscopy"* Wikipedia, The Free Encyclopedia: Available from: *https://en.wikipedia.org/w/index.php?title=Microscopy&oldid=1213024045*

[122] Ordoñez Casanova, E.G., Trejo Mandujano, H.A., and Aguirre, M.R., **(2019)**. *"Microscopy and spectroscopy characterization of carbon nanotubes grown at different temperatures using cyclohexanol as carbon source"*. Journal of Spectroscopy. **2019**, p. 6043523. *https://doi.org/10.1155/2019/6043523*

[123] Diaspro, A. and Usai, C., **(2006)**. *"Optical Microscopy"*. Wiley Encyclopedia of Biomedical Engineering. *https://doi.org/10.1002/9780471740360.ebs0869*

[124] Wikipedia contributors, (accessed **March 26, 2023**), *"Electron Microscope"*. Wikipedia, The Free Encyclopedia: Available from: *https://en.wikipedia.org/w/index.php?title=Electron_microscope&oldid=1211270906*

[125] Gajghate, S.S., **(2017)**. *"A presentation on: introduction to microscopy"*. PhD Research Scholar. Mechanical Engineering Department, National Institute of Technology Agartala. *https://doi.org/10.13140/RG.2.2.24105.49768*

[126] Safarova, K., Dvorak, A., Kubinek, R., Vujtek, M., and Rek, A., **(2007)**. *"Usage of AFM, SEM and TEM for the research of carbon nanotubes"*. Modern Research and Educational Topics in Microscopy. **2**, p. 513-519. *https://www.researchgate.net/publication/242769931*

[127] Saito, Y., Seko, K., and Kinoshita, J.-i., **(2005)**. *"Dynamic behavior of carbon nanotube field emitters observed by in situ transmission electron microscopy"*. Diamond and Related Materials. **14**(11), p. 1843-1847. *https://doi.org/10.1016/j.diamond.2005.07.023*

[128] Wikipedia contributors, (accessed **March 1, 2023**), *"Atomic Force Microscopy"*. Wikipedia, The Free Encyclopedia: Available from: *https://en.wikipedia.org/w/index.php?title=Atomic_force_microscopy&oldid=1202288565*

[129] Slattery, A.D., Shearer, C.J., Shapter, J.G., Blanch, A.J., Quinton, J.S., and Gibson, C.T., **(2018)**. *"Improved application of carbon nanotube atomic force microscopy probes using peakforce tapping mode"*. Nanomaterials. **8**(10), p. 807. *https://doi.org/10.3390/nano8100807*

[130] Bani-Fwaz, M.Z., **(2016)**. *"Introduction to spectroscopy: spectroscopic identification of organic compounds"*. Published by ResearchGate, 102 pages. *https://doi.org/10.13140/RG.2.2.29741.59360/1*

[131] Das, R., Hamid, S.B.A., Ali, M.E., Ramakrishna, S., and Yongzhi, W., **(2015)**. *"Carbon nanotubes characterization by X-ray powder diffraction – a review"*. Current Nanoscience. **11**(1), p. 23-35. *http://dx.doi.org/10.2174/1573413710666140818210043*

[132] Shindo, D. and Oikawa, T., **(2002)**. *"Energy dispersive X-ray spectroscopy*", in: Analytical Electron Microscopy for Materials Science, Editors: Shindo, D. and Oikawa, T., Springer Japan: Tokyo. p. 81-102. *https://doi.org/10.1007/978-4-431-66988-3_4*

[133] Nakajima, H., Morimoto, T., Zhou, Y., Kobashi, K., Ata, S., Yamada, T., and Okazaki, T., **(2019)**. *"Nonuniform functional group distribution of carbon nanotubes studied by energy dispersive X-ray spectrometry imaging in SEM"*. Nanoscale. **11**(44), p. 21487-21492. *http://dx.doi.org/10.1039/C9NR07619K*

[134] Wikipedia contributors, (accessed **July 31, 2023**), *"Raman Spectroscopy"*. Wikipedia, The Free Encyclopedia: Available from: *https://en.wikipedia.org/w/index.php?title=Raman_spectroscopy&oldid=1205291263*

[135] Bokobza, L. and Zhang, J., **(2012)**. *"Raman spectroscopic characterization of multiwall carbon nanotubes and of composites"*. Express Polymer Letters. **6**(7), p. 601 - 608. *https://doi.org/10.3144/expresspolymlett.2012.63*

[136] Wikipedia contributors, (accessed **June 3, 2023**), *"Rheology"* Wikipedia, The Free Encyclopedia: Available from: *https://en.wikipedia.org/w/index.php?title=Rheology&oldid=1191992729*

[137] Kim, J.A., Seong, D.G., Kang, T.J., and Youn, J.R., **(2006)**. *"Effects of surface modification on rheological and mechanical properties of CNT/epoxy composites"*. Carbon. **44**(10), p. 1898-1905.

https://doi.org/10.1016/j.carbon.2006.02.026

[138] Neves, M.G.d.C., Arruda, M.A.N.d.C.d., Freitas, J.C.S., Batista, E.A., Prado, T.A., and Naka, M.H., **(2012)** *"Construction of a tribometer for tests with biolubricants".* in: 2012 10th IEEE/IAS International Conference on Industry Applications, Fortaleza, Brazil, p. 1-7.
https://doi.org/10.1109/INDUSCON.2012.6452601

[139] Salinier, A., Dagréou, S., Léonardi, F., Derail, C., and Navascués, N., **(2013)**. *"Electrical, rheological and mechanical characterization of multiscale composite materials based on poly(etherimide)/short glass fibers/multiwalled carbon nanotubes".* Composite Structures. **102**, p. 81-89.
https://doi.org/10.1016/j.compstruct.2013.02.025

[140] Wikipedia contributors, (accessed **May 14, 2023**), *"Tribometer".* Wikipedia, The Free Encyclopedia: Available from: *https://en.wikipedia.org/w/index.php?title=Tribometer&oldid=1190735232*

[141] Holmberg, K., Andersson, P., and Erdemir, A., **(2012)**. *"Global energy consumption due to friction in passenger cars".* Tribology International. **47**, p. 221-234.
https://doi.org/10.1016/j.triboint.2011.11.022

[142] Tung, S.C. and McMillan, M.L., **(2004)**. *"Automotive tribology overview of current advances and challenges for the future".* Tribology International. **37**(7), p. 517-536.
https://doi.org/10.1016/j.triboint.2004.01.013

[143] Kałużny, J., **(2004)**. *"Wpływ kształtu powierzchni nośnej tłoka na parametry filmu olejowego pokrywającego gładź cylindra ".* praca doktorska. Politechnika Poznańska.
https://scholar.google.com/scholar?cluster=17410952017661780 45&hl=en&oi=scholarr

[144] Czech, P., Łazarz, B., and Wojnar, G., **(2007)**. *"Detection of local defects of gear teeth using artificial neural networks and genetic algorithms".* Radom: ITE. **182**.
https://scholar.google.com/scholar?hl=en&as_sdt=0%2C5&q=Detection+of+local+defects+of+gear+teeth+using+artificial+neural+networks+and+genetic+algorithms&btnG=

[145] Qinghua, W., Youyun, Z., Lei, C., and Yongsheng, Z., **(2009)**. *"Fault diagnosis for diesel valve trains based on non-negative matrix factorization and neural network ensemble".* Mechanical Systems and Signal Processing. **23**(5), p. 1683-1695.
https://doi.org/10.1016/j.ymssp.2008.12.004

[146] Madej, H. and Czech, P., **(2010)**. *"Discrete wavelet transform and probabilistic neural network in IC engine fault diagnosis".* Eksploatacja i Niezawodnosc-Maintenance and Reliability, (4), p. 47-54.
https://scholar.google.com/scholar?hl=en&as_sdt=0%2C5&q=Discrete+wavelet+transform+and+probabilistic+neural+network+in+IC+engine+fault+diagnosis&btnG=

[147] Czech, P. and Madej, H., **(2011)**. *"Application of cepstrum and spectrum histograms of vibration engine body for setting up the clearance model of the piston-cylinder assembly for RBF neural classifier".* Eksploatacja i Niezawodność-Maintenance and Reliability, (4), p. 15-20.
https://archive.ein.org.pl/sites/default/files/2011-04-03.pdf

[148] Figlus, T., **(2009)**. *"Diagnosing the engine valve clearance, on the basis of the energy changes of the vibratory signal".* Maintenance Problems. **1**, p. 75-84.
https://scholar.google.com/scholar?cluster=8825954207020800624&hl=en&oi=scholarr

[149] Yadav, S.K. and Kalra, P.K., **(2009)** *"Fault diagnosis of internal combustion engine using Empirical Mode Decomposition".* in: 2009 Proceedings of 6th International Symposium on Image and Signal Processing and Analysis, IEEE, Salzburg, Austria, p. 40-46.
https://doi.org/10.1109/ISPA.2009.5297760

[150] Desbazeille, M., Randall, R.B., Guillet, F., El Badaoui, M., and Hoisnard, C., **(2010)**. *"Model-based diagnosis of large diesel engines based on angular speed variations of the crankshaft".* Mechanical Systems and Signal Processing. **24**(5), p. 1529-1541.
https://doi.org/10.1016/j.ymssp.2009.12.004

[151] Yıldırım, H., Çınar, A., Şayli, Ö., and Köylü, H., **(2015)** *"Vibration and noise analysis of an engine fuelled with diesel and biodiesel blends".* in: International Conference on Advances in Mechanical Engineering.

[152] Fischer, A., **(1996)**. *"Well-founded selection of materials for improved wear resistance".* Wear. **194**(1), p. 238-245.
https://doi.org/10.1016/0043-1648(95)06738-8

[153] Rapoport, L., Nepomnyashchy, O., Lapsker, I., Verdyan, A., Soifer, Y., Popovitz-Biro, R., and Tenne, R., **(2005)**. *"Friction and wear of fullerene-like WS_2 under severe contact conditions: friction of ceramic materials".* Tribology Letters. **19**(2), p. 143-149.
https://doi.org/10.1007/s11249-005-5095-2

[154] Tevet, O., Von-Huth, P., Popovitz-Biro, R., Rosentsveig, R., Wagner, H.D., and Tenne, R., **(2011)**. *"Friction mechanism of individual multilayered nanoparticles".* Proceedings of the National Academy of Sciences. **108**(50), p. 19901-19906.
https://doi.org/10.1073/pnas.1106553108

[155] Chen, C.-S., Cian, H.-J., Yu, C.-H., and Huang, C.-W., **(2014)**. *"Friction coefficient calculation and mechanism analysis for MoS_2 nanoparticle from molecular dynamics simulation".* Procedia Engineering. **79**, p. 617-621.
https://doi.org/10.1016/j.proeng.2014.06.388

[156] Vadgama, B.N., **(2014)**. *"Molecular dynamics simulations of dry sliding asperities to study friction and frictional energy dissipation".* PhD dissertation. Auburn University, Mechanical Engineering.
http://hdl.handle.net/10415/4015

[157] Schlick, T., **(2010)**. *Molecular modeling and simulation-an interdisciplinary guide*. 2nd Edition, Interdisciplinary Applied Mathematics, Editors: Antman, S.S., Marsden, J.E., and Sirovich, L. Vol. 21. Springer-Verlag New York.
https://doi.org/10.1007/978-1-4419-6351-2

[158] Haile, J.M., **(1992)**. *Molecular Dynamics Simulation: Elementary Methods*. John Wiley & Sons, Inc., USA. 487 pages.
https://dl.acm.org/doi/abs/10.5555/531139

[159] Plimpton, S., **(1995)**. *"Fast Parallel Algorithms for Short-Range Molecular Dynamics".* Journal of Computational Physics. **117**(1), p. 1-19.
https://doi.org/10.1006/jcph.1995.1039

[160] Mauch, A., Tophoven, J., Trzebiatowski, T., and Raatz, T., **(2011)**. *"Potenziale und grenzen des downsizings beim dieselmotor".* MTZ - Motortechnische Zeitschrift. **72**(7), p. 530-537.
https://doi.org/10.1365/s35146-011-0124-1

[161] GmbH, M., **(2016)**. *Pistons and engine testing*. 2nd Edition, ATZ/MTZ-Fachbuch, Editor: GmbH, M.: Springer Vieweg Wiesbaden.
https://doi.org/10.1007/978-3-658-09941-1

[162] Golloch, R. and Merker, G.P., **(2005)**. *"Downsizing bei Verbrennungsmotoren".* MTZ - Motortechnische Zeitschrift. **66**(2), p. 126-131.
https://doi.org/10.1007/BF03227254

[163] Deuss, T., Ehnis, H., Bassett, M., and Bisordi, A., **(2011)**. *"Reibleistungsmessungen am befeuerten dieselmotor zyklusrelevante CO_2-ersparnis".* MTZ - Motortechnische Zeitschrift. **72**(12), p. 954-959.
https://doi.org/10.1365/s35146-011-0206-0

[164] Kennedy, M., Hoppe, S., and Esser, J., **(2012)**. *"Kolbenringbeschichtung zur reibungssenkung im ottomotor".* MTZ - Motortechnische Zeitschrift. **73**(5), p. 400-403.
https://doi.org/10.1007/s35146-012-0325-2

[165] Olek, M., Kempa, K., Jurga, S., and Giersig, M., **(2005)**. *"Nanomechanical Properties of Silica-Coated Multiwall Carbon NanotubesPoly(methyl methacrylate) Composites".* Langmuir. **21**(7), p. 3146-3152.
https://doi.org/10.1021/la0470784

[166] Meng, H., Sui, G.X., Xie, G.Y., and Yang, R., **(2009)**. *"Friction and wear behavior of carbon nanotubes reinforced polyamide 6 composites under dry sliding and water lubricated condition".* Composites Science and Technology. **69**(5), p. 606-611.
https://doi.org/10.1016/j.compscitech.2008.12.004

[167] Hwang, H.J., Jung, S.L., Cho, K.H., Kim, Y.J., and Jang, H., **(2010)**. *"Tribological performance of brake friction materials containing carbon nanotubes".* Wear. **268**(3), p. 519-525.
https://doi.org/10.1016/j.wear.2009.09.003

[168] Tehrani, M., Safdari, M., Boroujeni, A.Y., Razavi, Z., Case, S.W., Dahmen, K., Garmestani, H., and Al-Haik, M.S., **(2013)**. *"Hybrid carbon fiber/carbon nanotube composites for structural damping applications".* Nanotechnology. **24**(15), p. 155704.
https://dx.doi.org/10.1088/0957-4484/24/15/155704

[169] Cui, L.-J., Geng, H.-Z., Wang, W.-Y., Chen, L.-T., and Gao, J., **(2013)**. *"Functionalization of multi-wall carbon nanotubes to reduce the coefficient of the friction and improve the wear resistance of multi-wall carbon nanotube/epoxy composites".* Carbon. **54**, p. 277-282.
https://doi.org/10.1016/j.carbon.2012.11.039

[170] Yan, L., Wang, H., Wang, C., Sun, L., Liu, D., and Zhu, Y., **(2013)**. *"Friction and wear properties of aligned carbon nanotubes reinforced epoxy composites under water lubricated condition".* Wear. **308**(1), p. 105-112.
https://doi.org/10.1016/j.wear.2013.10.007

[171] Golchin, A., Wikner, A., and Emami, N., **(2016)**. *"An investigation into tribological behaviour of multi-walled carbon nanotube/graphene oxide reinforced UHMWPE in water lubricated contacts".* Tribology International. **95**, p. 156-161.
https://doi.org/10.1016/j.triboint.2015.11.023

[172] Matczak, L., Johanning, C., Gil, E., Guo, H., Smith, T.W., Schertzer, M., and Iglesias, P., **(2018)**. *"Effect of cation nature on the lubricating and physicochemical properties of three ionic liquids".* Tribology International. **124**, p. 23-33.
https://doi.org/10.1016/j.triboint.2018.03.024

[173] Qu, J., Bansal, D.G., Yu, B., Howe, J.Y., Luo, H., Dai, S., Li, H., Blau, P.J., Bunting, B.G., Mordukhovich, G., and Smolenski, D.J., **(2012)**. *"Antiwear performance and mechanism of an oil-miscible ionic liquid as a lubricant additive".* ACS Applied Materials & Interfaces. **4**(2), p. 997-1002.
https://doi.org/10.1021/am201646k

[174] Yu, Q., Wang, Y., Huang, G., Ma, Z., Shi, Y., Cai, M., Zhou, F., and Liu, W., **(2018)**. *"Task-specific oil-miscible ionic liquids lubricate steel/light metal alloy: a tribochemistry study".* Advanced Materials Interfaces. **5**(19), p. 1800791.
https://doi.org/10.1002/admi.201800791

[175] Yu, Q., Zhang, C., Dong, R., Shi, Y., Wang, Y., Bai, Y., Zhang, J., Cai, M., and Zhou, F., **(2019)**. *"Novel N, P-containing oil-soluble ionic liquids with excellent tribological and anti-corrosion performance".* Tribology International. **132**, p. 118-129.
https://doi.org/10.1016/j.triboint.2018.12.002

[176] Wang, B., Wang, X., Lou, W., and Hao, J., **(2010)**. *"Rheological and tribological properties of ionic liquid-based nanofluids containing functionalized multi-walled carbon nanotubes".* The Journal of Physical Chemistry C. **114**(19), p. 8749-8754.
https://doi.org/10.1021/jp1005346

[177] Yu, B., Liu, Z., Ma, C., Sun, J., Liu, W., and Zhou, F., **(2015)**. *"Ionic liquid modified multi-walled carbon nanotubes as lubricant additive".* Tribology International. **81**, p. 38-42.
https://doi.org/10.1016/j.triboint.2014.07.019

[178] Mortazavi, V. and Nosonovsky, M., **(2011)**. *"Friction-Induced Pattern Formation and Turing Systems".* Langmuir. **27**(8), p. 4772-4779.
https://doi.org/10.1021/la200272x

[179] Xue, L., Iturri, J., Kappl, M., Butt, H.-J., and del Campo, A., **(2014)**. *"Bioinspired orientation-dependent friction".* Langmuir. **30**(37), p. 11175-11182.
https://doi.org/10.1021/la502695d

[180] Kałużny, J., Kulczycki, A., Dzięgielewski, W., Piasecki, A., Gapiński, B., Mendak, M., Runka, T., Łukawski, D., Stepanenko, O., Merkisz, J., and Kempa, K., **(2020)**. *"The indirect tribological role of carbon nanotubes stimulating zinc dithiophosphate anti-wear film formation".* Journal. **10**(7), p.
https://doi.org/10.3390/nano10071330